A STUDY OF PRESTRESSED CONCRETE

Presented in Partial Fulfillment of the Requirements
for the Degree of Master of Engineering.

McGILL UNIVERSITY

MONTREAL

April 1957 Lionel Issen

ACKNOWLEDGEMENTS

This investigation was undertaken as a continuation of an investigation into prestressed concrete begun by Mr. R. Banks and Mr. G. A. Jakobson.

The beam was designed jointly by the author and Mr. Banks, Mr. Banks selecting the beam section and the author designing the end blocks.

To Professor J. L. De Stein, who acted as research director, the author is indebted for a number of helpful suggestions.

To Professor V. W. Wilson, head of the Strength of Materials Laboratory, who assisted in obtaining materials, in the layout for the instrumentation, and suggesting alternative procedures when desired instruments were unavailable.

To the Precompressed Concrete Engineering Company Limited for supplying the wedges and anchorages used, and for supplying the necessary jacks and fittings for tensioning the wires.

To the Hesmont Concrete Company for providing the H.T. steel wire.

To the Mount Royal Ready Mixed Company for supplying the concrete, and for suggesting handling and curing procedures.

To Mr. I. Ginsberg for assistance in wiring up the gages and checking the circuits.

To Mr. G. Matsell, of the McGill Strength of Materials Laboratory, for assistance in rigging the beam and setting up the ancillary equipment.

T A B L E   O F   C O N T E N T S

Table of Contents Continued

NOMENCLATURE

The following symbols used in this thesis are those which appear to be most commonly used by designers and writers in prestressed concrete.

A - cross sectional area

A_s - area of steel

a - portion of span between support and load; subscript "condition or loading applied after prestressing has been completed"

b - width of section; subscript "bottom"

C - permissible compressive stress in concrete

C_t - permissible tensile stress in concrete

C_{at}, C_{ab} - calculated stress in top and bottom fibres due to loads W_a applied after prestressing has been completed

C_{dt}, C_{db} - calculated stress in top and bottom fibres due to loads W_d acting at time of prestressing

d - depth of section; subscript "dead load"

δ - deflection of the neutral axis of a beam from its unloaded state, elongation of a test piece under load

e - eccentricity of the prestressing force from the neutral axis of the cross section

E_c - modulus of elasticity of concrete

E_s - modulus of elasticity of steel

ϵ - unit strain

ϵ_1 ϵ_2 ϵ_x - unit strain in direction 1,2,x etc

f'_c	- ultimate compressive strength of concrete, usually the 28-day strength of a standard 6 x 12 cylinder
f'_{ci}	- ultimate compressive strength of concrete at time of prestress
f_e	- stress in concrete at eccentricity "e"
f_g	- stress in concrete at the center of gravity of the cross-section
f'_s	- ultimate unit stress of the prestressing steel
f_y	- unit stress at the equivalent yield point of the hi-tensile steel
γ	- shearing strain
I	- moment of inertia
L	- span length
n	- modular ratio = E_s/E_c
μ	- Poisson's ratio for concrete
M_a, M_d	- bending moments due to loads W_a and W_d respectively
M_t	- total bending moment at a section
P	- applied concentrated load; prestressing force
P_i	- initial prestressing force
P_u	- ultimate prestressing force
r	- radius of gyration
τ	- unit shearing stress
σ	- unit normal stress
σ_x σ_y	- unit normal stress in the directions of the x and y axes
σ_{MAX} σ_{MIN}	- maximum and minimum principal stress

t	- thickness; subscript "top" or "tensile"
W_a	- loading applied after prestress has been established
W_d	- loading acting at time that prestress is applied
y	- distance to a fibre from the neutral axis of the cross section
Z	- section modulus = I/y

INTRODUCTION

HISTORY OF PRESTRESSED CONCRETE

Almost from the beginning of the use of reinforced concrete as a structural material, attempts were made to improve the quality and strength of the material by applying prestressing forces. In a patent applied for in 1886 entitled "Constructions of Artificial Stone and Concrete Pavements", P. H. Jackson of San Francisco described several methods of applying prestress forces by stretching ties by turnbuckles, screws and nuts and wedges. Later in 1888 C. F. W. Doehring in Germany, and in 1896 J. Mandl in Austria secured patents for applications of steel and concrete that may quite properly be described as prestressed concrete.

These early attempts at prestressing, and later attempts prior to 1920 were unsuccessful because the properties of the concrete were unknown and in particular the relative importance of shrinkage, and plastic flow was not realized.

Around 1923 F. V. Emperger in Austria, W. H. Hewett and R. H. Dill in the United States independently of one another proposed that high strength steel wire be used to apply prestress forces to circular structures such as tubes and pipes. However, the problem of deferred strains due to shrinkage and plastic flow was still not clearly understood.

Successful linear prestressing dates from 1928 when

Freyssinet, drawing on the results of work done in the United States and Britain by Faber and Glanville, was able to evaluate the magnitude of the deferred strains and establish his theory of prestressing.

Quoting from a lecture by Eugene Freyssinet:

"The idea of modifying the nature of the forces and defects in structures caused by the application of load first began to haunt my mind towards 1903-04 under the influence of my professors at the Ecole des Ponts et Chaussees ....

"Even at that early date, there was nothing new in the idea of stretching the reinforcement in reinforced concrete...

"In 1905 .... I attempted to put my ideas into practice. In 1907 a 100 foot span arch over the River Bresbres was decentered by pressure at the crown .... This was followed by the construction of a series of these bridges over the River Allier each having three very flat arches of more than 230 ft. span.

"The deflections of the test arch, and the observations made on the first of the bridges about a year after its construction, showed strains so much larger than those calculated that the bridge would have collapsed had the arches not been jacked up and the crown hinges made solid; this compelled the admission of a modulus varying considerably with time and stress. But this question prompted the consideration of the maintenance of permanent forces in concrete and, indeed the whole basic of prestressing. The first world war ..... held up the pursuit of these ideas for more than ten years and it was only in 1926-27 that I was able to form a clear idea of the phenomena of delayed strain.

"At that moment, research carried out in America and England was published and provided confirmation of my results."

Since this date, there have, of course, been many developments in prestressed concrete theory, design, construction and prestressing procedures. But to Freyssinet we are indebted for the first workable theory of linear prestressed concrete and for pioneering its use in all branches of engineering construction.

TYPES AND METHODS OF APPLYING PRESTRESS

Prestressing is usually applied through tensioned steel bars or wires.

The various ways of transferring the stress from the steel to the concrete are grouped into two classes; they are pretensioning and posttensioning.

In pretensioning the steel is first stretched and the concrete is cast around it. When this has attained sufficient strength, the steel is released and stress is retained by bond with the concrete. The steel is usually in the form of wires less than 0.2 inches diameter. The diameter being kept small to increase the bond, bonding may be further improved by notching or indenting the wire.

The pretensioning methods can be applied to either the long-line process or to individual molds.

In the long-line process, a long casting bed usually 200 to 300 feet long is used to cast similar linear units. The units are separated by sheet metal or fibre inserts, or the units may be sawn into suitable lengths after curing. At the ends of the casting bed the stressing wires are tensioned against a heavy frame and anchored to it by suitable devices. The anchoring devices are usually based on the wedge-in-a-slot principle. However, great care must be taken with the anchoring devices as they can only be reused a few times before they lose their gripping qualities. A number of serious accidents have occurred when reused wedges slipped, allowing tensioned wires to snap back very much in the manner of a stretched elastic band. The wires are tensioned by either a hydraulic jack acting against the frame, or by moving the anchoring frame away from the mold. In either case the net result is the same; namely the wires are elongated a predetermined amount.

The individual mold method is similar to the long-line process except that the lengths of the casting beds are much shorter, being only that required for a single unit. The mold must be designed to carry the full prestress force.

In posttensioning, the concrete is cast and allowed to harden before the prestress is applied. The wires or cables or bars may be placed in position and cast into the concrete, being prevented from bonding to the concrete by some form of sheath or other means, or holes may be cast into the concrete and the wires or cables passed through after hardening has taken place. They may then be stressed and anchored against the ends of the unit. subsequently, the wires or cables may be grouted in to protect the steel and give the additional safeguard of bond between the steel and concrete.

Up to the present, the two main systems of posttensioning anchorage for wire cables that have been evolved are the Freyssinet system developed in France by Eugene Freyssinet, and the Magnel system developed in Belgium by Professor Gustave Magnel. These two methods have been applied to a great number and variety of structures ranging from stringers to bridges, and their soundness have been proved by the tests of time and use.

Because these two methods are covered by patents, their basic principles have often been adapted in ways to circumvent the patents.

In the Freyssinet system, a number of wires - the number ranging between 8 and 18 - are grouped around a mild steel helical wire core and covered with a thin sheet metal sheath.

In practise, the sheath is cast into the concrete and the cable may either be placed loosely in the sheath or drawn through the sheath after the concrete has set.

The anchorage system consists of a concrete cylinder with a central conical hole into which a conical plug is forced, after the wires have been tensioned. The conical hole is lined with a closely spaced spiral of high tensile wire. The cylinder is of sufficient size to distribute its load to the concrete and is almost always cast into the beam with its end flush with end of the beam. The cone is made of concrete but with any spiral reinforcement or surface covering, but it is made with longitudinal grooves to grip the cable wires. A hole runs through the center of the cone to allow grout to be injected after the cables are stressed. The cable wires are threaded between the cylinder and the cone, after the wires are tensioned the cone is forced into the cylinder, gripping the wires tightly.

In the Magnel system, the method of anchorage consists of steel sandwich plates with four trapezoidal slots, two of each on the upper and lower surfaces. A trapezoidal wedge fits into each slot and fixes two wires, thus each sandwich plate holds eight wires and a prestressing cable will have a number of wires equal to eight times the number of sandwich plates. The sandwich plate bears upon a cast steel distribution plate which has a central hole through which the cable passes. The distribution plate serves to distribute the prestressing force at the point of application to the end of the beam or unit.

In both systems the ends of the beams must be suitably reinforced to withstand the concentrated forces applied through the anchorage units. Additional secondary mild steel reinforcement is usually placed along the beam, this serves to tie the unit together and improves the behaviour of the unit under severe loading.

Two other systems deserve mention here, they are typified by the Lee-McCall system and the Roebling system. In the first the large number of wires is replaced by a small number of high tensile alloy bars. The ends of the bars are threaded and the anchorage is through nuts bearing on distribution plates. The main disadvantage of the system is that the ends of the rods are not made of a larger diameter than the body, so that the weakest portion is at the anchorage. In tests carried out at the Illinois Institute of Technology in 1951, and elsewhere, the bars failed in every case at the nut anchorages. Also, cases have occurred where the anchorages have failed during stressing operations. Notwithstanding these shortcomings, the Lee-McCall system has been successfully applied to engineering structures.

The Roebling system replaces the large number of wires by a smaller number of stranded cables. The anchorage system is via a nut and collar arrangement. Here again, the anchorage is the weakest part of the system. However, this system has been used successfully for several heavy structures on the Pacific Coast.

For a complete discussion of the various methods of prestressing, the reader should consult the references at the end of this thesis.

After the prestressed units are cast, they are almost steam cured if they are being pretensioned, and are generally steam cured if they are posttensioned. The setup for steam curing can often be made very simply; for example, a light canvas over a wooden frame has been used satisfactorily. However, for a factory installation it would be advisable to have a fairly elaborate steam curing installation.

STRUCTURAL EFFICIENCY OF PRESTRESSED CONCRETE

Prestressed concrete has been applied successfully to pipes, tanks, runway and highway slabs, building frames and components, bridges, flat arches, shell structures and dams. In short, apart from structures requiring the use of mass concrete, there are no structures which can be built of reinforced concrete that cannot be built in prestressed concrete. The particular advantages of prestressed concrete are its lighter weight, freedom from cracks, economy of steel and of concrete. Prestressed concrete structures, because of their greater length to depth ratio, are of particular advantage where the headroom is restricted. Also because of the combining effect of the prestress forces, and because the entire concrete section is effective, the deflections are smaller than with an equivalent reinforced concrete structure.

The two factors that contribute to the structural economy of prestressed concrete as compared with reinforced concrete are as follows: firstly, its greater structural efficiency; that is the whole cross-sections of the structural number is effective in resisting the bending moments: secondly, shearing stresses are rarely critical, because the prestress acts to reduce the magnitude and inclination of principal tensile stresses. The magnitude of the principal tensile stresses are further reduced by bending the cable so that it is formed into a parabolic arc. Here the vertical component of prestress produced by curving the cable acts in the opposite sense to the shear force, and the maximum effect is at the ends of the beams where the shear force is greatest.

The reduction in principal tensile stress results in an additional saving in stirrups. In reinforced concrete, the principal tensile stress is assumed to act at an angle of 45^{o} to the neutral axis, this assumption follows mathematically if no horizontal forces are considered below the neutral axis. In prestressed concrete, the flatter angle of the principal tensile stress permits a greater spacing of the shear reinforcement and the use of much lighter shear reinforcement.

In practise, the amount of shear reinforcement is usually nominal with 3/8-inch or 1/4-inch diameter mild steel stirrups being spaced between .7 to .8 of the overall depth of the beam.

This rule of thumb for stirrup spacing grew out of the Theories of Kommendant, Magnel and Billig, and the later work of Guyon, Betaille and Robinson.

The first group of writers assume that the concrete will fail in the direction of greatest tensions; viz., in the direction of the principal tensile stress, thus conforming to the maximum principal stress Theory of Failure. Guyon drew on the work of Betaille and Robinson which predicts that failure will occur at the angle of maximum slip, which is somewhat more inclined than the angle of principal tension, thus conforming to the Mohr Theory of Failure.

The discussion is developed further in the sections entitled "Theories of Failure" and "Discussion of Results."

SAFETY OF PRESTRESSED CONCRETE STRUCTURES

Safety with prestressed concrete as with other forms of construction depends on both the design and its execution. If the available conventional methods of design are used, and if the design is executed in an adequate manner, the prestressed concrete structure will be at least as safe as any equivalent structure executed in another material. This is because, during the prestressing operation, the concrete and steel are subjected to greater loads than they will be subjected to during their subsequent life in the structure. Because of the higher strength concrete, the smaller sections, and the critical or delicate design features involved, prestressed concrete structures require greater care in their design and erection than do the equivalent concrete sections.

CHAPTER I

THE EXPERIMENT

PURPOSE OF THE EXPERIMENT

During the summer of 1955, the writer undertook the experimental work on a full size prestressed concrete beam, following a similar project carried out jointly by Mr. G. A. Jakobson and Mr. R. H. Banks.

Though considerable testing on prestressed concrete members has been carried out in North America during the past six or seven years, the testing has usually had limited objectives and has usually been concerned with such things as cracking loads, ultimate loads, deflections, and verification of safety factors. Deflections are usually close to the predicted up to the cracking load, the safety factors are verified and that is the extent of the test. In rare cases, where strain gages are applied to the structure under test, the results are almost always reported in terms of stress, and the resulting stress distributions almost invariably seem to agree with those predicted by the elastic theory. A notable exception is the report on the Walnut Lane Bridge, in Magnel's book "Prestressed Concrete" 2nd and 3rd editions.

Too little consideration has been given to the actual internal behaviour of the structural member. How do the stress conditions under prestress, working and ultimate loads, compare with those predicted by the classical theory? With the increased use of prestressed concrete, it becomes more important to know if the elastic theory can be applied and its limitations, or whether other more rational techniques should be employed. Though a mathematical analysis of principal stresses, using the Mohr circle, indicates that the principal tension stresses in the web of a prestressed beam are low, there have been very few attempts made to verify this. The verification of the actual stresses in a full size beam with the theoretical stresses is thus the main concern of this thesis. A secondary concern is a qualitative examination of current construction and prestressing techniques.

In order to obtain results that could easily be applied to current problems, a full size I-beam was cast. This beam had a conventional cross-section; however, because of space limitations in the laboratory, the depth/span ratio was only 1:8.5, whereas in practise this ratio is usually of the order of 1:15 to 1:30. This, however, has little effect on the critical properties of the beam, viz, bending and shear strength. However, the bending deflections were increased by some 10% due to secondary shear effects.

THE INSTRUMENTATION FOR THE EXPERIMENT

The instrumentation used in the test on the experimental beam consisted mainly of SR4-A3 linear gages, SR4-A9 linear gages, and SR4-AR14 rosettes. The last were used instead of the SR4-AR1 rosettes beacuse of their availability. The A3 and AR14 gages were bonded to the concrete, while the A-9 gages were bonded to the prestressing wires. A Baldwin-Lima-Hamilton static strain indicator was used to give direct strains readings.

Deflections at the supports and center of the test beam were measured by 1/1000 Ames dials. Net deflection at the center line were obtained by deducting the mean deflection over the supports from the mean deflection at the center line.

The experimental beam was tested in the 220 ton Baldwin-Lima-Hamilton testing machine in the McGill University test laboratory.

The beam was supported on two 8" x 10" x 3'0" concrete blocks resting on a sand cushion on the laboratory floor. One end of the beam rested on a fixed rocker which consisted of a 2" diameter steel roller welded to a 5" x 14" x 1-1/2" steel plate; the other end of the beam rested on roller placed between two plates 5" x 14" x 1-1/2". See Fig. I-1.

On the sides of the beam, gages were placed directly opposite each other, while on the top and bottom faces of the flanges three gages were placed in a line perpendicular to the axis of the beam. The mean of the gages was taken as the true strain for calculation purposes.

Twelve A-9 gages were attached to the prestressing cables, six to each cable. The mean of these strain readings was taken to represent the mean strain in each wire.

Compensating gages for the gages were prepared by attaching A3 and AR14 gages to a test cylinder made from the same mix as that used for the experimental beam, and by attaching an A9 gage to a block of high grade steel. The method of attaching the gages to the structure is discussed farther in Chapter IV.

The location of the strain gages is shown in Fig. I-2, while the numbering code for the gages is shown in Fig. I-3a and 3b. Photographs of the test setup and instrumentation are shown in Fig. I-4, I-5, and Fig. IV-13.

Because of the availability of the anchoring devices, the beam was prestressed using the Magnel-Blaton system.

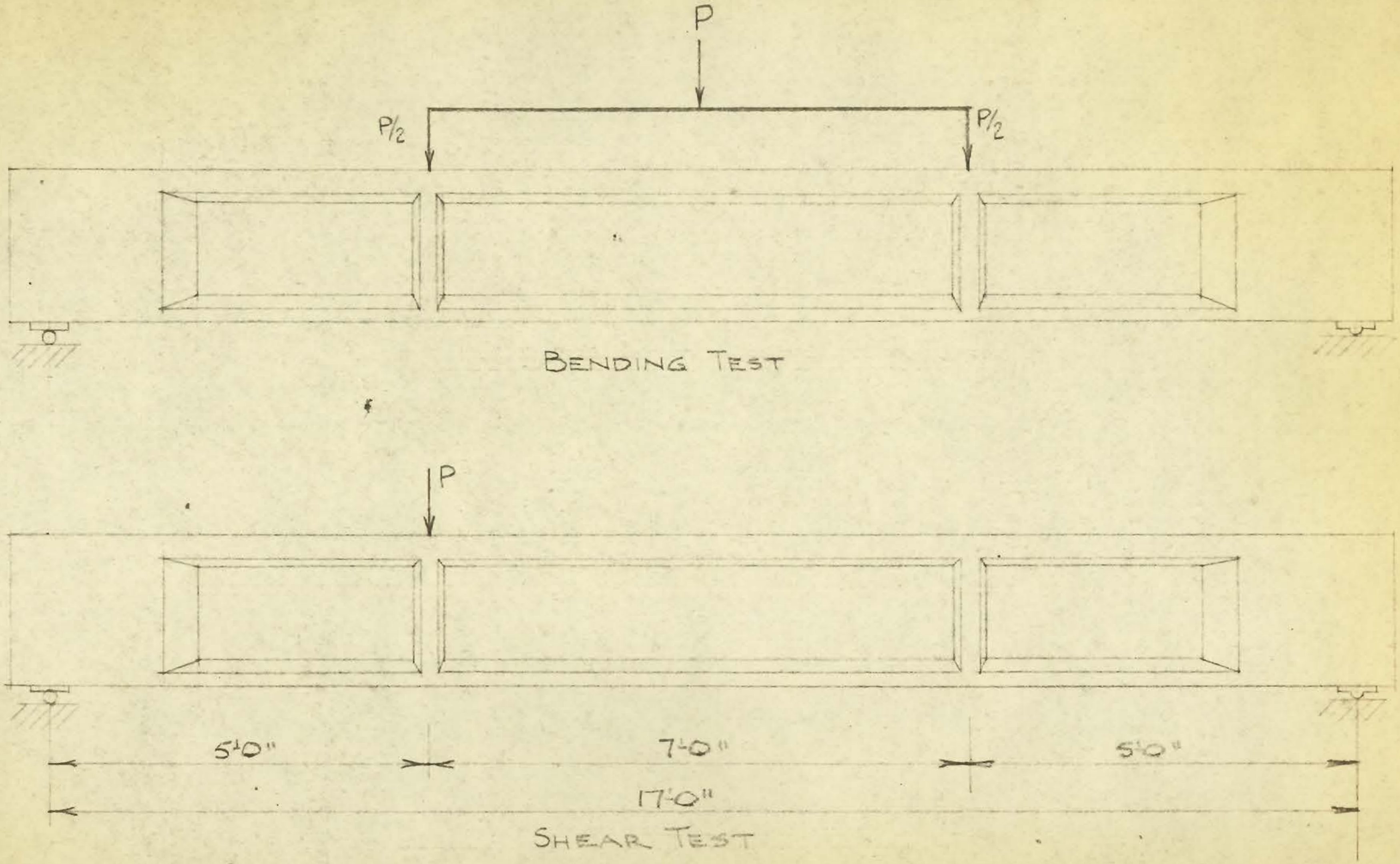

FIG I-1
BEAM LOADING TEST SETUP

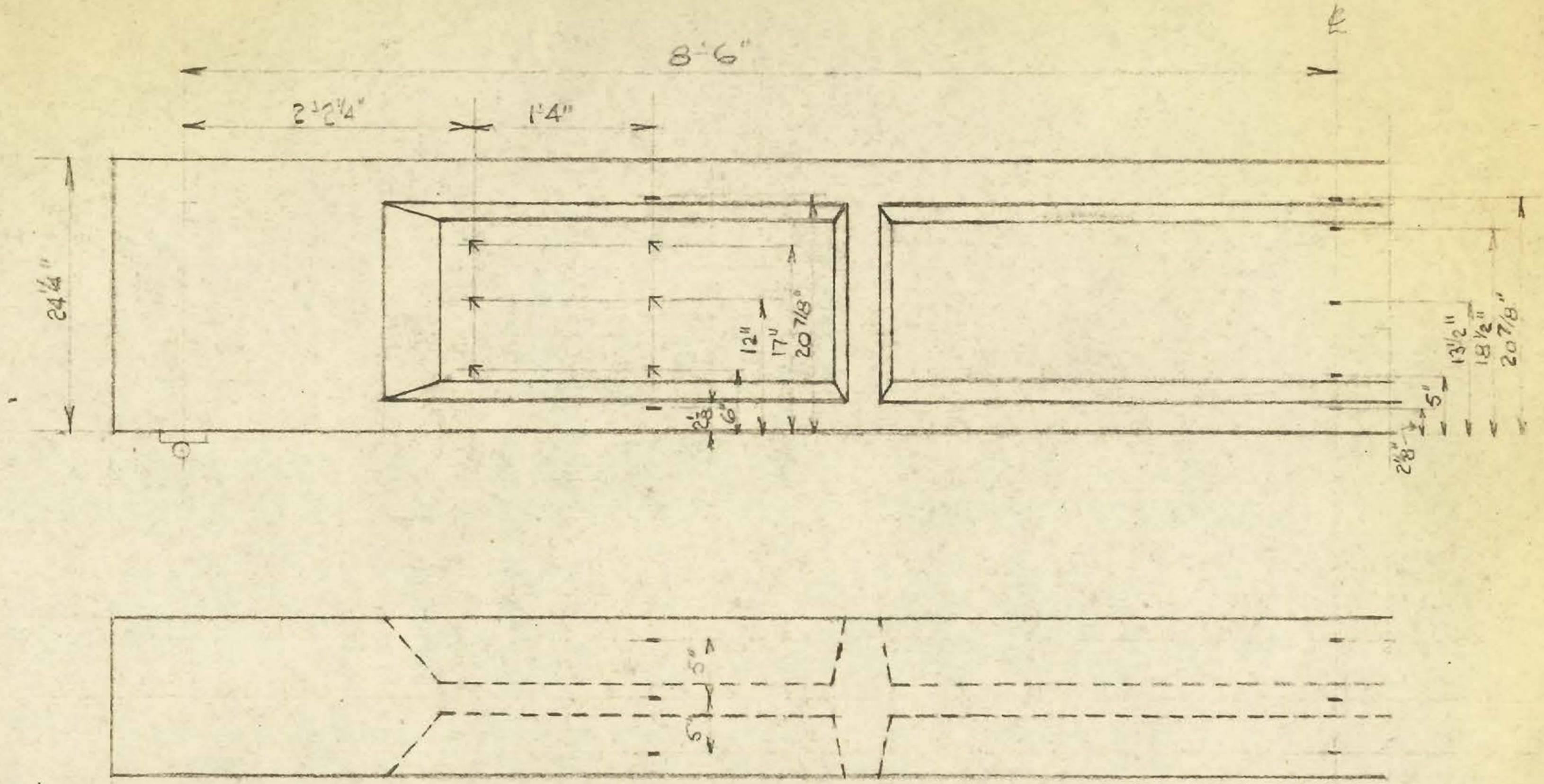

FIG I-2
LOCATION OF STRAIN GAGES ON TEST BEAM

SCALE $\frac{3}{4}$" = 1'-0'

↖ - ROSETTE

— - LINEAR GAGE

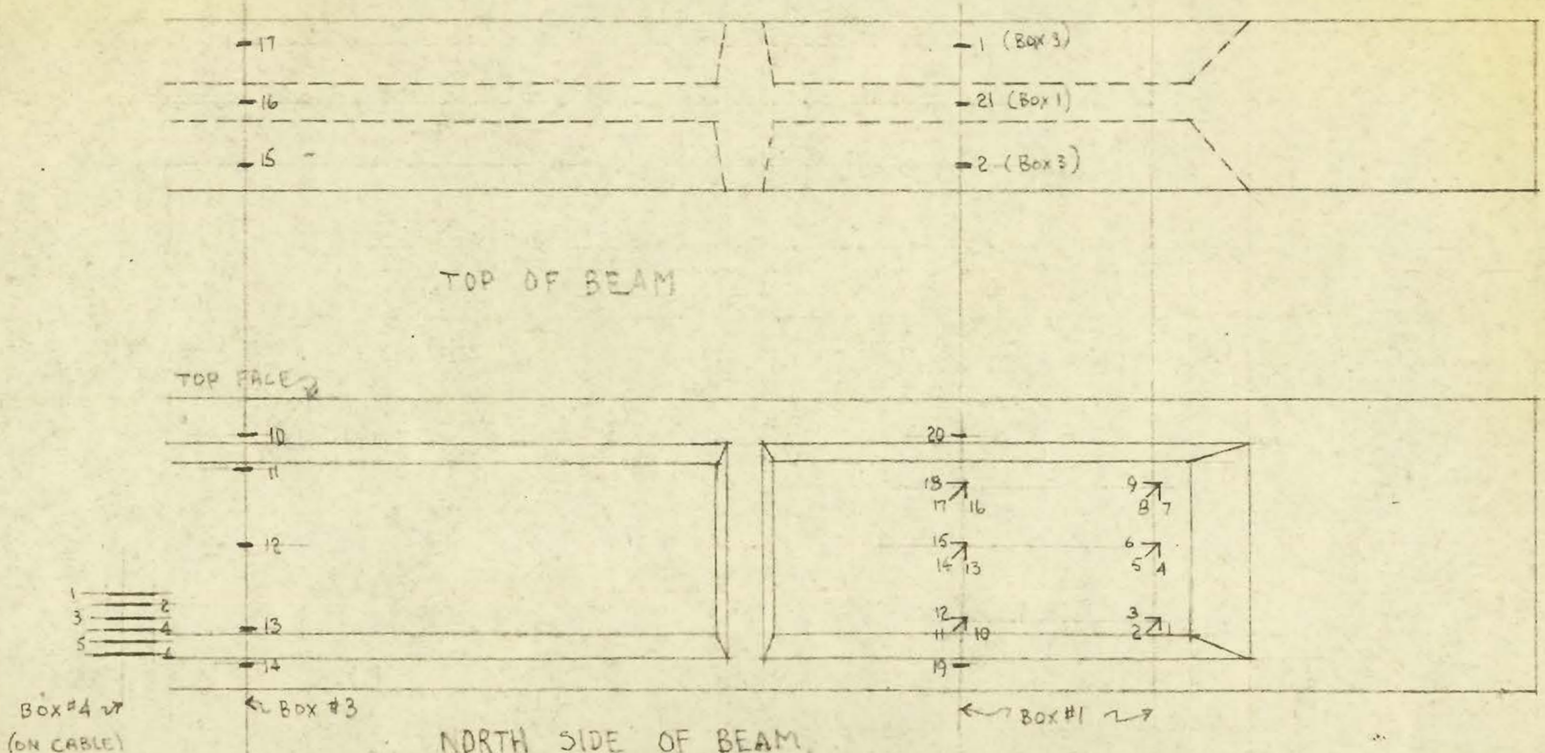

FIG I-3a
NUMBERING CODE FOR STRAIN GAGES

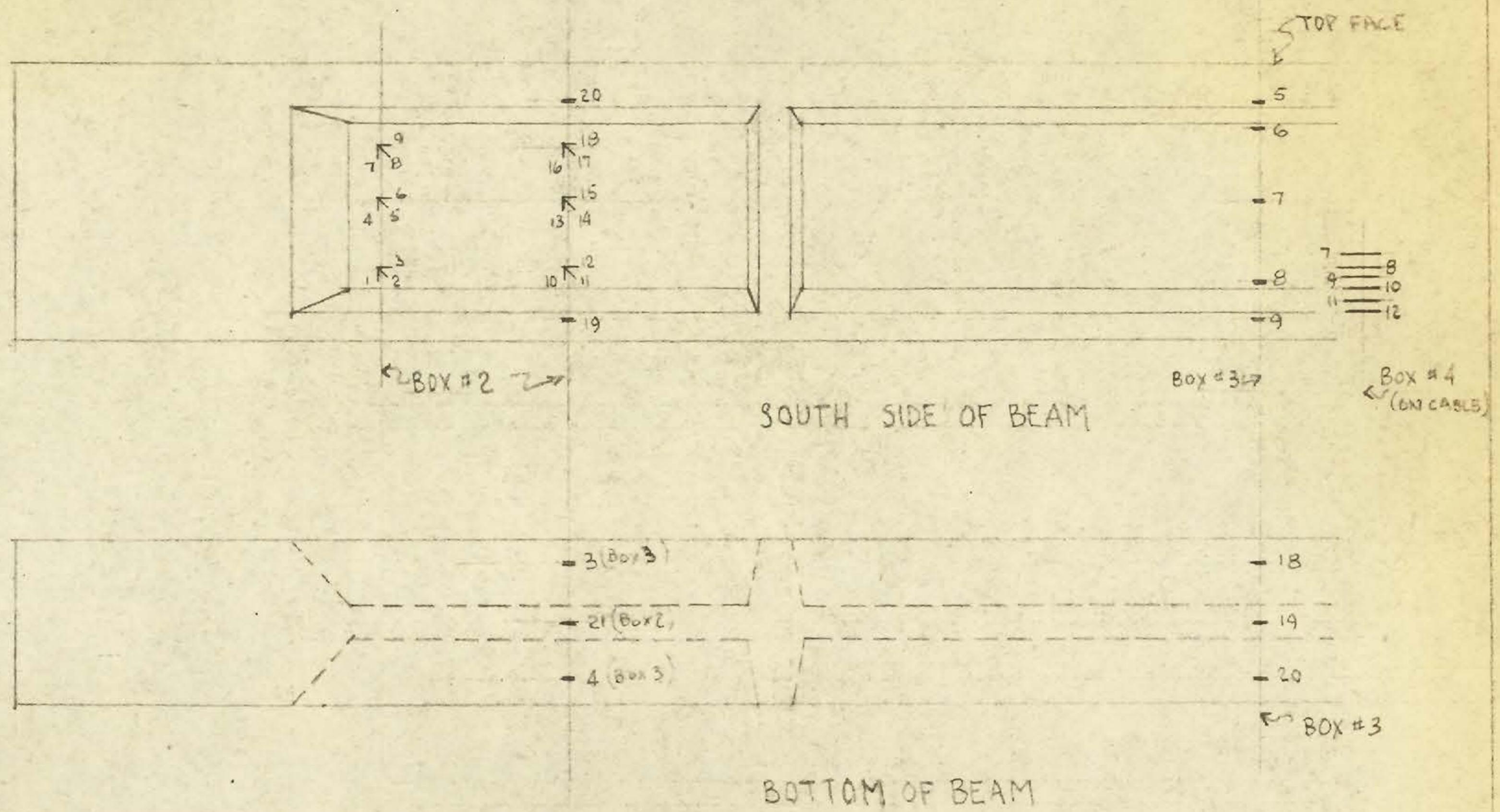

FIG I-3b,
NUMBERING CODE FOR STRAIN GAGES.

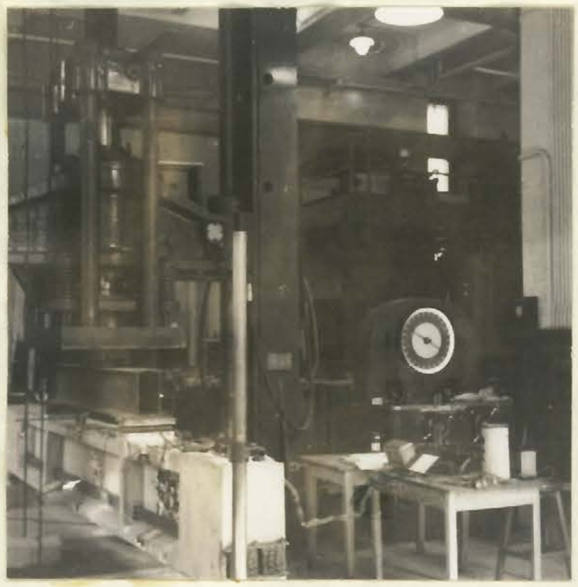

FIG. I-4

SETUP FOR BENDING TEST

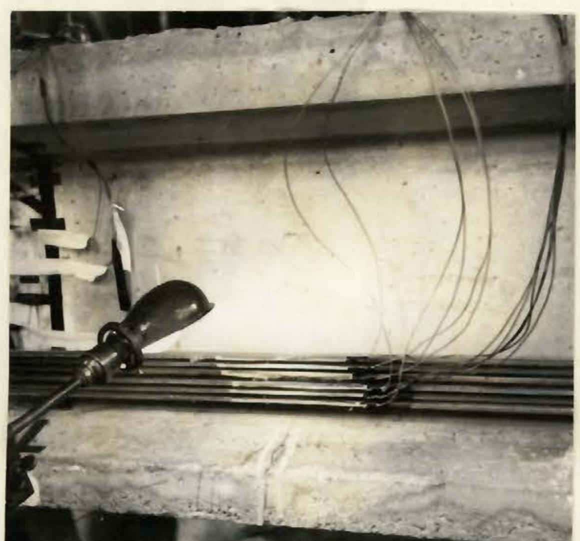

FIG. I-5

A-9 GAGES ON PRESTRESSING CABLE

THE DESIGN OF THE EXPERIMENTAL PRESTRESSED CONCRETE BEAM

The experimental beam was similar to that used in a previous series of experiments by G. A. Jakobson and R. H. Banks, which were carried out at McGill during the early part of the 1955-56 school year.

In the original design, the overall length was 18'0", with an unsupported length of 16'6"; however, in this experiment the unsupported length was increased to 17'0", which gave slightly higher moments at the centre of the beam. The depth of 2 feet and cross section was otherwise the section.

Specifications for prestressed concrete beam:

Span	18'0" overall, supported length 17'0"	
Depth	24"	
Web	$3\frac{1}{2}$" (this is a minimum thickness)	
Concrete Stresses	bending at time of initial prestress	.40f'c compression 0 tension
	bending under loading conditions	.30f'c - .35f'c compression 0 tension
	principal tension	.08f'c for reinforced sections .03f'c for non-reinforced sections
Steel Stresses	in prestressing steel the lesser value of .80 equivalent yield stress or .60 ultimate stress.	
	Note: the equivalent yield stress is that stress	

which, after an application of 10 seconds, produces a permanent set of 0.2% the total strain.

Loading 3700 p.l.f. live load, 180 p.l.f. dead load (assumed).

There are a number of graphical and semi-graphical methods for selecting a section for a prestressed concrete beam. Notable among these is the method suggested by G. Magnel in his book "Prestressed Concrete". This method bears a close resemblance to the methods used in limit design and in linear programming, and it would be of value to investigate this line of approach further. However, on the basis of the author's experience in prestressed concrete design, and in the opinion of many experienced designers, the fastest approach is to use cut and try methods, startingwhere possible with a number of previously designed sections whose properties are known and do not have to be recalculated.

A number of sections were designed and the final selected section was as shown in Fig. II-1.

During the pouring operations the bottom end of the forms spread slightly giving an average "as cast" cross section as shown in Fig. III-1.

The prestressing force was applied through 2 - 24 wire cables placed outside the web. This facilitated casting and made it easier to place strain gages on the prestressing wire. The eccentricity of the cables was 6.24 inches.

The initial prestressing force was calculated to be:

$$132{,}600 \times .0289 \times 48 \quad = \quad 184{,}000 \text{ lbs.}$$

The measured initial prestressing force was:

$$48 \times 5137 \times 10^{-6} \times 26 \times 10^{+6} \times .0289 = 185{,}100 \text{ lbs.}$$

a difference of less than 1%

Whence under initial prestress conditions the bending stresses are as follows:

Prestress

$$\frac{P}{A}\left(1 \pm \frac{ey}{r^2} \right)$$

$$\frac{185{,}100}{170.09}\left(1 - \frac{6.24 \times 11.84}{75.5} \right) = \quad 24 \text{ p.s.i. at top flange.}$$

and

$$\frac{185{,}100}{170.09}\left(1 + \frac{6.24 \times 12.41}{75.5} \right) = \quad 2210 \text{ p.s.i. at bottom flange.}$$

Dead load

$$C_d = \frac{M}{Z} = \quad \frac{wL^2}{8} \times \frac{1}{Z}$$

$$C_{dt} = \frac{170.09}{144} \times \frac{150}{1} \times \frac{17^2}{8} \times 12 \times \frac{1}{1085} = \quad 71 \text{ p.s.i. at top flange.}$$

$$C_{db} = \frac{170.09}{144} \times \frac{150}{1} \times \frac{17^2}{8} \times 12 \times \frac{1}{1034} = \quad -74 \text{ p.s.i. at bottom flange.}$$

Though the maximum compressive stress in the bottom flange is about 7% higher than 0.40f'c (or 2000 psi). This is not serious for the following reasons: this is the highest compressive stress that the bottom flange will ever be subjected to, loss of prestress and future loading will relieve this stress; construction experience has shown that an overstress of 10% in the bottom flange, at the time of prestressing, can be safely tolerated.

The secondary reinforcement consisted of 3/8-inch diameter deformed mild steel stirrups placed at 6 inches on centres in one end panel and 18 inches on centres in the rest of the beam, and four 3/8-inch deformed mild steel longitudinal bars placed two in the top and two in the bottom flange. The difference in stirrup spacing was to assess the value of the stirrups and the effect of different stirrup at overloads. The longitudinal bars serve to both tie the stirrups together and to take the "rigging" stresses when the beam was moved and turned prior to application of the prestress.

The end block reinforcement was designed according to the method of G. Magnel and these bars were tied together into a quite rigid cage. (See photo II-2.) In practise, the end block reinforcement is often spot welded together, which not only insures positive interaction between the bars, but facilitates handling and placing of the cage.

The distribution plate was made out of a single block of steel. This facilitated fabrication and to a lesser extent its casting into the beam. The bearing pressure under the distribution plate at time of prestressing was 2850 p.s.i.

Magnel recommends that 1.75 x C be used to proportion the size of distribution plate, which in this case would be 1.75 x 1700 = 3000 p.s.i.

The justification for these high bearing pressures permitted under the distribution plate follow from qualitative analysis and consideration of test results. In the end block, immediately under the sandwich plates there exists a highly stressed zone, which is surrounded by a relatively unstressed zone which serves to support this highly stressed zone. In tests on concrete cylinders and cubes, Magnel noted that when the loaded area, in a compression test was less than one third of the total end area of the test cylinder or cube, the crushing strength of the concrete rose to 18,000 p.s.i. from 5,000 p.s.i. In the literature there are no recorded failures of end blocks that have been designed according to the methods of either Magnel or Freyssinet.

ELONGATION OF CABLE

The elongation of the cable (or individual wire) is that extension of the cable (or individual wire) measured from the end face of the anchorage which will give the designed force (or stress) in the cable (or individual wire). This definition requires that the losses due to creep, shrinkage, and plastic flow are considered when computing the total force required in the cable.

Whence the factors to be considered when computing the extension of the cable are as follows: shortening of the concrete along the axis of the cable; slippage of the wires in the anchorage; lastly, elongation of the wire to produce the desired force.

These factors were computed and gave the following values:-

Shortening of the concrete	.086"
Slippage of wires	.125
Elongation of wires	1.148
Total extension	1.359"
Extension used on test beam	1-3/8"

LOSS OF PRESTRESS

After a beam is prestressed, the value of prestress gets smaller with time. The loss of prestress is due to shrinkage, creep of the concrete and steel, and plastic flow of the concrete. Though elaborate calculations may be made, involving parameters whose actual value may vary considerably from that assumed, in particular the value of Young's modulus, of the shrinkage coefficient and of the plastic flow coefficient for the concrete may differ considerably from that assumed; long-time studies carried out in Europe have shown that if a value of 15% for the losses is used, the structure will not fail due to loss of prestress.

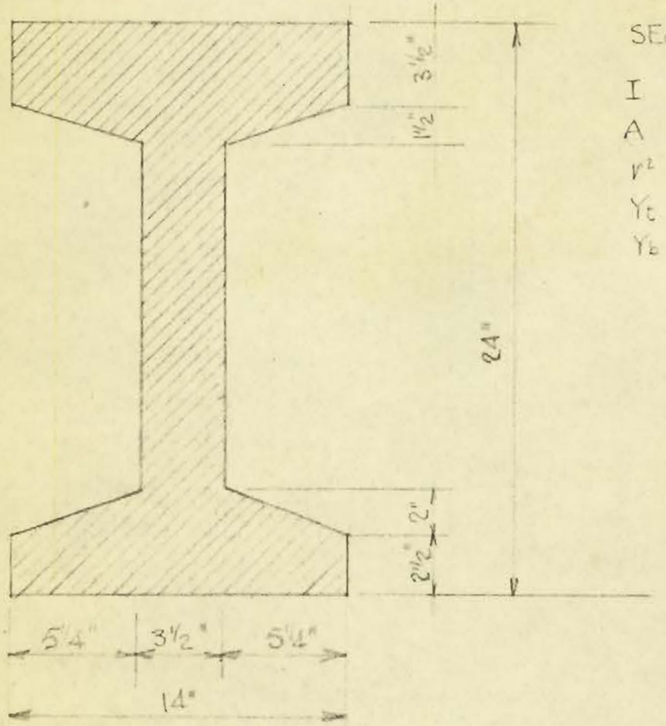

SECTION PROPERTIES

$I = 12{,}200$ IN^4
$A = 165.4$ IN^2
$r^2 = 73.6$ IN^2
$Y_t = 11.6$ IN
$Y_b = 12.4$ IN.

FIG. II-1

AS DESIGNED CROSS SECTION

FIG. II-2

ASSEMBLY OF END BLOCK REINFORCING

CHAPTER III

CONSTRUCTION OF THE CONCRETE FORM

Because of the somewhat complicated I - section, considerable time and energy was spent on the construction of the forms. The forms were made in 6 panels, 3 to each side and were built of both 3/4-inch plywood and 1-inch spruce stiffened by 1-inch spruce ribs bolted to 2 x 4 inch joists. In order to have a level platform and to facilitate stripping the forms and moving the beam, the forms were placed on a frame platform which was made of 4 x 8 inch timbers. The panels were nailed together to form a complete side of the form and could be easily opened for inspection and oiling prior to casting. The panels were held vertical by diagonal 1 x 4 inch spruce braces bolted to the joists and, in addition, just prior to casting the form was further tightened by suitably wrapping the two sides together with stove wire. Holes for the cables were cast into the beam by placing sheet metal inserts in the forms. The inserts were stiffened with wooden blocks and there was no difficulty in removing these wood blocks after the beam had set. The sheet metal inserts, of course, remained an integral part of the beam. Photographs and details of these forms are given in Fig. III-1, and Fig. III-2.

It should be noted that though great care was taken in the construction of the forms, and in oiling them before casting the beam, the forms could be stripped only with great difficulty and were not salvageable. If forms are to be used many times, particularly for the usual I - shapes used in prestressed concrete with their reentrant angles, it would be necessary to line the forms with this gauge sheet metal, and to provide gripping devices to assist in pulling the forms away from the concrete surfaces.

The concrete, provided by the Mount Royal Ready Mixed Concrete Co., arrived in good condition and was placed in about one hour. One of the laboratory windows was removed and the concrete was chuted into a 1/2-yard bucket suspended from an overhead crane. Concrete was also chuted into rubbertired barrows, then transported to the form and then the concrete was shoveled into the form. This latter procedure was necessary as the crane could not carry the bucket over the full strength of the form. During the pouring, the slump was three inches. The concrete was poured in four lifts of approximately 6 inches each. The concrete was vibrated with an internal vibrator for about 15-20 seconds after each life and thoroughly revibrated at the end of the last lift. After the forms were stripped, no honeycombing and no segregation due to placing or vibration could be detected.

During the placing of the concrete, ten standard test cylinders were cast - 6 in standard steel cylinder molds, 4 in fibre cylinders. These cylinders were filled in the manner outlined by the A.S.T.M. Also two small rectangular test beams 6'6" long were cast. These were for comparative deflection tests and to determine the modulus of elasticity of the concrete.

The Mount Royal Ready Mixed Concrete Co., also cast a number of small test beams and cylinders. These were for determining the tensile strength and the crushing strength of the concrete.

After the concrete had taken its set, the forms, test beams, and cylinders were covered with wetted burlap. The next day, the form on the prestressed beam was loosened slightly in order to permit water to enter. The concrete was then cured by keeping the burlap covering wet. This was done by wetting down the burlap every morning and evening with a water hose for a period of ten days, the forms were then stripped and the surfaces of the beam prepared for the attachment of the strain gages.

After the forms had been stripped, it was found that the bottom of the forms has pushed out slightly. To determine the as-constructed cross section of the beam, cross sections were taken at three foot intervals along the beam and the dimensions averaged. The as-constructed cross section is shown in Fig. III-1.

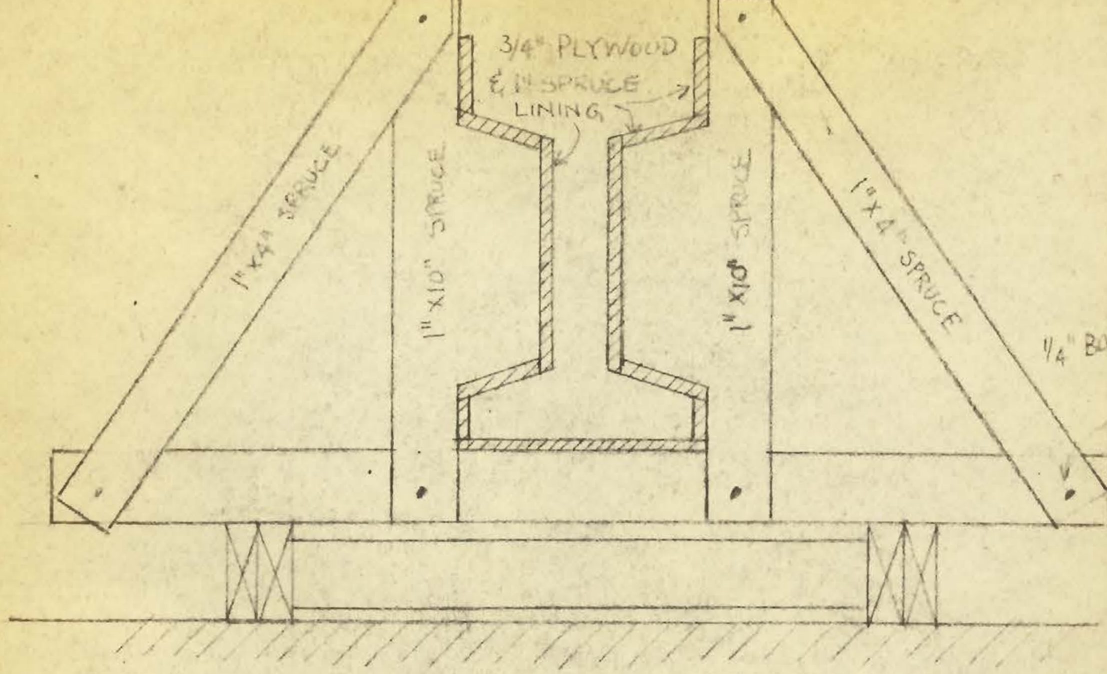

SECTION THROUGH FORM

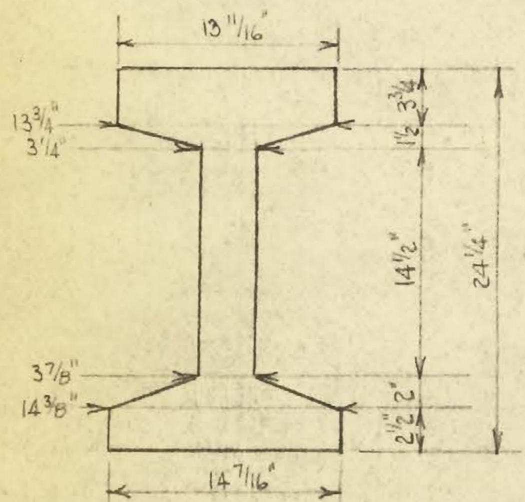

SECTION AS CAST

$A = 170.09\ IN^2$
$I = 12{,}850\ IN^4$
$r^2 = 75.5\ IN^2$
$Y_t = 11.84\ IN$
$Y_b = 12.41\ IN$
$Z_t = 1085\ IN^3$
$Z_b = 1034\ IN^3$
$e = 6.03\ IN$

FIG III-1

FIG. III-2a

FORMS OPENED FOR OILING

(note sheet metal ducts at stiffener)

FIG. III-2b

FORM ASSEMBLED JUST PRIOR TO POURING

CHAPTER IV

PROPERTIES OF THE MATERIALS

THE PROPERTIES OF THE STEEL

The prestressing steel used for the test beam was supplied by the Hesmont Concrete Company of Montreal, and was manufactured by the Steel Company of Canada.

The steel wire was delivered in a six foot diameter roll. This diameter of roll is too small, as the wire did not lay flat when unwound, which increased the difficulties of assembling and stressing the cables, and produces secondary stresses in the wire when it is tensioned.

As five tests on this roll of wire had previously been carried out by Mr. Ron Banks, only one test was carried out on a length of wire which was cut from the end of the roll that remained after the cables had been assembled. The results of this test were in agreement with the results obtained by Mr. Banks, thus obviating more extensive testing.

The test on the wire, as in the previous tests by Mr. Banks, were performed on the Tinius-Olsen wire testing machine in the test laboratory at McGill University. The arrangement of the tension test is shown in Fig. IV-1.

The loading rate was approximately 10,000 p.s.i. per minute. The strains were measured over a 40-inch gage length by means of a 1/1000th Ames dial gage, and over a 6-inch gage length by means of an SR4-A9 electric resistance gage located at the middle of the 40 inch gage length. In order to improve the agreement between the Ames dial gage and the SR4 electric strain gage, the wire under the electric gage was not polished, but was cleaned thoroughly with solvent. The results of this test are shown in Fig. IV-2. It is evident from the series of tests, the wire is of very uniform quality.

The Ames dial and electric gage results were in good agreement with each other. However, being a mechanical device, the Ames dial had to be tapped lightly as the needle exhibited some stickiness in its action, and too, the Ames dial had to be removed before failure of the wire to avoid being damaged. The only difficulty with the electric gage was affixing it to the wire. After some trials, it was determined that if the electric gage was adequately attached at its ends, the quality of the attachment along the middle part of the gage was relatively unimportant in this type of tension test. This discovery was of great importance because these relatively long gages were difficult to fix to the small diameter high tensile wire, exhibiting a tendency to wrap themselves around the wire while being cemented to it.

PROPERTIES OF THE CONCRETE

The concrete used in this experiment was required to have an ultimate crushing strength of 5,000 p.s.i. at 28 days. Because of the limited facilities available at the McGill Engineering Laboratories for mixing this volume of concrete, it was decided to obtain the concrete from a local concrete supplier.

The requirements, as sent to the Mount Royal Ready Mixed Concrete Co., were that the concrete was to have a 28-day strength of 5,000 p.s.i., a maximum size coarse aggregate of 3/8-inch trap rock (a crushed igneous stone), grading to conform to the A.S.T.M. specifications, and slump not to exceed 3 inches. The maximum size of 3/8-inch for the coarse aggregate was selected to facilitate placing and to avoid honeycombing. In order to prevent flocculation and to improve the dispersion of the cement throughout the mix, a dispersion agent consisting of 2-1/2 pounds of pozzolith per cubic yard was added to the mix.

The mix used was as follows:-

cement	800 lbs.
sand	1520
3/8" trap rock	1450
water	350
Total	4120 lbs. per cubic yard

The finess modulus of the sand was 2.58. The sand was obtained from glacial deposits near St. Gabriel de Brandon, Quebec. This is a clean quartz sand with no deleterious substances, and with a grading as shown in Fig. IV-3.

According to Blanks and Kennedy, in "The Technology of

Cement and Concrete", published by Wiley, pozzoliths have the effect of lowering both the value of the modulus of elasticity and Poisson's ratio, increasing the tensile strength and delaying the development of compressive strength.

However, on examination of the test values for the mix used in the test beam, no significant deviation from the values for these factors occurred, as compared to those obtained from the mix used in the Banks - Jakobson beam, except that in this beam the compressive strength was slightly lower at the time of the test. The mix used in the Banks - Jakobson beam was similar to that used in this experiment except that no pozzolith was used.

Test cylinders broken at the end of 7 days showed an average strength of 4,000 p.s.i., and at the end of 28 days, an average strength of 5,200 p.s.i. After 28 days, no cylinders broke at under 5,500 p.s.i., so that a reserve compressive strength of not less than 10% over design was realized.

MODULUS OF ELASTICITY AND POISSON'S RATIO

The modulus of elasticity for the concrete was determined by tests on concrete cylinders, deflection test on a small unreinforced concrete beam, deflections of the prestressed concrete test beam, and by balancing the forces across a cross section where strain gages had been placed. For details of this last method, see Appendix 2.

The standard method of evaluating Poisson's ratio for metals using the relationship $G = \frac{E}{2\ (1+\mu)}$ was unsuitable because of the difficulty of arranging satisfactory torsion tests on concrete. Instead, Poisson's ratio was determined by comparing the longitudinal strains with the lateral strains during a compression test on a concrete cylinder. Eight linear SR4 gages were placed equidistant, at mid-height, around a standard 6 x 12 concrete cylinder. The gages were placed alternately, vertically and horizontally. The curves of load versus vertical strain, and load versus horizontal strain are shown in Fig. IV-4 and Fig. IV-5 respectively. The ratio of the initial tangent slopes of the two curves gave a value of Poisson's ratio of 0.16, which compares with the usual range of values of from 0.10 to 0.25 for concrete. Because of the restraint at the ends of the cylinder, and the fact that the cylinder tends to assume a barrel shape under a compressive loading, the value of Poisson's ratio will vary somewhat along the height of the cylinder. However, since the gages were applied at mid-height - where the effects of the end restraint would be at a minimum - and because the gages were uniformly spaced around the circumference and the strains in the longitudinal and lateral directions averaged, it is believed that this method is satisfactory.

The instantaneous modulus of elasticity of the concrete, as determined by the different methods, gave a fairly narrow range of values with the exception of the value determined by the test on the plain concrete beam. This method gave a value of 3.6×10^6 p.s.i. and 3.4×10^6 p.s.i., for the tangent and secant moduli respectively. This value was somewhat lower than that given by the other methods which ranged from about 4.0 to 4.7×10^6 p.s.i. for the tangent modulus. The load deflection curve for this test is shown in Fig. IV-6.

The stress-strain diagram for the compression tests on the concrete cylinders was automatically drawn by a Peter's Recording Compressometer attached to the Baldwin testing machine (see Fig. IV-11). This device records the average strain on two diametrically opposite 6-inch gage lengths. The device is so designed that on a standard 6 x 12 concrete cylinder the gage lengths are centered about the mid-height of the cylinder. Three of the stress-strain diagrams for different loading cycles are shown in Fig. IV-8, -9, and -10.

From the compression tests on the concrete cylinders the initial tangent modulus ranged from 3.9 to 4.3×10^6 p.s.i. with an average value of 4.2×10^6 p.s.i.

The initial tangent modulus from the deflection test on the plain concrete beam, as determined from the center line deflection under third-point loading, was 3.56×10^6 p.s.i. Under this loading condition, the deflection due to shear was 3.4% of the total deflection, so that the modulus of elasticity for bending alone would be 3.6×10^6 p.s.i. However, it should be noted that, when analysing a beam structure, we are usually interested in that value for E that will enable prediction of deflections rather than the value due to bending alone. For details of the method of computing shear and bending deflections, see Appendix 3.

This beam was 6 inches wide by 8 inches deep by 6 feet 6 inches long. It was tested under third point loading on a 6 foot span. The deflection was measured by two Ames dials, located on opposite sides of the beam at the center line, and the average of these two readings was taken as the center line deflection. The test setup is shown in Fig. IV-12, and the load deflection curve is shown in Fig. IV-6. The beam failed at an ultimate load of 2200 pounds, breaking into three equal pieces. The ultimate tensile stress at failure was 412 p.s.i. This compares with value of 415 p.s.i. on a similar test by Mr. R. Banks.

The modulus of elasticity of the concrete from the tests on the prestressed concrete beam was determined in two ways: the first method was by balancing forces across a section at the linear gages at the center of the beam, this method is outlined in Appendix 2; the second method was by noting the slope of the load deflection curve. In this latter method, the deflection due to shear was equal to 9.6% of the deflection due to bending alone. For details of the method of calculating the deflection due to shear, see Appendix 3. The load - deflection curve is shown in Fig. IV-7. The results of the first method are shown in Table IV-1, and for the second method in

Table IV-2.

In the second method, if the prestressing force is constant, it has no effect on the deflection since its function is merely to change the allowable stresses in the concrete. If, as in this case, there is an increase in prestressing force under load, the deflections will be reduced by an amount proportional to the increase in this force. The maximum increase in prestressing force at the cracking load was 2.5 percent. This percentage increase in steel stress at a load of 80,000 pounds would be equivalent to a constant moment along the beam of

$$\frac{2.5}{100} \times 185{,}000 \times 6.38 = 86{,}000 \text{ in lbs.}$$

The corresponding decrease in deflection would be

$$\frac{1}{8} \times \frac{86{,}000 \times \overline{17.0 \times}^{\,2}\ 144}{4.0 \times 10^6 \times 12850} = .008 \text{ inches}$$

Since the total deflection of the beam due to a load of 80,000 lbs. was .250 inches, the effect of this increase in prestressing force is small and may be neglected.

The test setup for the test on the prestressed concrete beam is shown in Fig. IV-13a, b, and c.

TABLE IV-1

MODULUS OF CONCRETE BY THE METHOD OF BALANCING FORCES ACROSS THE MIDSECTION

flexural load kips	shear load kips	calculated E p.s.i.
20		4.43×10^6
30		4.42×10^6
40		4.18×10^6
50		4.18×10^6
60		3.95×10^6
70		3.91×10^6
	20	4.41×10^6
	40	4.32×10^6
	60	4.10×10^6
	mean	4.2×10^6

TABLE IV-2

MODULUS OF CONCRETE

METHOD	E p.s.i.
Deflection of concrete beam	3.6×10^6
Deflection of prestressed beam	4.6×10^6
Test cylinders	4.3×10^6
	4.3×10^6
	3.9×10^6

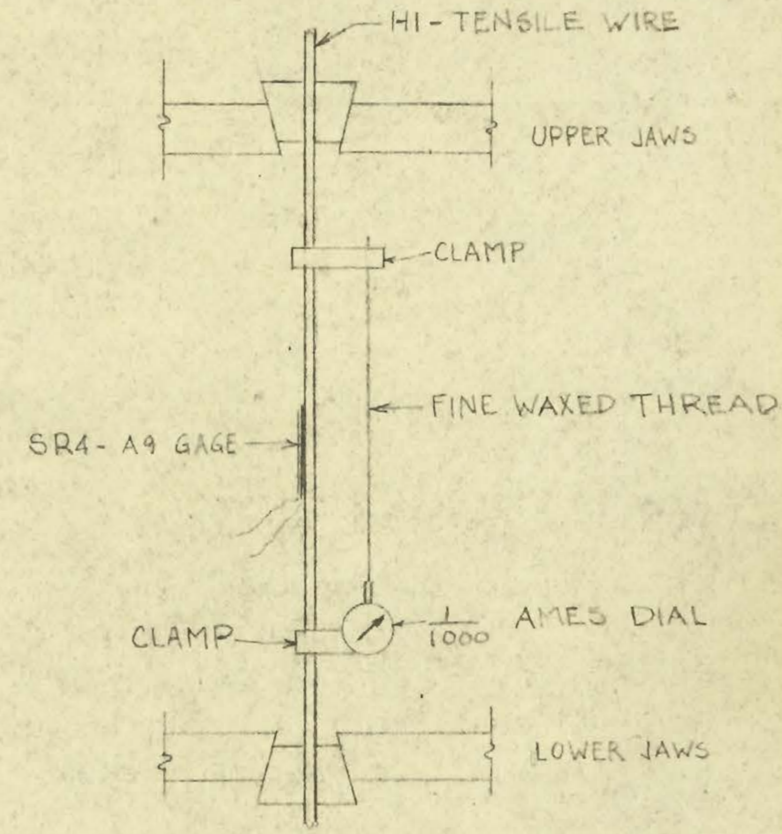

FIG IV - 1

ARRANGEMENT OF WIRE TEST IN TINIUS - OLSON WIRE TESTING MACHINE

TENSION TEST ON HI-TENSILE WIRE

DIAMETER — ·192 INCH
GAGE LENGTH — 40 INCHES
INITIAL LOAD — 1000 LBS.

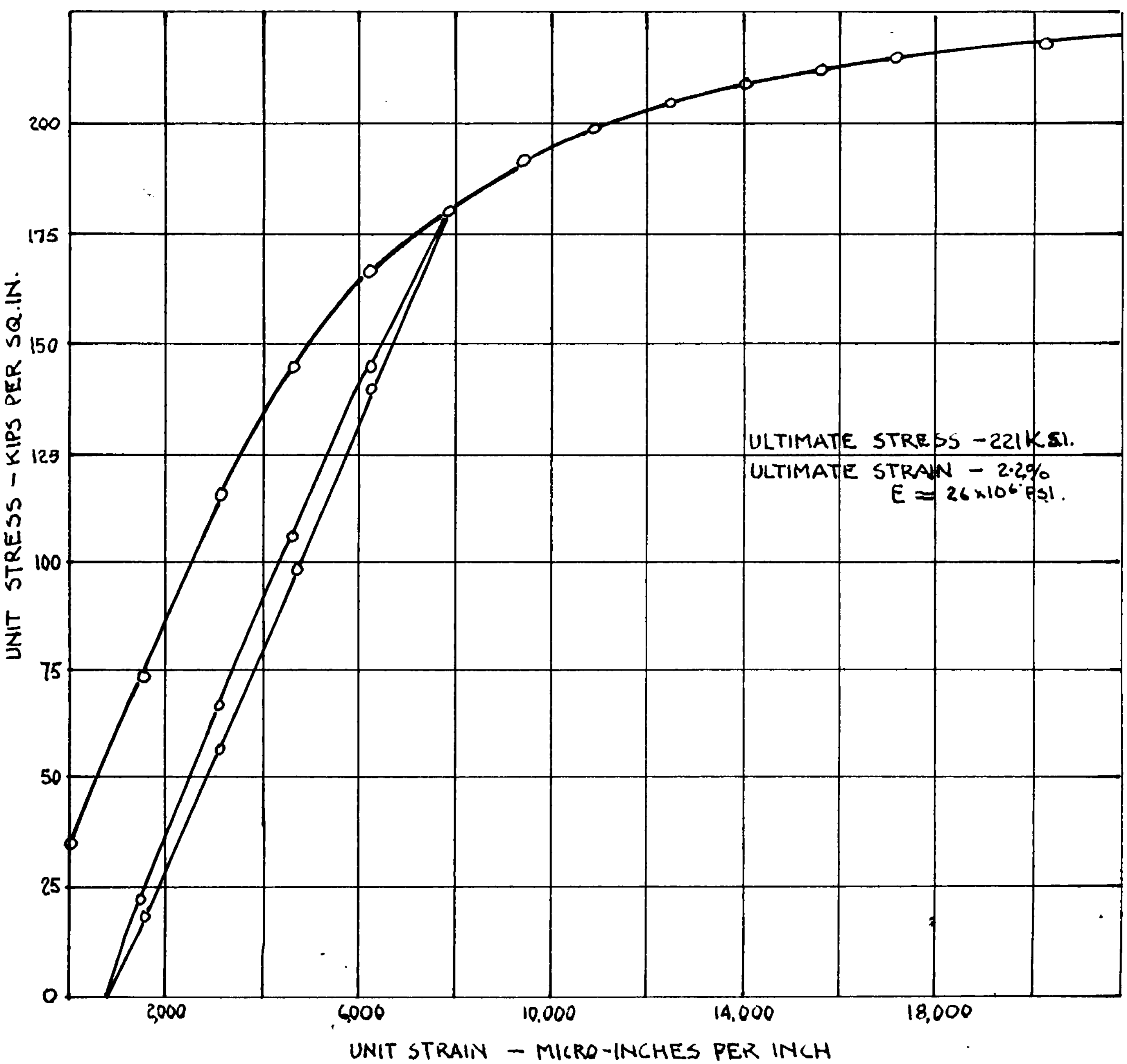

FIG IV -2

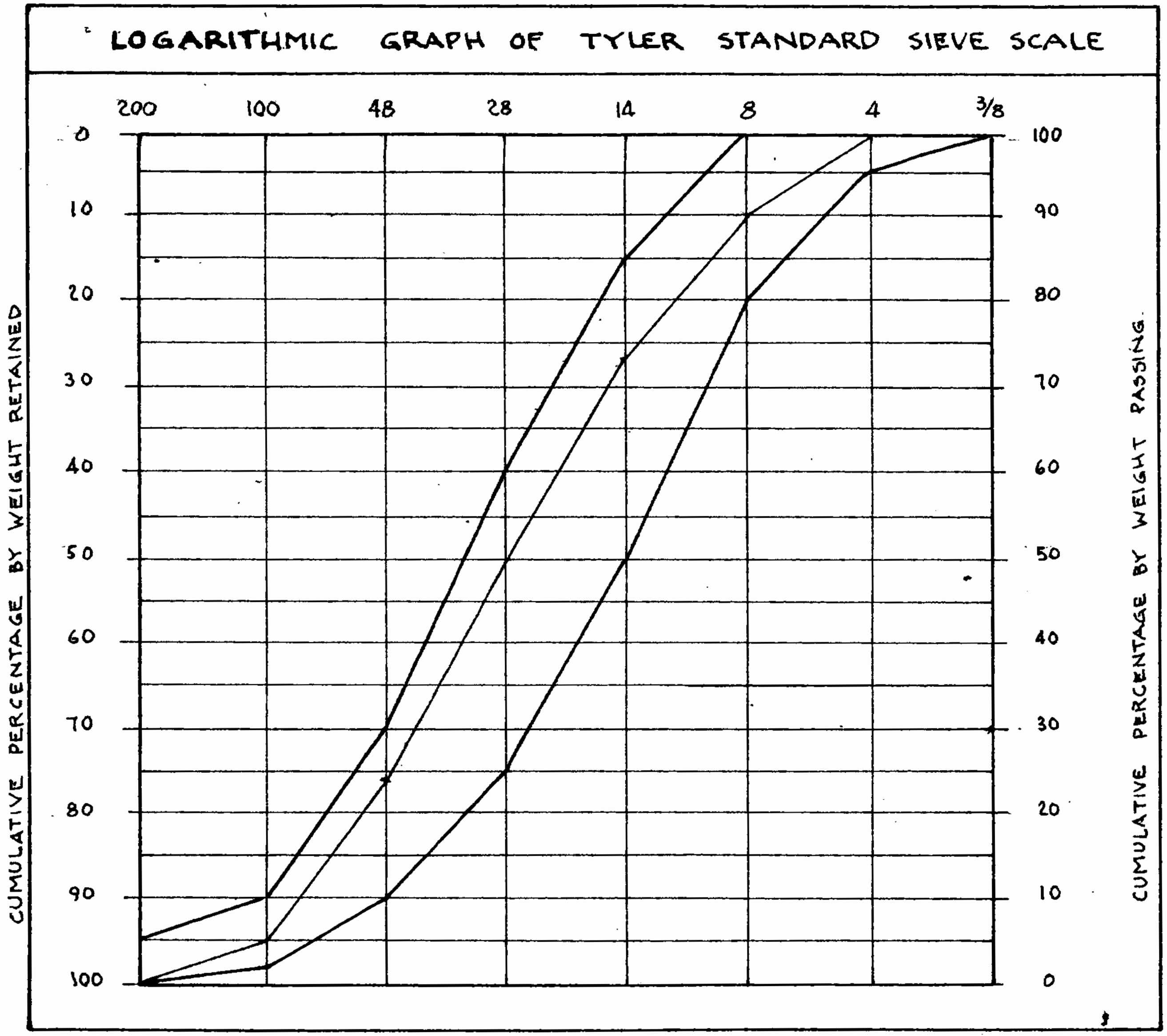

RESULTS OF SCREENING	
No OF SAMPLE	
No. OF SIEVE	CUMULAT. % BY WT. RETAINED
3/8	5.8
4	16.5
8	9.6
14	26.6
28	50.0
48	76.8
100	95.0
200	99.2
PAN	100.0
F. M.	2.58

NOTE;
GRADING LIMITS
ASTM C33-52T

SIEVE ANALYSIS OF FINE AGGREGATE

FIG. IV - 3

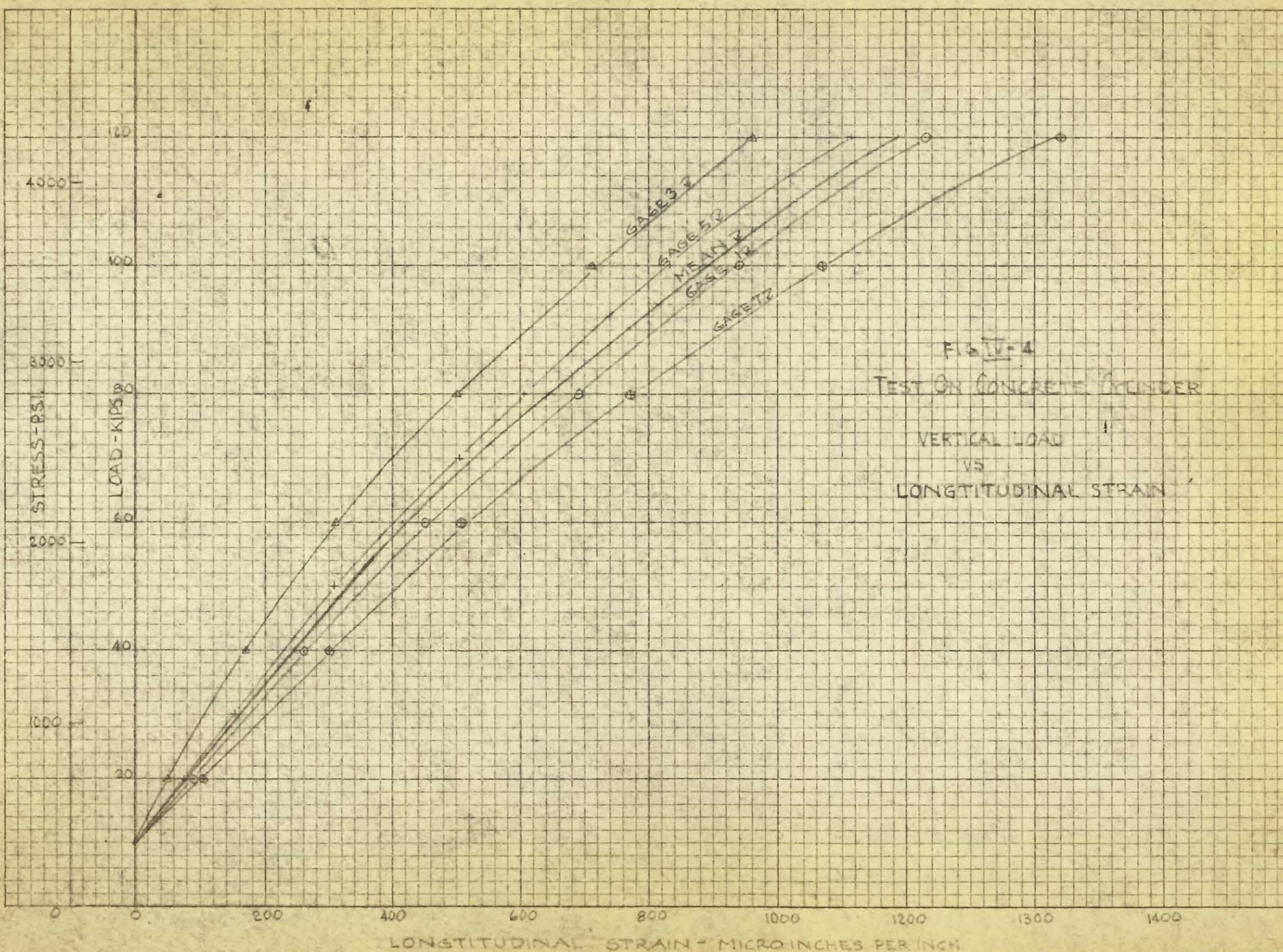

FIG IV-4
TEST ON CONCRETE CYLINDER
VERTICAL LOAD
VS
LONGTITUDINAL STRAIN

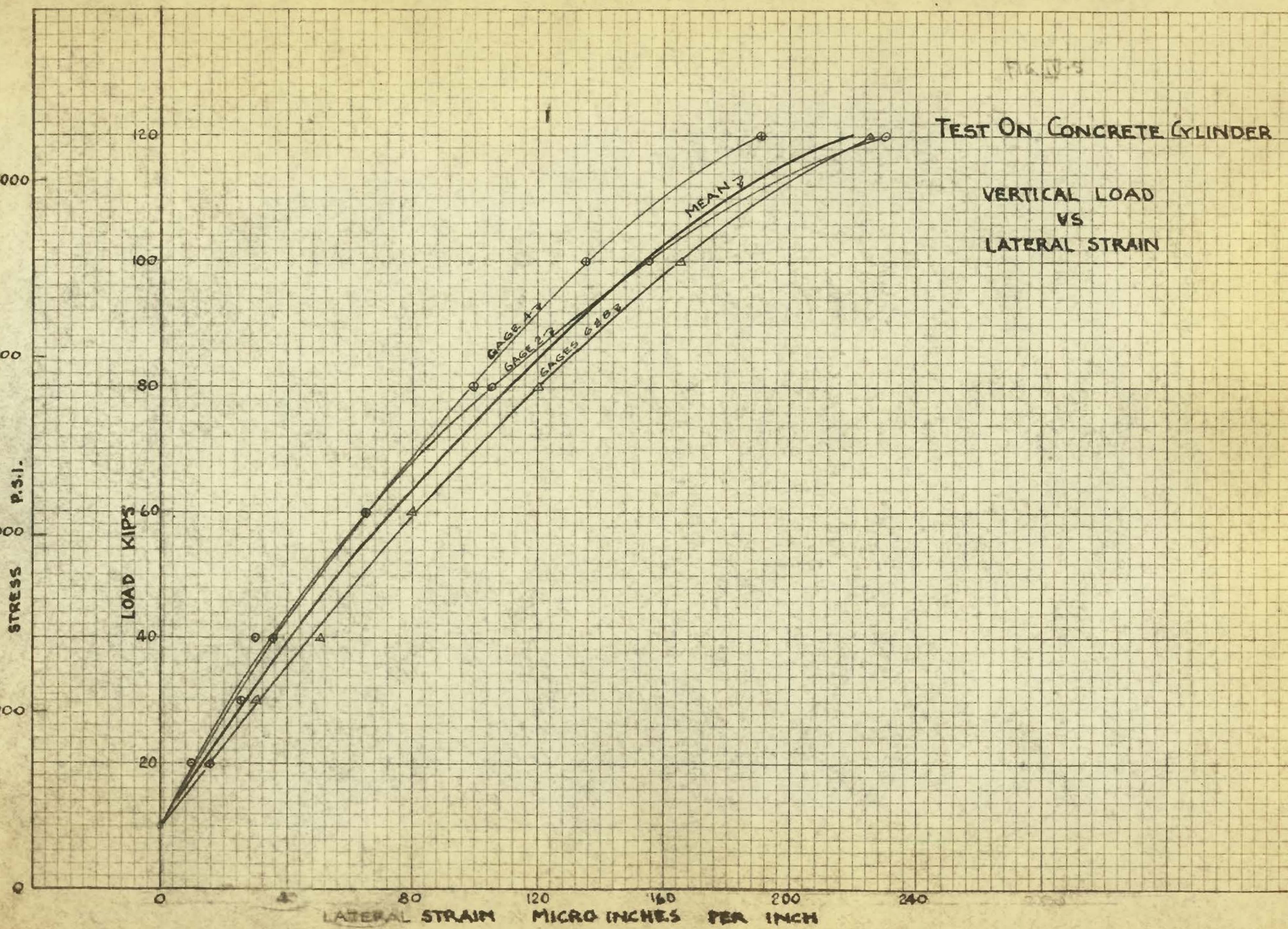
TEST ON CONCRETE CYLINDER
VERTICAL LOAD
VS
LATERAL STRAIN
MEAN
LOAD KIPS
STRESS P.S.I.
LATERAL STRAIN MICRO INCHES PER INCH
0
40
80
120
160
200
240
20
60
100
1000
2000
3000
4000

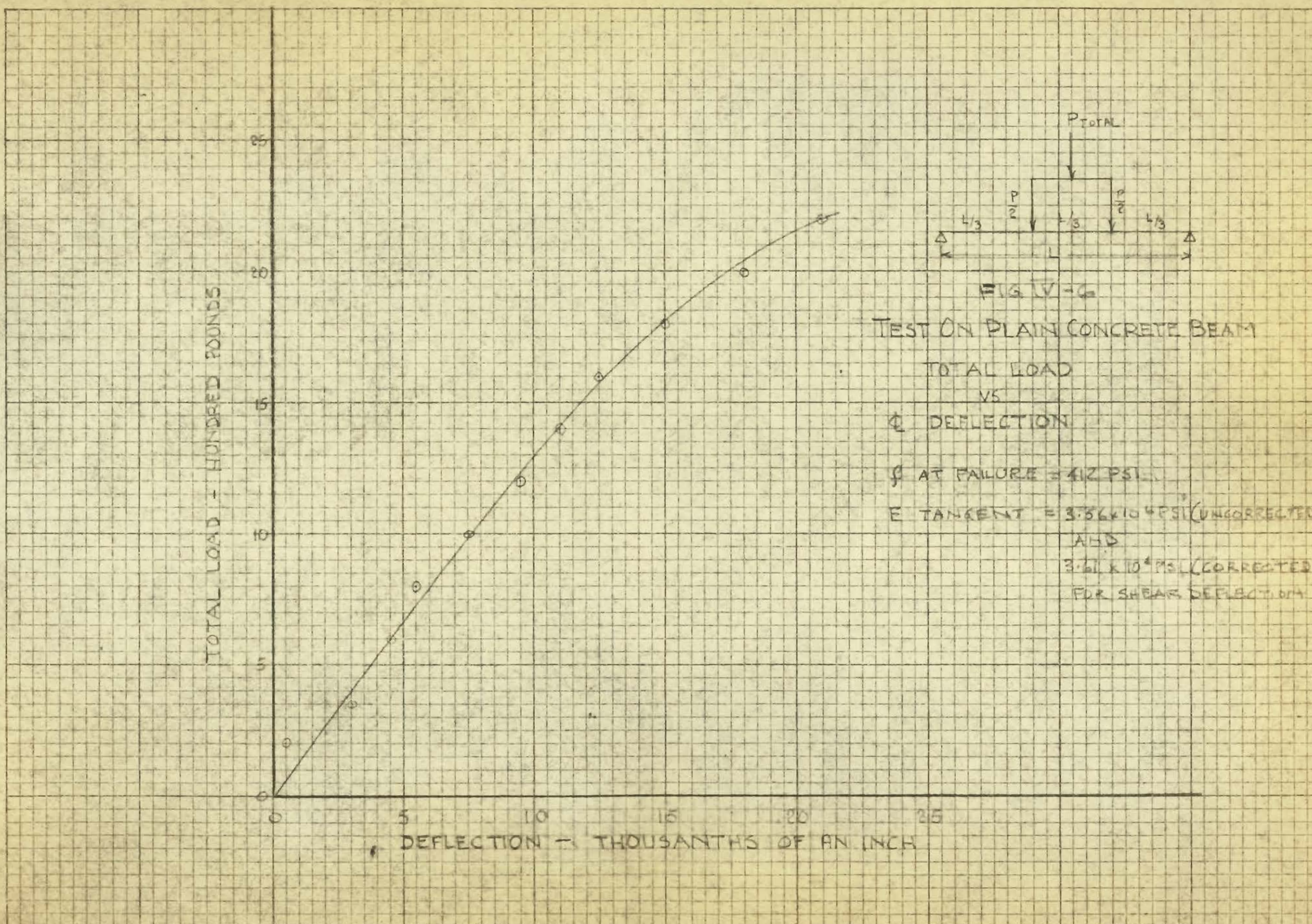
P TOTAL
P/2
P/2
L/3
L/3
L/3
L
FIG IV-6
TEST ON PLAIN CONCRETE BEAM
TOTAL LOAD
VS
℄ DEFLECTION
f AT FAILURE = 412 PSI.
E TANGENT = 3.56 x 10^6 PSI (UNCORRECTED)
AND
3.61 x 10^6 PSI (CORRECTED
FOR SHEAR DEFLECTION
TOTAL LOAD - HUNDRED POUNDS
0
5
10
15
20
25
DEFLECTION - THOUSANTHS OF AN INCH

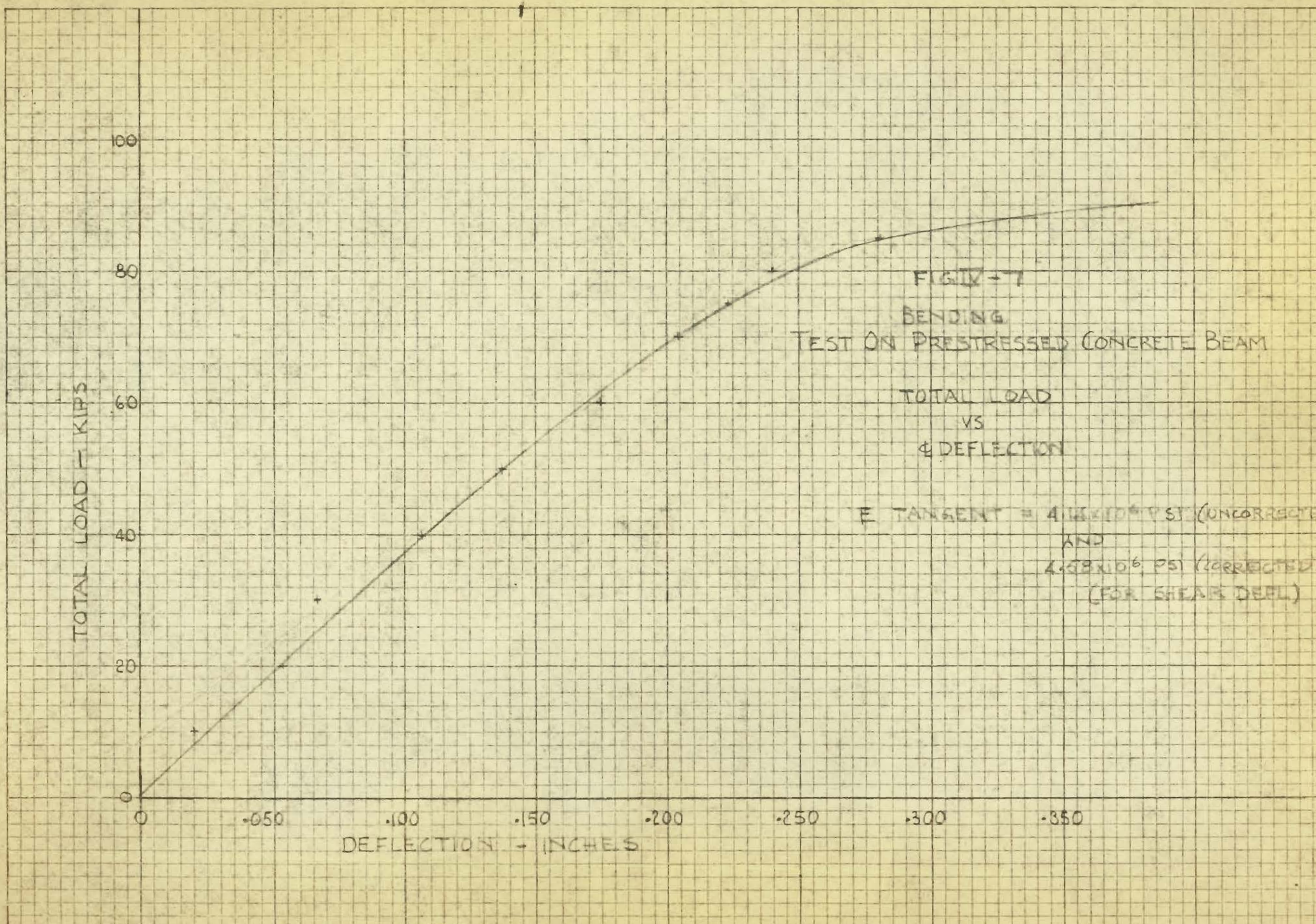
FIG IV - 7
BENDING
TEST ON PRESTRESSED CONCRETE BEAM
TOTAL LOAD
VS
℄ DEFLECTION
E TANGENT = 4.14 x 10^6 PSI (UNCORRECTED)
AND
4.58 x 10^6 PSI (CORRECTED
(FOR SHEAR DEFL)
TOTAL LOAD — KIPS
0
20
40
60
80
100
0
.050
.100
.150
.200
.250
.300
.350
DEFLECTION - INCHES

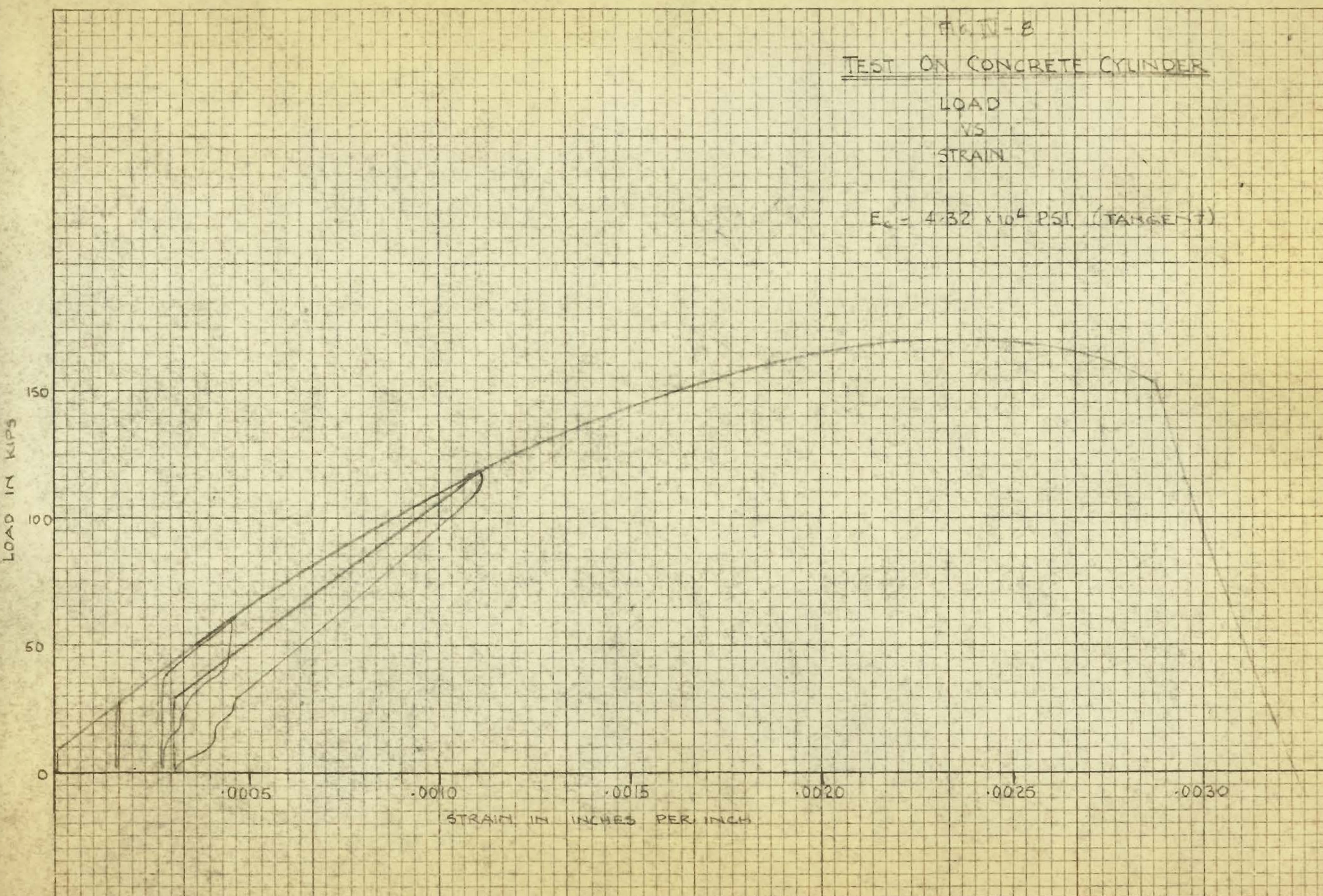
FIG. IV-8
TEST ON CONCRETE CYLINDER
LOAD
VS
STRAIN
$E_c = 4.32 \times 10^4$ PSI. (TANGENT)
LOAD IN KIPS
0
50
100
150
·0005
·0010
·0015
·0020
·0025
·0030
STRAIN IN INCHES PER INCH

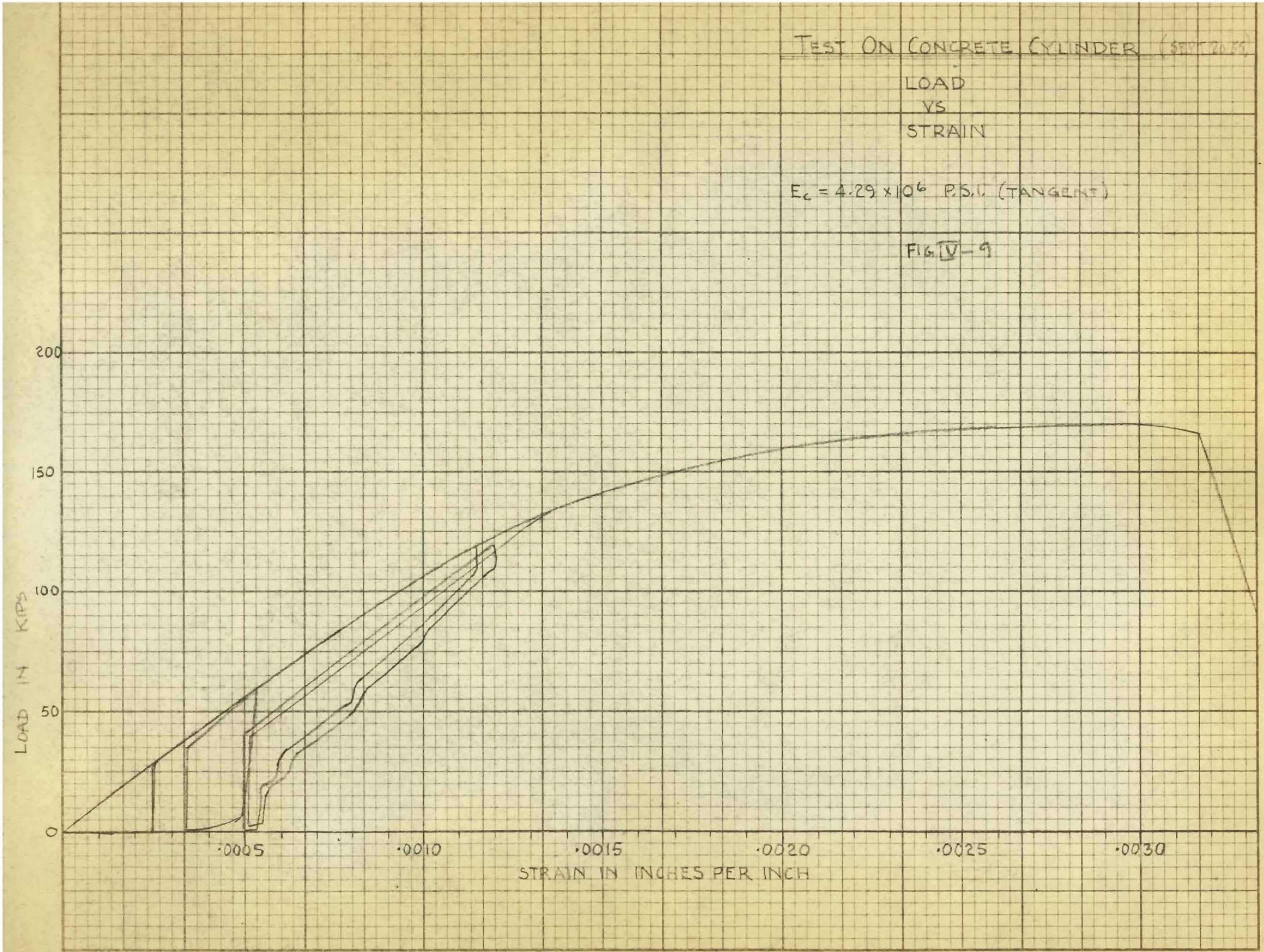
TEST ON CONCRETE CYLINDER
LOAD
VS
STRAIN
$E_c = 4.29 \times 10^6$ P.S.I. (TANGENT)
FIG. IV-9
LOAD IN KIPS
0
50
100
150
200
·0005
·0010
·0015
·0020
·0025
·0030
STRAIN IN INCHES PER INCH

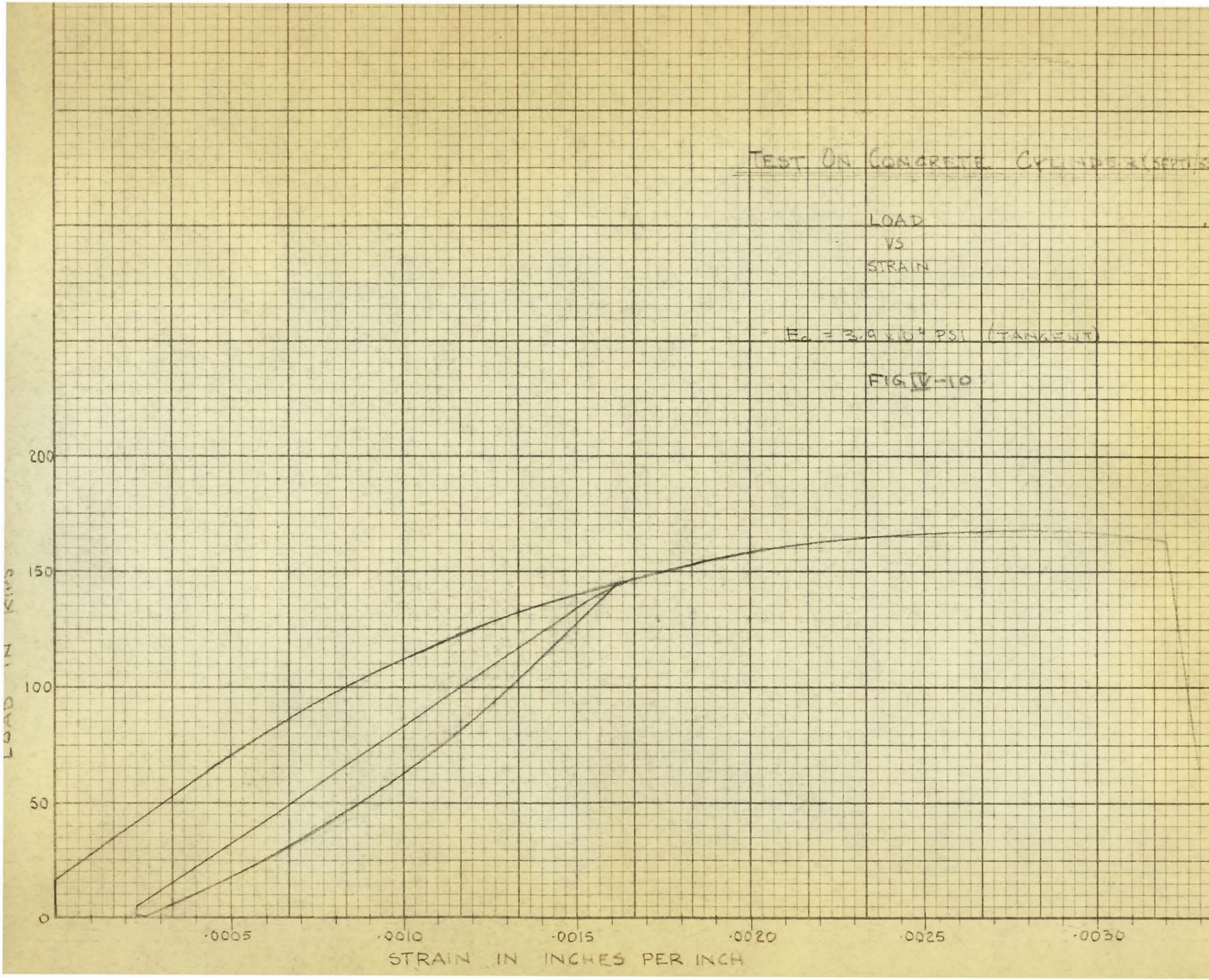
TEST ON CONCRETE CYLINDER (SEPT/55)
LOAD
VS
STRAIN
$E_c = 3.9 \times 10^4$ PSI (TANGENT)
LOAD IN KIPS
0
50
100
150
200
.0005
.0010
.0015
.0020
.0025
.0030
STRAIN IN INCHES PER INCH

FIG IV-10

FIG. IV-11

PETERS COMPRESSOMETER ATTACHED TO TEST CYLINDER

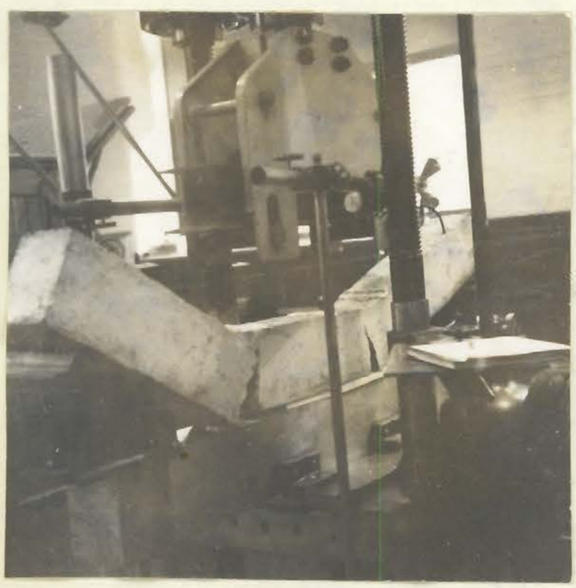

FIG. IV-12a

FAILURE OF PLAIN CONCRETE BEAM

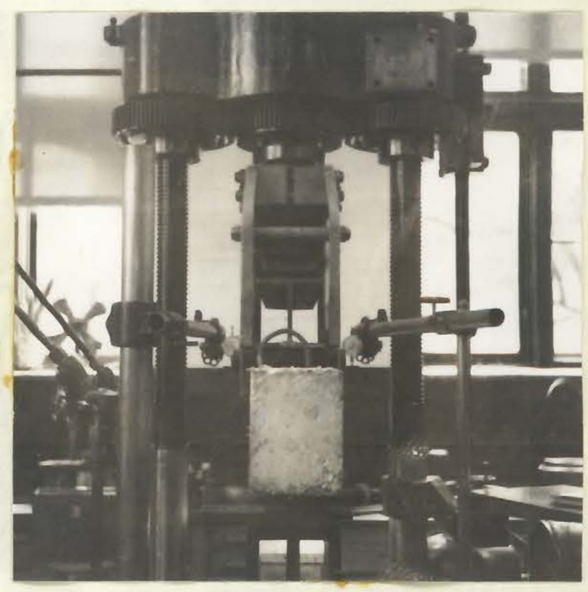

FIG. IV-12b

SETUP FOR TEST ON PLAIN CONCRETE BEAM

FIG. IV-13

TEST SETUP FOR THE EXPERIMENTAL BEAMS

CHAPTER V

DESCRIPTION OF THE ELECTRIC STRAIN GAGE

The SR-4 bonded wire electric strain gage was developed by Simmons and Ruge in the United States during the 1930's. These gages are characterized by their lightness, relative ease of application, and sensitivity.

The SR-4 strain gage consists of a length of 1 mil wire cemented between two pieces of thin paper. The paper serves as a carrier for the wire, for ease in handling, and to insulate the wire from the surface on which it is to be bonded. On some strain gages, a protective layer of felt is used to cover the top side of the gage.

It is apparent from the sketch in Fig. V-1 that some of the wire is at right angles to the axis of the gage. Thus, the change of electrical resistance of the gage is affected both by the lingitudinal strains, but also by the transverse strains perpendicular to the axis of the gage. This effect is small and may be taken into account by considering the auxiliary factor of transverse sensitivity. However, for the rosette and linear gages used in this experiment, this effect is of the order of 1% and 2% respectively and was ignored.

Rosettes are an assembly of three or more SR-4 gages with various angular inclination. This type of assembly is used to measure the strains at a point but in different directions. From these simultaneous strains, the principal strains (and stresses) and their inclinations from a given axis can be computed.

The basic principle of this gage is that the resistance of the wire varies with the tensions (or compression) to which it is subjected to. However, it must be pointed out that the change of resistance is not due solely to the dimensional changes accompanying the longtitudinal strain of the wire. In using electric resistance gages the two physical quantities that are of particular interest are the unit change in gage resistance and the unit change in length. The dimensionless relationship between these two variables is called the gage factor of the strain gage and is expressed mathematically as:

$$F = \frac{\Delta R}{R} \div \frac{\Delta L}{L}$$

on this relationship R and L respectively the initial resistance and length of the strain gage; while ΔR and ΔL are the change of resistance and length that occur as the gage is strained along with the surface to which it is bonded. The gage factor is thus an index of the strain sensitivity of the gage. The higher the gage factor, the more sensitive the gage and the greater the electrical output for indicating or recording purposes.

Special problems are encountered when attaching the strain gages to concrete. These problems are due mainly to the lack of homogeneity of the concrete, and the shrinkage of the concrete, and the hygrostatic changes of the concrete. Most of these difficulties are overcome by having a compensating gage suitably incorporated in the strains gage indicator circuit.

The strain gages were attached to the concrete in the following manner. The surface of the concrete was sanded smooth; then if any voids larger than pinholes were present they were filled with plaster of Paris and the surface was again smoothed down. The area under the gage was cleaned with acetone, then two coats of Baldwin Pre-coat were applied to the concrete and each allowed to set. Then one coat of Duco cement was applied and allowed to become tacky, and then the gage was pressed into place using a foam rubber pressure pad until an initial set had occurred. A two pound weight was then applied to the gage through the foam rubber pad, which was separated from the gage by a piece of wax paper. After 24 hours, the gage was considered secure but no load was applied for several days. No unusual difficulty was noted when applying the linear A-3 and the rosette A-14 gages, but it was found that the gages were easier to apply and formed a better bond if cement was applied to the back of the gage before affixing it to the structure. The slightly different method of applying the longer A-9 gages to the prestressing wire is discussed in Chapter IV.

The compensating gages for the A-3 and A-14 gages circuits were constructed by affixing an A-13 and an A-14 gage to a test cylinder from the same mix, and keeping this cylinder near the beam during the experiment. The compensating gage for the A-9 circuits was applied to a rectangular piece of high quality steel. It was not applied to a piece of hi-tensile wire because these wires had a slight initial curvative and because the round cross-section of the wire would have exposed the compensating gage to unnecessary risk of damage.

After the gages were applied to the beam and wired up to the junction boxes, they were covered with beeswax in order to protect them from humidity in the air and chance short circuits. However, during the placing of the prestressing cables and rigging of the beams, two rosettes were damaged. These could not be replaced because of the narrow clearance between the cable and the beam. However, the readings on the operating gage on the opposite side of the beam gave consistent values which have been incorporated in the tables of observation.

The accuracy of the gages and the suitability of the method of applying them was proven in two ways:

For the concrete, they were attached to a test cylinder in various ways and then loaded in the testing machine. The strains as measured by the electric gages and by the mechanical gages were compared, and it was seen that both results were in agreement. For the steel, the gage was attached to the wire and a mechanical gage was made up using an Ames dial, the piece of wire was then placed in a testing machine and the strains as measured by the mechanical and electric gages were compared and again found to be in agreement.

After a series of these tests, it was concluded that the strain gage can be attached in almost any manner, providing the bonding medium enforces the gage to follow the strains occurring on the surface to which it is attached.

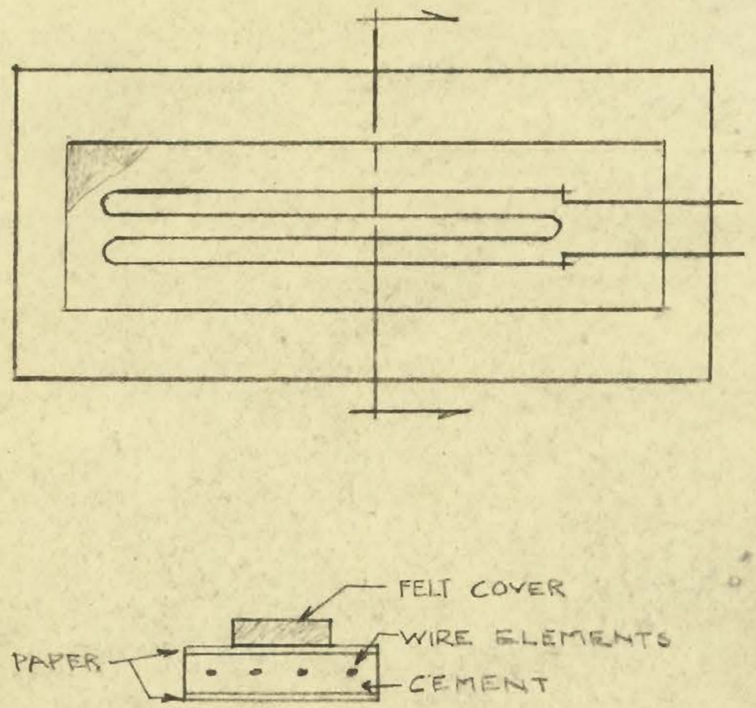

FIG VI-1

SKETCH SHOWING METHOD
OF STRAIN GAGE CONSTRUCTION

C H A P T E R VI

PRINCIPAL STRESSES AND STRAINS FROM STRAIN GAGE ROSETTES

A strain gage measures strains along its longitudinal axis only. In order to determine the directions and magnitudes of the principal strains and stress, several strain gages (usually three) are placed on one sheet of backing paper and so oriented that they measure the stress in different directions at a point. The point being usually either at the intersection of the axes of the gages, or at the center of the rosette.

Though the following explanation applies specifically to electric resistance strain gages, the discussion is quite general and applies equally well to mechanical or other types of strain gages.

The total strain in any direction can be considered to consist of three separate parts:

1. Due to temperature change - eliminated by instrumentation.
2. Due to Poisson effect which is a strain unaccompanied by stress.
3. Primary strain that is directly related to stress by Hooke's law.

The maximum and minimum values of the strain at any point lie along mutually perpendicular directions. These are called the principal strains. The accompanying stresses, which lie along the same directions as the principal strains, are called the principal stresses.

The relationship between principal stress and principal strain will be shown by considering the deformation of an isotropic unit cube subjected to forces in the x, y and z directions.

Considering the deformation due to a force in the x direction as shown in Fig. VI-1.

In the x direction, strain $= \frac{\sigma_x}{E}$

In the y direction, strain $= -\frac{\mu \sigma_x}{E}$

In the z direction, strain $= -\frac{\mu \sigma_x}{E}$

Similarly for a force applied in the y direction

$$\epsilon_y = \frac{\sigma_y}{E}$$

$$\epsilon_x = \epsilon_z = -\frac{\mu \sigma_y}{E}$$

Again for a force applied in the z direction

$$\epsilon_z = \frac{\sigma_z}{E}$$

$$\epsilon_x = \epsilon_y = -\frac{\mu \sigma_z}{E}$$

Hence, if all three forces are applied simultaneously, the strain in any direction may be found by adding the above results.

$$\epsilon_x = \frac{\sigma_x}{E} - \frac{\mu \sigma_y}{E} - \frac{\mu \sigma_z}{E} \qquad (1)$$

$$\epsilon_y = -\frac{\mu \sigma_x}{E} + \frac{\sigma_y}{E} - \frac{\mu \sigma_z}{E} \qquad (2)$$

$$\epsilon_z = -\frac{\mu \sigma_x}{E} - \frac{\mu \sigma_y}{E} + \frac{\sigma_z}{E} \qquad (3)$$

For a plane, or two-dimensional stress field $\sigma_z = 0$. Re-writing the above equations to obtain the principal stresses in terms of the principal strains

$$\sigma_x = \frac{E}{1-\mu^2}\left[\epsilon_x + \mu \epsilon_y \right] \qquad (4)$$

$$\sigma_x = \frac{E}{1-\mu^2}\left[\mu \epsilon_x + \epsilon_y \right] \qquad (6)$$

Note that σ_x and σ_y are functions of both ϵx and ϵy.

In most cases, the principal stress directions are unknown, therefore, means must be found to express the <u>principal stress</u> in terms of the <u>strains</u> in any direction. This is done by examining the geometric relationship existing between the <u>principal strains</u> and the <u>strain</u> in any direction: See Fig. VI-2, VI-3, and VI-4.

Fig. VI-2 shows a gage applied on the line A-B at an angle ϕ with the x-axis along which a strain ϵ_x exists. Since only the geometry of the problem is being considered, the Poisson strain in the y direction is not introduced.

After applying the strain in the x direction, the line OA, of length x has been stretched by the amount δx to OA', and the gage whose original length was L, now lies along the line OB' and is stretched by the amount δL. The strain in the x direction is then

$$\epsilon_x = \frac{\delta x}{x}$$

The strain measured by the gage is:

$$\epsilon_\phi = \frac{\delta L}{L}$$

Since L = $\frac{x}{\cos\phi}$ and $\delta L = \delta x \cos\phi$

then $\epsilon_\phi = \frac{\delta x \cos^2\phi}{x} = \epsilon_x \cos^2\phi$

similarly for a strain applied in the y direction

$$\epsilon_\phi = \epsilon_y \cos^2(90-\phi) = \epsilon_y \sin^2\phi \qquad (7)$$

Referring to Fig. VI-6, after applying a shearing strain γ_{xy}, the gage lies along the line OB' and has lengthened by the amount δL. The strain recorded by the gage is:

$$\epsilon_\phi = \frac{\delta L}{L}$$

but $L = \frac{y}{\sin\phi}$ $\qquad \delta L = \delta x \cos\phi \qquad \delta x = y \tan\gamma_{xy} \equiv y\gamma_{xy}$

then $\delta L = y\gamma_{xy} \cos\phi$

and $\epsilon_\phi = \frac{\delta L}{L} = \gamma_{xy} \sin\phi \cos\phi$

$$= \frac{1}{2}\gamma_{xy} \sin 2\phi \qquad (8)$$

Now if strains ϵ_x , ϵ_y , and γ_{xy} act simultaneously, the gage will record the sum of the strains, or .

$$\epsilon_\phi = \epsilon_x \cos^2\phi + \epsilon_y \sin^2\phi + \gamma_{xy} \sin\phi\cos\phi$$

$$= \frac{\epsilon_x+\epsilon_y}{2} + \frac{\epsilon_x-\epsilon_y}{2}\cos 2\phi + \frac{\gamma_{xy}}{2}\sin 2\phi \qquad (9)$$

Since ϵ_ϕ can be measured with a strain gage, the strains in any selected x and y directions can be determined. By measuring ϵ_ϕ along any three lines making angles ϕ_1, ϕ_2 and ϕ_3 with the x-axis selected, we then have 3 equations and 3 unknowns, or

$$\left.\begin{aligned}\epsilon_1 &= \frac{\epsilon_x+\epsilon_y}{2} + \frac{\epsilon_x-\epsilon_y}{2}\cos 2\phi_1 + \frac{\gamma_{xy}}{2}\sin 2\phi_1 \\ \epsilon_2 &= \frac{\epsilon_x+\epsilon_y}{2} + \frac{\epsilon_x-\epsilon_y}{2}\cos 2\phi_2 + \frac{\gamma_{xy}}{2}\sin 2\phi_2 \\ \epsilon_3 &= \frac{\epsilon_x+\epsilon_y}{2} + \frac{\epsilon_x-\epsilon_y}{2}\cos 2\phi_3 + \frac{\gamma_{xy}}{2}\sin 2\phi_3\end{aligned}\right\} \quad (10)$$

The relations between ϵ_x, ϵ_y and γ_{xy} and the principal strains existing at a given point will now be developed.

Since by definition the principal strains are the maximum and minimum values existing at a given point, the general expression for ϵ_ϕ can be differentiated with respect to ϕ to obtain the angle ϕ_p giving the direction of the principal strains.

$$\frac{d\epsilon_\phi}{d\phi} = -\frac{2(\epsilon_x-\epsilon_y)}{2}\sin 2\phi_p + \frac{2\gamma_{xy}}{2}\cos 2\phi_p = 0$$

$$\text{whence} \quad \tan 2\phi_p = \frac{\gamma_{xy}}{\epsilon_x-\epsilon_y} \qquad (11)$$

The magnitude of the principal strain is then obtained by substituting the value of $2\phi_p$ in the general expression for ϵ_ϕ in equation (9). The easiest method for obtaining the trigonometric functions of the angle $2\phi_p$ is to construct an angle whose tangent is $\frac{\gamma_{xy}}{\epsilon_x-\epsilon_y}$ as shown in Fig.VI-5.

From the figure VI-5

$$\sin 2\phi_p = \pm \frac{\gamma_{xy}}{\sqrt{(\epsilon_x - \epsilon_y)^2 + \gamma^2_{xy}}}$$

$$\cos 2\phi_p = \pm \frac{\epsilon_x - \epsilon_y}{\sqrt{(\epsilon_x - \epsilon_y)^2 + \gamma^2_{xy}}}$$

Substituting in equation (9) and simplifying

using positive values

$$\epsilon_{MAX} = \frac{\epsilon_x + \epsilon_y}{2} + \frac{1}{2}\sqrt{(\epsilon_x - \epsilon_y)^2 + \gamma^2_{xy}} \qquad (12)$$

using negative values

$$\epsilon_{MIN} = \frac{\epsilon_x + \epsilon_y}{2} - \frac{1}{2}\sqrt{(\epsilon_x - \epsilon_y)^2 + \gamma^2_{xy}} \qquad (13)$$

MOHR'S CIRCLE FOR STRAIN

It is possible to employ a graphical method to show the relationship that exists between normal and shearing strains in any direction at a point. The construction is called Mohr's Circle for Strain. It uses ϵ and $\frac{\gamma}{2}$ as the axis of a co-ordinate system. Thus a single point can be used to represent the state of strain on some plane in a strained body: in this system the positive direction of the $\frac{\gamma}{2}$ axis is downwards, see Fig. VI-6.

Mohr's Circle can now be used to obtain a solution of the problem under consideration. The strain gage readings ϵ_1, ϵ_2, and ϵ_3 when substituted in the equations, give values of ϵ_x, ϵ_y and γ_{xy} which can be plotted in the ϵ, $\frac{\gamma}{2}$ co-ordinate system. ϵ_x and $\frac{\gamma_{xy}}{2}$ are represented by a single point A; ϵ_y and $\frac{\gamma_{yx}}{2}$ $\left(= -\frac{\gamma_{xy}}{2} \right)$ are represented by a single point B. The line joining A and B is the diameter of Mohr's Circle for strain, which can now be drawn. All points on the circumference of the circle represent the strain conditions on some plane at the point being considered. The principal strains occur where the circle crosses the axis, since the shearing stresses are zero at these points.

Referring to Fig. VI-6, the distance from the centre of the circle to the point representing ϵ_x on the x-axis is $\frac{\epsilon_x - \epsilon_y}{2}$ and the distance between the origin and the centre of the circle is $\frac{\epsilon_x + \epsilon_y}{2}$. The right triangle in the circle having the sides $\frac{\epsilon_x - \epsilon_y}{2}$ and $\frac{\gamma_{xy}}{2}$ will have for its hypotenuse (and the radius of the circle)

$$\frac{1}{2}\sqrt{(\epsilon_x - \epsilon_y)^2 + \gamma^2_{xy}}$$

If the angle between this hypotenuse and the ϵ-axis is called $2\phi_p$, then $\tan 2\phi_p = \frac{\gamma_{xy}}{\epsilon_x - \epsilon_y}$ which is the same as the value obtained algebraically. From the above figure

$$\epsilon_{\substack{MAX \\ MIN}} = \frac{\epsilon_x + \epsilon_y}{2} \pm \frac{1}{2}\sqrt{(\epsilon_x - \epsilon_y)^2 + \gamma^2_{xy}}$$

which is identical with equations (12) and (13).

Again from Fig. VI-6, it is apparent that the angles measured around the circumference of Mohr's Circle are twice as great as those measured in the x, y co-ordinate system. For example, point A, which represents the strains along and perpendicular to the x plane, is 180 degrees from point B, which represents the strains along and perpendicular to the y plane, but the x and y planes are, of course, only 90 degrees apart. The maximum principal strains will be found in a direction making a counterclockwise angle ϕ_p with the x-axis.

To summarize, the steps required to determine the maximum and minimum stresses existing at a point are as follows:-

1. An x axis is selected and magnitudes of strain are determined in three directions, making angles ϕ_1, ϕ_2, and ϕ_3 with the chosen axis. ϕ_1 is usually made equal to zero for convenience; that is, the first strain is measured along the x axis.
2. The three strains obtained are substituted in equations (10), which are solved simultaneously for ϵ_x, ϵ_y and γ_{xy}.
3. The values of ϵ_x, ϵ_y and γ_{xy} obtained in the second step are substituted in equations (12) and (13) to obtain the principal strains ϵ_{MAX} and ϵ_{MIN}. In place of these equations, Mohr's Circle for Strain can be substituted to obtain the principal strains graphically or algebraically.
4. If the directions of the principal strains and stresses are required, the values of ϵ_x, ϵ_y and γ_{xy} must be substituted in equation (11), to determine the angle ϕ_p which the maximum principal strain (and stress) make with the original selected x axis. ϕ_p can also be obtained from Mohr's Circle for Strain.

The maximum and minimum principal stresses are now obtained by substituting ϵ_{MAX} and ϵ_{MIN} in equations (4) and (5).

Since the algebraic procedure is somewhat lengthy, graphical procedures have been developed by means of which the principal strains and their directions can be obtained fairly rapidly. The graphical methods eliminate step 2 in the analytic procedure. However, in this experiment only rectangular rosettes were used, this resulted in simplified equations so that there was no great advantage in using the graphical procedure. Instead, a semi-graphical method which is developed below, was used throughout the calculations:

The relationship between the stresses existing on any two mutually perpendicular planes and those on any other planes are of a similar nature to the relationship for strains. Beginning with an element of volume in which a general two-dimensional state of stress exists in the x and y directions, it is possible to write the expression for the stress conditions on a plane whose normal makes an angle ϕ with the x-axis.

First an element of volume is isolated as shown in Fig. VI-7 and the area of the slant face is labelled A. The area of the horizontal face will then be A sin ϕ, of the vertical face, A cos ϕ. Summing up the forces perpendicular and parallel to the slant face, collecting terms and cancelling etc.

$$\sigma_\phi = \sigma_x \cos^2\phi + \sigma_y \sin^2\phi - 2\tau_{xy} \sin\phi \cos\phi$$

$$\tau_\phi = (\sigma_x - \sigma_y) \sin\phi \cos\phi + \tau_{xy} (\cos^2\phi - \sin^2\phi)$$

These equations may be rewritten

$$\sigma_\phi = \frac{\sigma_x + \sigma_y}{2} + \frac{\sigma_x - \sigma_y}{2} \cos 2\phi - \tau_{xy} \sin 2\phi \qquad (14)$$

$$\tau_\phi = \frac{\sigma_x - \sigma_y}{2} \sin 2\phi - \tau_{xy} \cos 2\phi \qquad (15)$$

It is apparent that the equations for σ_ϕ and ϵ_ϕ , and τ_ϕ and $\frac{\gamma_\phi}{2}$ are of the same form.

The expression for the angle at which the normal stress becomes a maximum can then be written as:

$$\tan 2\phi_p = \frac{2\tau_{xy}}{\sigma_x - \sigma_y} \qquad (16)$$

Since the equations for stress are of similar form to those for strain, a Mohr's Circle for Stress can also be constructed by substitution of σ and τ for the co-ordinate axis, with the positive τ axis drawn in the opposite direction to the positive $\frac{\gamma}{2}$ axis.

The general construction of Mohr's Circle for Stress is shown in Fig. VI-8. As long as the stress conditions are known on any two orthogonal planes, they can be plotted as points on the σ , τ co-ordinate system and the line joining the two points will be the diameter of Mohr's Circle for Stress. The circle having been constructed, the stress conditions on any plane can be determined directly. The greatest utility of Mohr's Circle for Stress, as is the case for the Strain Circle, is not in the graphical construction, but rather in the fact that an analytic solution is readily obtained from the geometry of freehand construction, so that it is not necessary to remember the complex equations defining σ and τ .

THE RECTANGULAR ROSETTE

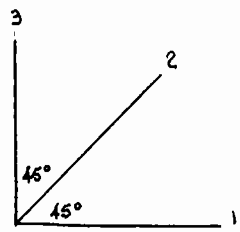

In this case $\phi_1 = 0$

$\phi_2 = 45^\circ$

$\phi_3 = 90^\circ$

Substituting the numerical values of sin 2ϕ and cos 2ϕ in the fundamental equation (9)

$$\epsilon_\phi = \frac{\epsilon_x + \epsilon_y}{2} + \frac{\epsilon_x - \epsilon_y}{2}\cos 2\phi + \frac{\gamma_{xy}}{2}\sin 2\phi$$

we obtain

$$\left.\begin{aligned} \epsilon_1 &= \frac{\epsilon_x + \epsilon_y}{2} + \frac{\epsilon_x - \epsilon_y}{2} \\ \epsilon_2 &= \frac{\epsilon_x + \epsilon_y}{2} + \frac{\gamma_{xy}}{2} \\ \epsilon_3 &= \frac{\epsilon_x + \epsilon_y}{2} - \frac{\epsilon_x - \epsilon_y}{2} \end{aligned}\right\} \quad (16)$$

solving for ϵ_x , ϵ_y , and γ_{xy}

$$\left.\begin{aligned} \epsilon_x &= \epsilon_1 \\ \epsilon_y &= \epsilon_3 \\ \gamma_{xy} &= 2\epsilon_2 - (\epsilon_1 + \epsilon_3) \end{aligned}\right\} \quad (17)$$

From equations (11), (12) and (13)

$$\epsilon_{MIN}^{MAX} = \frac{\epsilon_x + \epsilon_y}{2} \pm \frac{1}{2}\sqrt{(\epsilon_x - \epsilon_y)^2 + \gamma_{xy}^2}$$

$$\gamma_{MAX} = \frac{1}{2}\sqrt{(\epsilon_x - \epsilon_y)^2 + \gamma_{xy}^2}$$

$$2\phi_P = \tan^{-1}\frac{\gamma_{xy}}{\epsilon_x - \epsilon_y}$$

substituting equations (17) into the above, we obtain the following:

$$\left.\begin{aligned} \epsilon_{MIN}^{MAX} &= \frac{1}{2}(\epsilon_1 + \epsilon_3) \pm \frac{1}{2}\sqrt{(\epsilon_1 - \epsilon_3)^2 + [2\epsilon_2 - (\epsilon_1 + \epsilon_3)]^2} \\ \gamma_{MAX} &= \frac{1}{2}\sqrt{(\epsilon_1 - \epsilon_3)^2 + [2\epsilon_2 - (\epsilon_1 + \epsilon_3)]^2} \\ \phi_P &= \frac{1}{2}\tan^{-1}\frac{2\epsilon_2 - (\epsilon_1 + \epsilon_3)}{\epsilon_1 - \epsilon_3} \end{aligned}\right\} \quad (18)$$

Using the previously developed relationships,

$$\sigma_{MAX} = \frac{E}{1-\mu^2}\left[\epsilon_{MAX} + \mu\epsilon_{MIN}\right]$$

$$\sigma_{MIN} = \frac{E}{1-\mu^2}\left[\epsilon_{MIN} + \mu\epsilon_{MAX}\right]$$

$$\tau_{MAX} = \frac{E}{2(1+\mu)}\gamma_{MAX}$$

We obtain for the principal stresses and maximum shearing stress:

$$\sigma_{\substack{MAX \\ MIN}} = \frac{E}{2}\left[\frac{\epsilon_1+\epsilon_3}{1-\mu} \pm \frac{1}{1+\mu}\sqrt{(\epsilon_1-\epsilon_3)^2+\left[2\epsilon_2-(\epsilon_1+\epsilon_3)\right]^2}\right]$$

$$\tau_{MAX} = \frac{E}{2(1+\mu)}\sqrt{(\epsilon_1-\epsilon_3)^2+\left[2\epsilon_2-(\epsilon_1+\epsilon_3)\right]^2}$$

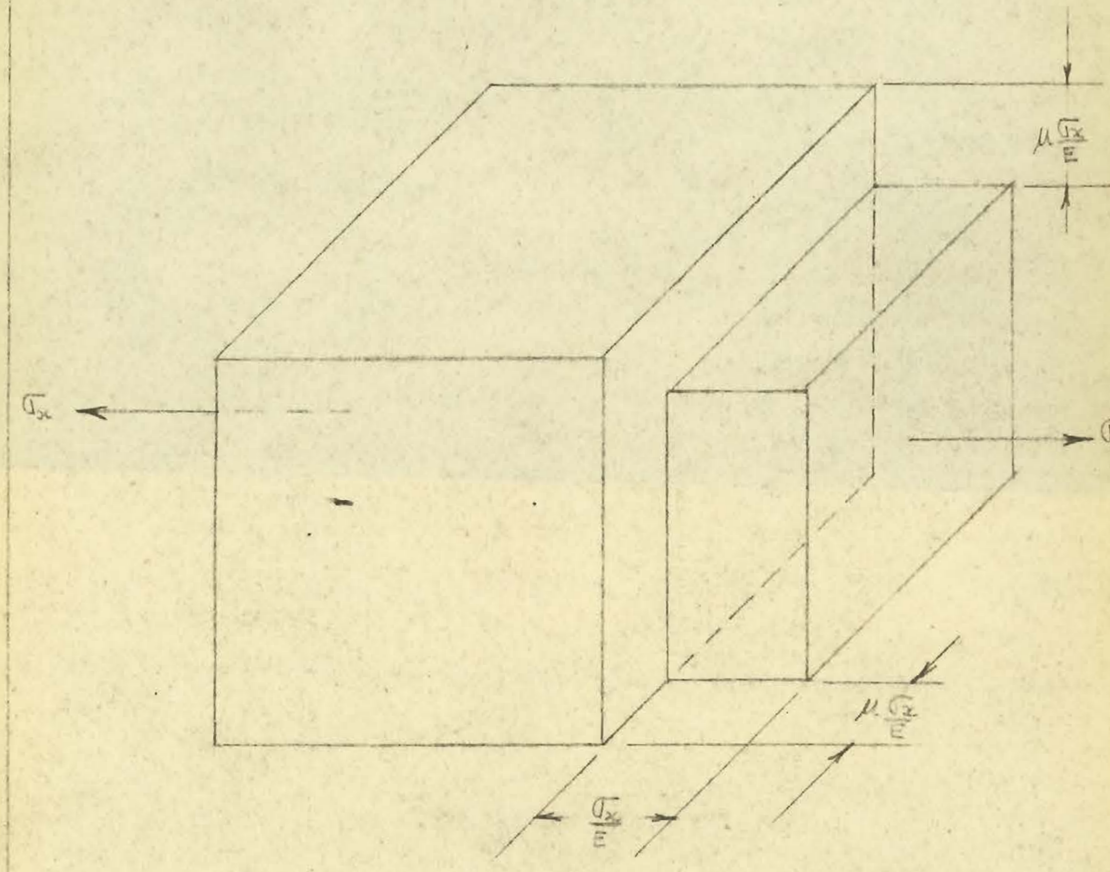

FIG $\overline{\underline{VI}}$-1

STRAINS PRODUCED IN A UNIT CUBE
BY A UNIAXIAL STRESS

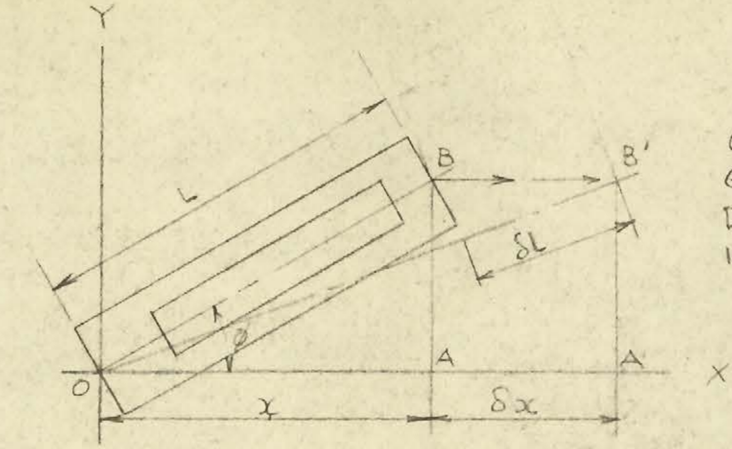

FIG VI-2
GEOMETRY OF STRAIN GAGE DEFORMATION DUE TO A STRAIN IN THE X DIRECTION

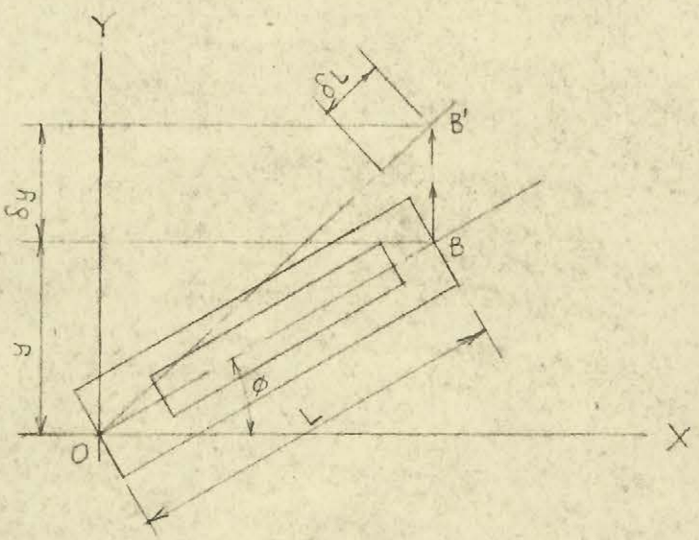

FIG VI-3 –
GEOMETRY OF STRAIN GAGE DEFORMATION DUE TO A STRAIN IN THE Y DIRECTION

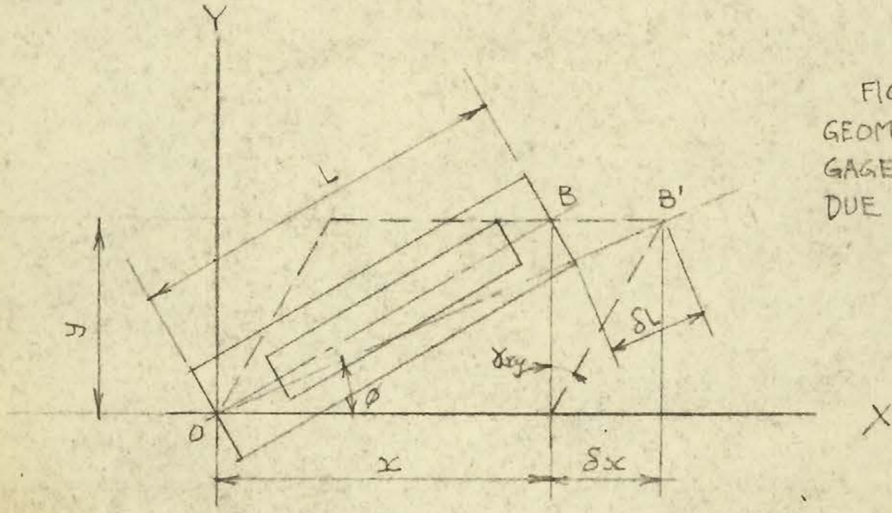

FIG. VI-4
GEOMETRY OF STRAIN GAGE DEFORMATION DUE TO A SHEARING STRAIN

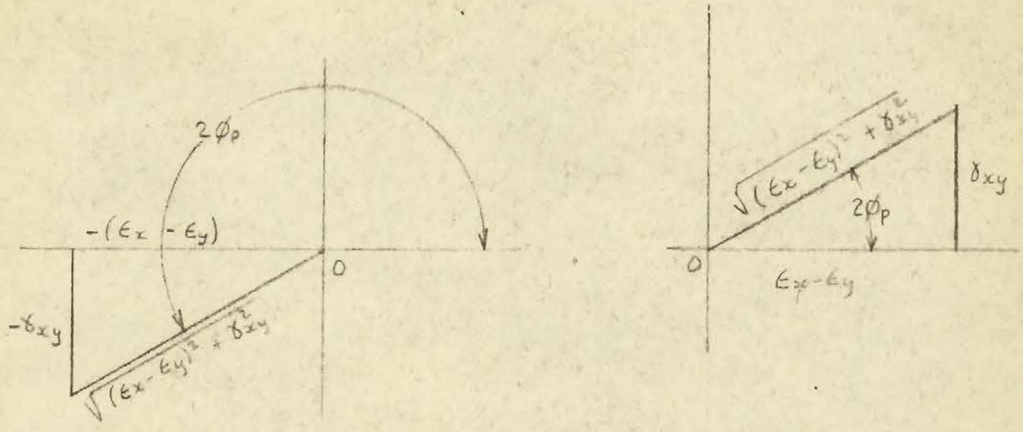

FIG. VI-5
TRIGONOMETRIC REPRESENTATION
OF STRAIN RELATIONSHIPS

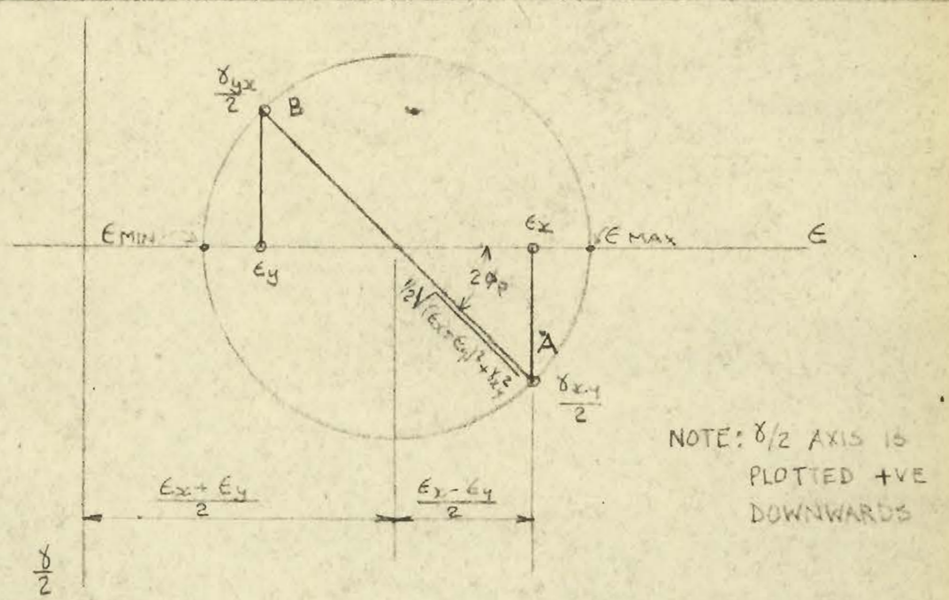

FIG. VI-6
MOHR CIRCLE FOR STRAIN

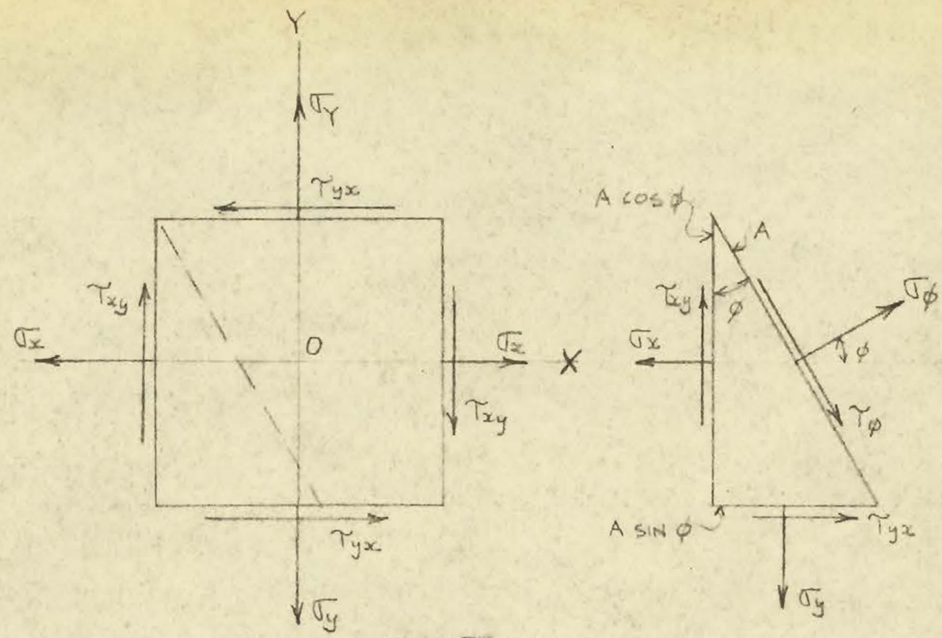

FIG VI - 7
FREE BODY DIAGRAM
OF AN ELEMENT
IN A BIAXIAL STRESS FIELD

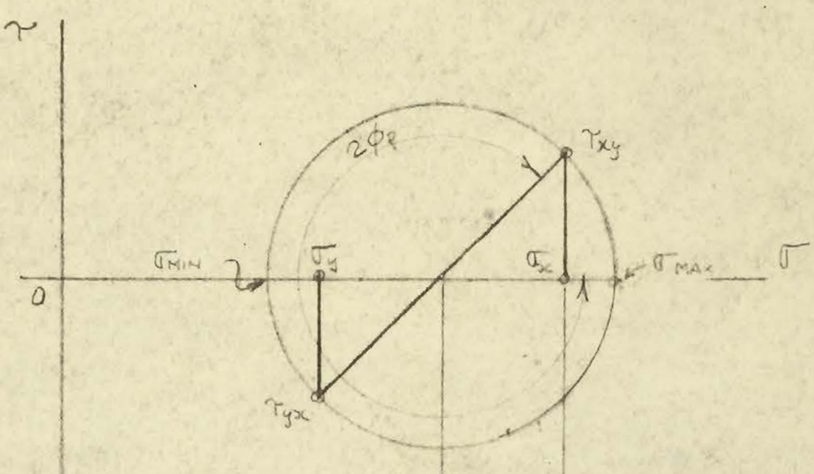

FIG VI - 8
MOHR CIRCLE FOR STRESS

THEORIES OF FAILURE WITH RESPECT TO CONCRETE

THE MAXIMUM PRINCIPAL STRESS THEORY

This theory, which is often called Rankine's Theory, states that inelastic action at any point in a material which any state of stress exists begins only when the maximum principal stress at the point reaches a value equal to the tensile (or compressive) elastic limit or yield strength of the material as found in a simple tension (or compression) test, regardless of the normal or shearing stresses that occur on other planes through the point provided that the latter are absolutely smaller,

$$\sigma_{critical} = \frac{P}{A}$$

For brittle materials, which do not fail by yielding, but fail by brittle fracture, this theory is considered to be reasonably satisfactory, although the maximum strain theory is considered to be preferable. Its limitations are evident mainly in the presence of shear or in the case of triaxial compressive forces of equal magnitude producing stresses of yield stress or greater magnitude, which according to this theory should cause failure: a fact not verified by experimental evidence.

THE MAXIMUM SHEARING STRESS THEORY

This theory is also known as Coulomb's Theory, or Guest's Law, states that inelastic action at any point in a body at which a state of stress exists, begins only when the maximum shearing stress on some plane through the point reaches a value equal to the maximum shearing stress in a tension specimen when yielding starts. This means that the shearing elastic limit must not exceed one-half the tensile elastic limit, since the maximum shearing stress in a tension specimen is one-half the maximum tensile stress in the specimen,

$$\tau_{critical} = \frac{1}{2}\frac{P}{A} = \frac{1}{2}\sigma_{critical}$$

This theory appears to be more suitable for ductile materials than for brittle materials. However, in the case of pure shear, as occurs in a torsion test, the shearing elastic limit varies somewhat but has an average value of about 0.57 critical. Hence for this condition the error is about 14% on the safe side. Like the maximum principal stress theory, this theory is inadequate under conditions of large equal triaxial tensile stresses where the shearing stresses would be very small and failure would be by brittle fracture rather than yielding. We should note that stirrup design in reinforced concrete is based on the maximum shear stress theory of failure. By considering no direct stresses below the neutral axis of a section (in a reinforced concrete beam), we automatically assume that the material is going to fail in shear along a plane at 45 degrees to the neutral axis. If the tensile and compressive strengths of a material are equal rupture coincides with the maximum shear stress theory, and this forms a special case where the Mohr theory of rupture, which is explained in the next section, coincides with that of the maximum shear stress theory.

MOHR THEORY OF RUPTURE

This theory states that the condition under which a stressed body begins to deform inelastically, or ruptures, can be formulated in a quite general manner. A material may fail by plastic slip or rupture when either the shearing stress in the planes of slip has increased to a certain value, or when the largest tensile stress has reached a limiting value depending upon the properties of the material. If the states of stress are graphically represented by Mohr circles it can be shown that the locus of limiting stress circles. This curve is called the Mohr envelope and the abscissas and ordinates of the points on this curve represent the normal and shear stresses in planes of slip.

The theory of slip planes is confirmed somewhat by experimental evidence. For example, concrete test cylinders usually break along surfaces obliquely inclined with respect to the axis of the cylinder forming the familiar failure cone (see photograph Fig. VII-1). Noting that, according to the assumptions made by Otto Mohr, the intermediate principal stress in a three dimensional stress system is without influence on the failure of the material, and that the stress conditions in this experiment, were investigated for conditions of two-dimensional stress only; the limiting conditions under this theory will be developed for two-dimensional stress instead of the general development, for three domensional stress.

One difficulty now presents itself; namely no reliable values for the shear strength of concrete are available, and shear tests for concrete are somewhat difficult to arrange. However, the Mohr envelope can be plotted if the tensile and compressive strengths of the material are known (see Fig. VII-2) and from the Mohr envelope we can deduce this shear strength of the concrete. Though the Mohr envelope is actually a curved line and Guyon considers it to be a parabola, Timoshenko in the second edition of "Theory of Elastic Stability" states that the Mohr envelope may be represented by straight lines tangent to the circles representing failure in compression and tension.

Referring to Fig. VII-2, if the Mohr circle for any state of stress falls inside the Mohr envelope, no failure would occur. If the Mohr circle is tangent to the envelope in the compression region, failure would be iminent in compression, and no stirrups would be necessary. However, if the points of tangency fall within the tensile region, failure would occur in diagonal tension and stirrups would have to be provided. If at a point in the stress field, the direction of principal stresses forms an angle β to the horizontal axis, then the worst inclination of cracks for stirrup design would be $\phi = \beta + \alpha$ While the inclination of principal stresses can be determined from either the corresponding Mohr circle, or analytically, the angle of slip α can be found either graphically from the plotted Mohr envelope, or analytically from the expression for the critical Mohr circle.

The following method of calculating the angle of slip from the Mohr theory of rupture is due to Messrs. Robinson and Betaille and is presented more fully in "Prestressed Concrete" by Y. Guyon.

Expressing the equation for a Mohr circle:

$$\left(\sigma_1 - \frac{\sigma_1 + \sigma_3}{2}\right)^2 + \tau^2 = \left(\frac{\sigma_1 - \sigma_3}{2}\right)^2 \qquad \begin{array}{l}\sigma_1 = \sigma_{MIN} \\ \sigma_3 = \sigma_{MAX}\end{array}$$

into a parametric form

$$(\sigma - p)^2 + \tau^2 = \tau_m^2 \qquad (1)$$

Eliminating the unknown σ and τ quantities equation (1) can be rewritten in a new parametric form

$$(p + p_0)^2 = \tau_m\left(1 + \frac{\tau_m}{r_0}\right) \qquad (2)$$

Where r_0 and p_0 are parameters depending solely on the strength of the concrete. These two parameters can be found if we know the compressive and tensile strengths of the concrete, which gives us two of the circles of the family of circles tangent to the Mohr envelope.

for pure compression

$$p = \frac{f'_c}{2} \qquad \tau_m = \frac{f'_c}{2}$$

for pure tension

$$p = -\frac{f'_t}{2} \qquad \tau_m = -\frac{f'_t}{2}$$

Inserting these values into equation (2) and solving the resultant two simultaneous equations we obtain:

$$p_0 = f'_c\left[\frac{1 + \frac{f'_t}{f'_c}}{1 + \left(\frac{f'_t}{f'_c}\right)^3} - 1\right]$$

and since f'_t/f'_c is small the term $(f'_t/f'_c)^3$ may be neglected, giving:

$$p_o = f'_t$$

$$r_o = \frac{f'_c}{8}\left[\frac{1}{\frac{f'_t}{f'_c}\left(1 - \frac{f'_t}{f'_c}\right)}\right]$$

The table below, giving the values of r_o as a function of f'_c, is due to Guyon.

$\left[\frac{f^1t}{f^1c}\right]$	$\left[\frac{r_o}{f^1c}\right]$
1/10	1.135
1/12	1.385
1/15	1.76
1/20	2.38
1/25	3.01
1/30	3.64

Assuming a reduction in concrete strength by a factor of λ, smaller than unity, or in other words a safety factor of $1/\lambda$, equation (2) becomes:

$$(p + \lambda p_o)^2 = \tau_m^2 \left(1 + \frac{\tau_m}{\lambda r_o}\right) \qquad (3)$$

The abscissas σ of the points of tangency to the Mohr envelope can be expressed mathematically as the abscissas of a straight vertical line through these points of tangency.

This line is represented by the derivative of equation (1) with respect to p;

$$\sigma - p + \tau_m \frac{d\tau_m}{dp} = 0 \qquad (4)$$

Again differentiating equation (3) with respect to p we obtain:

$$2(p + \lambda p_o) = \tau_m \frac{d\tau_m}{dp}\left(2 + \frac{3\tau_m}{\lambda r_o}\right) \qquad (5)$$

Eliminating $\frac{d\tau_m}{dp}$ from equations (4) and (5), the abscissa, σ, is expressed as:

$$\sigma = \frac{3p\tau_m - 2(\lambda p_o)(\lambda r_o)}{2\lambda r_o - 3\tau_m}$$

From the geometry of the critical Mohr circle and the envelope it follows that:

$$\cos 2\alpha = \frac{p - \sigma}{\tau_m}$$

Using either this calculated value for α , or the one obtained graphically from the Mohr envelope, the probable slip plane can be determined. At one end panel of the test beam the stirrups were placed at a distance of about 18 inches apart, or slightly greater than that given by this theory, in the other end panel, the stirrups were placed much closer together, being about six inches apart. In practise, stirrups are usually spaced at about .75 to .80 times the depth. For discussion of the effects of the different stirrup spacing see the section of this thesis entitled "Conclusions and Discussion of Results".

FIG. VII-1

CONE OF FAILURE OF CONCRETE

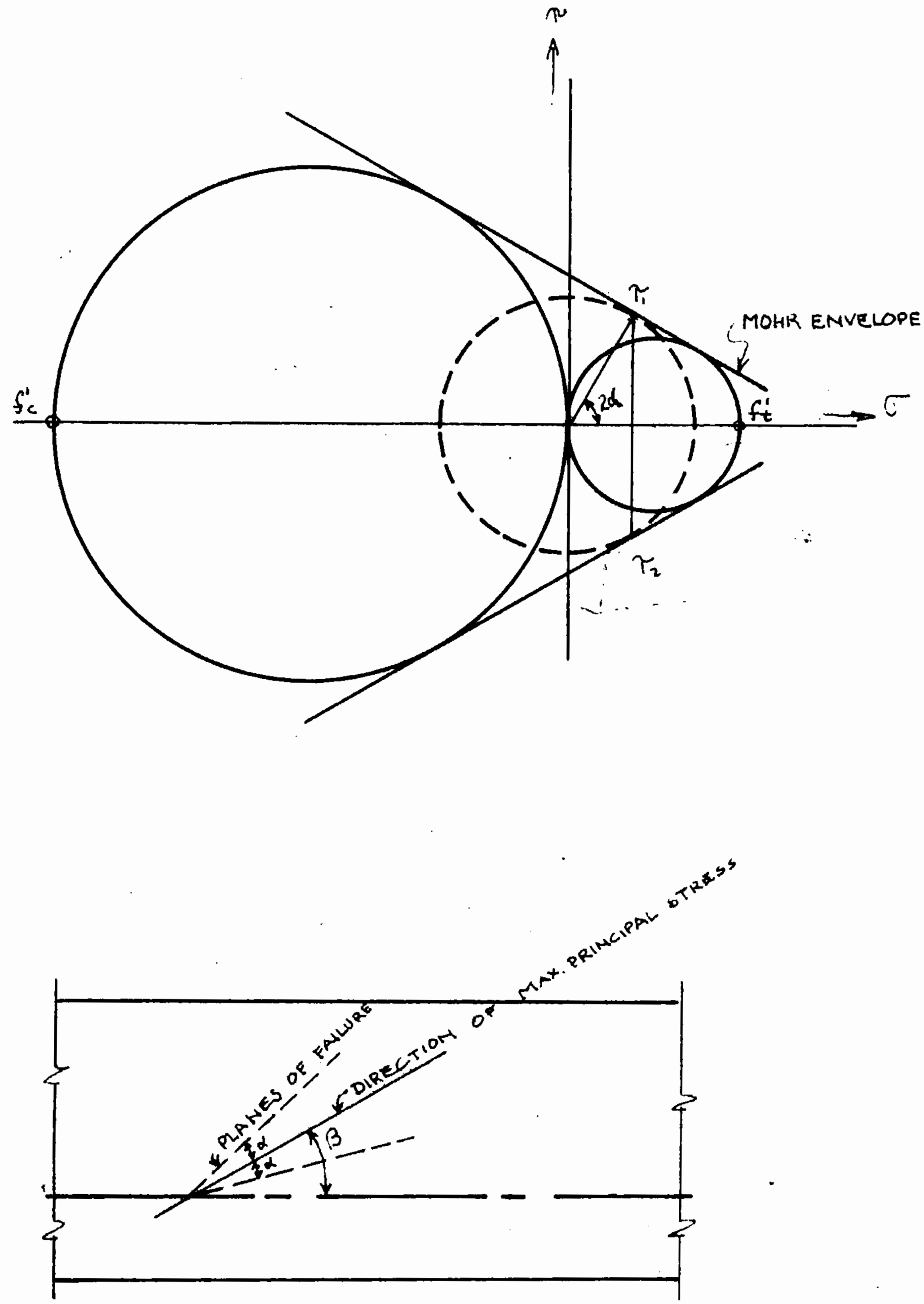

FIG VII-2
MOHR ENVELOPE AND
SLIP PLANES

CHAPTER VIII

DISCUSSION OF THE RESULTS OF THE EXPERIMENT

FORMS

The forms had been designed and assembled in panels in order to facilitate removal and reuse. In addition, the forms had been liberally oiled with two coats of oil. These efforts notwithstanding, the forms literally had to be broken up in order to remove them from the beam.

It follows that if forms are to be reused, and this is an economic necessity with the complicated I-shapes used with prestressed concrete, the forms should be made very rigidly. If wooden forms are used, it would be advisable to line the inside of the forms with light gage sheet metal, or with a light cheap material that will effectively separate the form from the concrete. Gripping devices should be attached to the form to assist in their removal, and if convenient, the form should be assembled into smaller units than a full panel, i.e., the web portion should be detachable from the flange portions.

CONCRETE

The concrete used was similar to the mix for the Banks-Jakobson beam, with a pozzolith dispersion agent added. It would be dangerous to make a broad generalization from what is really a very limited sample, and one that is not subject to scientific control; that is, the observations would have more validity if two batches of concrete had been made from the same mix, one with pozzolith, one without. The pozzolith seemed to delay the development of compressive strength, as in this test the cylinders failed at about 5500 p.s.i. versus 6200 p.s.i. for the Banks-Jakobson beam. Though the values of both E and μ differ slightly, 4.2 versus 4.5, and .16 versus .12, it would not be justified to attribute these differences solely to the pozzolith on the basis of the limited data available.

The value for the modulus of elasticity, as determined from the tests on the concrete test cylinders, and as determined by the method of balancing forces across a section, were in excellent agreement, being 4.2×10^6 p.s.i. for each method.

HI-TENSILE STEEL WIRE

The apparent creep (or loss of prestress) in the cable is less than recorded by Banks-Jakobson, being here of the order of 2.2% versus 18% between the time of prestress and the last day of the test, a period of 8 days.

There are several possible reasons for this. They are as follows. During the stressing operation, the wire was tensioned up to 100,000 p.s.i. in order to secure the end of the wire on the end opposite to the jack, the stress was then released and then raised to approximately 130,000 p.s.i. in order to apply the full prestress and anchor the jack end of the wire. Magnel recommends a similar procedure as this reduces the subsequent creep of the wire. The stressing operation itself took two working days, and during this operation no attempt was made to measure the strains in the wire. Undoubtedly, had continuous readings been taken of the strains in the wires, the first wires tensioned would have shown greater apparent losses of prestress as additional wires were tensioned.

STRAIN GAGES

Gages attached to the concrete

The linear A-3 gages gave consistent strain readings, and in general the stresses computed from their strains were in good agreement with those calculated from theoretical considerations. However the AR-14 rosettes gave poor, inconsistent results, in general, only in fair agreement with the theoretical values.

The AR-14 rosettes have a short gage length of only 3/8-inch and were designed for use on aircraft structures. They were used here because of their availability, the AR-1 rosettes not being available at the time of the test. The confirmation of the inaccuracy of these gages was shown when the web cracked in the direction of the computed principal stress. This is discussed further below.

GAGES ATTACHED TO THE HI-TENSILE WIRES

The A-9 gages attached to the hi-tensile wires gave consistent readings and the pattern of the strain readings was in good agreement with that predicted from experience. As mentioned earlier in this thesis, the long A-9 gages were somewhat difficult to attach to the wires because they exhibited a tendency to wrap themselves around the wire. However, after some trial, it was found that if the gages were well bonded at their ends, the quality of the bonding along the middle portion of the gage was not too important. Of course, this procedure is suitable only in a test of this type.

OBSERVED STRAINS AND STRESSES

The strains used in the calculations are the instantaneous elastic strains. At the beginning of each testing cycle the zero reading of each gage was taken, starting with the gages attached to box no.1 and finishing with those attached to box no.4. The increment of loading was then applied to the st ucture and the gages were then again read in the same order. The strain due to load being that due to the difference between the no-load reading and the under-load reading. The measured strains of the gages placed on opposite sides of the beam were averaged and then converted to the corresponding stresses.

Inclusion of the prestress effects in the calculations for principal stresses had to be done somewhat indirectly. For the gage values, the no-load readings at the time of prestress were considered to represent the prestress effects, and these readings were added algebraically to the instantaneous elastic strains due to loadings. For the computed values, the measured force in the cable at the time of prestress was taken to represent the prestress force, the computed effects of which were then added algebraically to the stresses due to external loading.

Though this procedure is open to discussion, it is one in which the small difference between the actual and the assumed prestress conditions would be the same for both the measured (or gage) values, and for the computed (or theoretical) values.

The magnitude and direction of the measured and computed principal stresses for the bending test are shown graphically in Fig. VIII-1, -2, -3, and VIII-4, -5, and -6, respectively. For the shear test, the computed values only are shown in Fig. VIII-7, -8, and -9.

The measured and computed instantaneous principal strains and stresses are shown in Tables VIII-1, -2, and -3 for the bending test, and in Tables VIII-4 and -5 for the shear test. For the instantaneous strains and stresses, the rosettes exhibited a somewhat better correlation between measured and computed values for both stress and direction.

From the diagrams for measured change of strain and stress at the center of the beam, see Fig. VIII-10 and -11, the maximum compressive strains and stresses occurred at some distance away from the compressive face. Similar results were reported on tests carried out on the Walnut Lane Bridge (Ref. "Prestressed

TABLE VIII-1

Measured Principal Strains and Stresses[1]
Bending Test

LOAD KIPS	ϵ_{MAX} IN/IN × 10^6	ϵ_{MIN} IN/IN × 10^6	γ_{MAX} IN/IN × 10^6	ϕ DEGREES	σ_{MAX} PSI	σ_{MIN} PSI	τ_{MAX} PSI	
ROSETTE	10, 11, 12							
20	33.1	-43.1	38.1	33	113	-163	68	
30	54.7	-59.7	57.2	33	195	-220	104	
40	74.9	-59.9	67.4	26	282	-207	122	
50	100.0	-70.0	85.0	24	383	-233	154	
60	123.8	-98.8	111.3	28	466	-350	202	
70	306.0	-231.0	268.5	67	1160	-786	486	*
80	180.0	-100.0	140.0	28	709	-308	254	
90	189.0	-124.0	159.0	29	727	-426	288	
ROSETTE	13, 14, 15							
20	15.0	-65.0	40.0	45	15	-270	72	
30	20.4	-50.4	35.4	41	53	-203	64	
40	11.0	-46.0	28.5	53	16	-191	52	
50	40.8	-80.8	60.8	50	120	-311	110	
60	50.8	-90.8	70.8	49	157	-358	128	
70	50.3	-60.3	55.3	48	175	-225	108	*
80	146.0	-124.0	133.5	49	546	-422	242	
90	107.0	-232.0	219.5	52	301	-965	397	
ROSETTE	16, 17, 18							
20	8.5	-58.5	33.5	58	-3	-241	6	
30	41.2	-111.2	76.2	57	101	-462	138	
40	46.6	-136.6	91.6	60	107	-560	166	
50	64.4	-179.4	121.9	59	154	-710	220	
60	82.5	-227.5	155.0	59	199	-925	271	
70	45.0	-185.0	115.0	57	66	-761	208	*
80	198.5	-323.5	261.0	57	604	-1260	476	
90	298.0	-238.0	268.0	58	1120	-824	485	

$\mu = .16$

$E = 4.2 \times 10^6$ psi

* Inelastic action, due to cracking, begins.

1 Neglecting prestress

TABLE VIII-2

MEASURED PRINCIPAL STRAINS AND STRESSES[1]
BENDING TEST

LOAD KIPS	ϵ_{MAX} IN./IN x 10⁶	ϵ_{MIN} IN/IN x 10⁶	γ_{MAX} IN/IN x 10⁶	ϕ DEGREES	σ_{MAX} PSI	σ_{MIN} PSI	τ_{MAX} PSI	
ROSETTE	1, 2, 3							
20	27.1	-2.1	14.6	15	116	10	26	
30	56.7	-141.7	99.2	50	147	-572	179	
40	72.5	-147.5	110.0	51	211	-586	198	
50	80.5	-165.5	123.0	48	233	-659	222	
60	105.5	-150.5	133.0	45	350	-576	241	
70	151.0	-91.0	121.0	33	588	-288	219	*
80	175.0	-76.0	125.0	31	704	-203	226	
90	198.5	-148.5	173.5	29	754	-503	314	
ROSETTE	4, 5, 6							
20	21.0	-52.0	36.5	46	55	-210	66	
30	35.0	-75.0	55.0	45	99	-249	100	
40	3.2	-102.2	52.2	49	—	-495	94	
50	110.0	-115.0	112.5	46	496	-420	202	
60	90.0	-215.0	152.5	46	240	-865	275	
70	126.0	-166.0	146.0	42	428	-624	264	*
80	105.5	-155.0	130.5	42	348	-546	236	
90	61.0	-266.0	163.5	42	75	-1110	246	
ROSETTE	7, 8, 9							
20	26.8	-58.8	42.8	71	75	-235	77	
30	44.2	-119.2	81.7	59	108	-485	148	
40	91.0	-186.0	138.5	65	264	-739	251	
50	180.5	-265.5	223.0	65	639	-1020	403	
60	298.5	-343.5	321.0	67	1050	-1215	580	*
70	620.0	-185.0	402.5	40	2550	-370	728	
80	1123.	-267.0	1365.	81	4660	-375	2410	
90	2150.	-370.0	1760	107	4040	-112	3180	

$\mu = .16$

$E = 4.2 \times 10^6$ psi

1 NEGLECTING PRESTRESS

* INELASTIC ACTION, DUE TO CRACKING, BEGINS.

TABLE VIII-3

COMPUTED STRESSES AT ROSETTES *
BENDING TEST

ROSETTE	LOAD KIPS	f PSI	τ PSI	σ_{MAX} PSI	σ_{MIN} PSI	φ DEGREES
1,2,3	20	160	126	229	-69	29
	40	319	252	457	-138	
	60	478	377	686	-207	
	80	638	503	916	-277	
4,5,6	20	10	156	157	-146	44
	40	20	312	314	-292	
	60	31	468	472	-438	
	80	41	624	628	-585	
7,8,9	20	-114	156	108	-222	56
	40	-229	309	216	-444	
	60	-343	464	324	-666	
	80	-457	619	432	-888	
10,11,12	20	240	126	293	-54	23
	40	480	252	577	-108	
	60	720	377	881	-161	
	80	960	503	1175	-215	
13,14,15	20	15	156	160	-144	43
	40	31	312	320	-288	
	60	46	468	480	-432	
	80	62	624	640	-576	
16,17,18	20	-172	156	91	-263	60
	40	-344	309	182	-526	
	60	-516	464	273	-789	
	80	-687	619	364	-1052	

*NEGLECTING EFFECTS OF PRESTRESS.

TABLE VIII-4

MEASURED PRINCIPAL STRAINS AND STRESSES[1]
SHEAR TEST

LOAD KIPS	ϵ MAX IN/IN x10^6	ϵ MIN IN/IN /10^6	γ MAX IN/IN /10^6	ϕ DEGREES	σ MAX PSI	σ MIN PSI	τ PSI
ROSETTE	1,2,3						
20	52	-62	57	26	181	-233	103
40	86	-126	106	24	285	-501	192
50	76	-166	121	26	216	-665	219
80	157	-187	172	26	548	-700	311
ROSETTE	4,5,6						
20	40	-70	55	48	125	-276	100
40	66	-216	141	54	134	-385	265
60	96	-346	221	52	177	-1430	400 *
80	132	-408	300	56	289	-1930	643
ROSETTE	7,8,9						
20	400	-30	216	87			
40	943	-67	605	85			
60	1392	-87	742	86		MEANINGLESS	
80	1611	-175	893	83			
ROSETTE	10,11,12						
20	61	-25	43	20	246	-65	78
40	128	-92	110	24	488	-311	199
60	196	-136	166	24	761	-463	300
80	241	-225	233	22	885	-863	422
ROSETTE	13,14,15						
20	10	-60	35	49	0	-251	63
40	51	-161	106	49	108	-661	192
60	91	-281	186	47	194	-1150	336
80	111	-341	226	43	233	-1396	409
ROSETTE	16,17,18						
20	36	-116	76	61	73	-475	138
40	80	-236	161	63	181	-963	291
60	186	-332	259	65	570	-1302	469 *
80	253	-419	336	69	846	-1632	608

$\mu = .16$

$E = 4.2 \times 10^6$ PSI

1 NEGLECTING PRESTRESS

* INELASTIC ACTION, DUE TO CRACKING BEGINS

TABLE VIII-5

COMPUTED STRESSES AT ROSETTES *
SHEAR TEST

ROSETTE	LOAD KIPS	f PSI	τ PSI	σ_{MAX} PSI	σ_{MIN} PSI	ϕ DEGREES
1,2,3	20	226	118	333	-107	29
	40	452	355	667	-215	
	60	678	533	1000	-322	
	80	904	710	1333	-429	
4,5,6	20	14	220	227	-213	44
	40	29	440	454	-425	
	60	43	660	682	-638	
	80	58	880	909	-851	
7,8,9	20	-162	219	152	-313	30°
	40	-324	437	303	-626	
	60	-485	665	454	-939	
	80	-647	873	606	-1252	
10,11,12	20	338	178	414	-76	23
	40	676	356	828	-152	
	60	1014	533	1242	-228	
	80	1352	710	1656	-304	
13,14,15	20	22	220	231	-209	44
	40	43	440	462	-418	
	60	65	660	693	-627	
	80	86	880	923	-836	
16,17,18	20	-242	219	129	-371	59
	40	-484	437	258	-742	
	60	-726	665	387	-1113	
	80	-968	873	516	-1484	

* NEGLECTING EFFECTS OF PRESTRESS

Concrete" by G. Magnel, 2nd Edition). A recent paper by E. Hognestad in the Proceedings of the A.S.C.E. entitled "Confirmation of Inelastic Stress Distribution in Concrete" (Paper No.1189) states that, "Test results show that the inelastic concrete stress distribution consists of a rising curve from zero to the maximum stress, and a descending curve beyond the maximum stress." The stress distribution under discussion being that in the compressive region. If the no-load prestress strains are added to the under-load strains, the non-linear distribution becomes even more pronounced than that shown in the figures. However, as shown in Fig. VIII-12, the correlation between observed and measured change of stresses is good except at the compression flange, where the non-linear distribution of stress is most pronounced.

Because of the poor performance of the rosettes, any measurement of shrinkage based on them is questionable. However, on Fig. VIII-13, and VIII-14 are plotted the no-load strains at the center of the beam, which shows the total of the instantaneous plus deferred strains, for the period of the test, at this section. In Table VIII-6, below, is listed the measured change of strain on the cable under no-load conditions on the concrete at gages 9 and 14 of box no.3. These gages are located on the web of the beams slightly below the C.G. of the cable. Because the cable and beam form a unit, any shortening of the beam along the axis of the cable will be followed by a corresponding shortening of the cable. Considering the small strain differences involved, the recorded shortening of the beam as indicated by the no-load strains at gages 9 and 14 are in good agreement with those recorded by the gages attached to the cable for the first 100 hours. As expected, the greatest rate of shortening occurred at the time of prestress, and decreased with time. This shortening appeared to be virtually complete by the end of the testing program.

TABLE VIII-6

DEFERRED STRAINS UNDER NO-LOAD

Time from Prestress Hours	Measured Increment of Strain In/In x 10^6	
	On cable	On concrete
0	0	0
48	53	60
96	70	65
144	113	80
192	120	75

In Table VIII-7, below, is shown the variation of prestress in the cable with time and with load. This table shows that within the working range, the increase in stress in the cable under loading did not exceed 3%, but that at close to failure loads, the increase in cable stress was of the order of 6%. Graphs showing the variation in strain in each wire with time are shown in Fig. VIII-15 to -20, and the mean no-load strains

T A B L E VIII-7

MEAN MEASURED STRAINS AND STRESSES IN PRESTRESSING CABLE

DATE	LOAD Kips	STRAIN In/In x 10^6	STRESS p.s.i.	TOTAL FORCE lbs.
Sept.7	0	0	0	0
8	P_i	5137	133,500	185,100
BENDING TEST				
10	D.L.	5084	132,100	183,800
	10	5100	132,700	186,700
	20	5115	132,900	184,600
12	D.L.	5067	131,900	183,000
	30	5115	132,900	184,600
	40	5133	133,200	185,000
	50	5148	133,900	186,000
	60	5200	135,100	187,900
13	D.L.	5037	131,000	182,000
	70	5163	134,100	186,200
	75	5174	134,200	184,400
14	D.L.	5024	130,200	180,900
	80	5174	134,200	184,400
	85	5224	135,500	188,100
	90	5331	138,600	192,100
SHEAR TEST				
16	D.L.	5017	130,200	181,000
	20	5049	131,100	182,100
	40	5080	132,100	183,600
	60	5151	132,900	184,200

for the cable are plotted in Fig. VIII-21.

FAILURE OF THE TEST BEAM

The beam failed at a load of 92 kips under the shear test setup. The failure was a flexural failure with the compression flange failing by buckling. A photograph of the failure is shown in Fig. VIII-22.

At failure, the maximum bending moment, at the L.H. stiffener was 3900 inch kips. As the failure occurred close to the stiffener, it is reasonable to take this figure as the failure moment at the failing section. At the time of failure, a large crack had opened up to the compression flange. Considering that the cable and the compression flange resists the full moment, the direct stress in the compression flange was approximately

$$\frac{3900}{16.0''} \times \frac{1000}{51.8''^2} = 4700 \text{ p.s.i.}$$

Though this value is lower than the test cylinder value for the compressive strength, it should be born in mind that the flange failed in buckling, and that this value of 4700 p.s.i. is somewhat approximate.

During the bending test at loads of 60 to 70 kips, two diagonal shear cracks developed in both end panels. The crack in the lightly reinforced end panel was inclined at an angle of approximately 23 degrees, while the crack in the more heavily reinforced panel (where the rosettes were applied) was inclined at an angle of approximately 26 degrees. At this load in the bending test, the direction of the principal stresses in the region of the cracks is about 22 degrees, while in the shear test the direction of cracks is about 26 degrees. The slightly greater inclination of the cracks in the heavily reinforced panel may be due to the additional stirrups inhibiting the spread at the cracks in that panel, but that during the subsequent shear test the stirrups were unable to prevent the spread of the cracks in the web, but the crack continued to develop at the new angle of the principal stress, which was about 26 degrees.

If the theories of Guyon et al were applicable, the inclination of the web cracks would have been greater; that is, had they developed along a slip plane, their inclination would have been approximately 14 degrees greater, or at an inclination of about 37 degrees. The graphical computation for the inclination of the slip planes is shown in Fig. VIII-23.

Jakobson had determined that the stirrup spacing required would be 13.5 inches, based on the theory of slip planes and web cracking occurring at an angle of 33 degrees.

Since the web cracking occurred at an angle of 23 degrees, e.g., along the direction of principal stress, we can derive a spacing based on the stirrups carrying the vertical component of the principal tensile stress, and assuming that the crack will penetrate the depth of the stirrups.

$$s = \frac{A_s f_s \cos\beta}{p_t \times t \times \frac{d'}{\tan\beta}}$$

$$= \frac{.22 \times 30{,}000 \times \cos 23 \times \tan 23}{180 \times 3.5 \times 22} = 18.6 \text{ inches}$$

It would appear that further research is warranted, however, before the Mohr-Guyon theory of failure is justified for application to prestressed concrete.

In view of the general results of the experiment, it would appear that the current methods used to proportion prestressed concrete structures are satisfactory, but that greater care should be taken when designing the stirrup layout.

TABLE VIII-8

BENDING TEST
COMPUTED PRINCIPAL STRESSES
(INCLUDING PRESTRESS)

LOAD KIPS	GAGE POS'N	P MAX PSI	P MIN PSI	ϕ DEGREES
20	1,2,3.	9	-1515	4°45'
40		47	-1391	10°16'
60		111	-1297	16°15'
20	4,5,6.	22	-1132	7°50'
40		57	-1187	14°45'
60		172	-1262	20°20'
20	7,8,9.	30	-818	10°45'
40		95	-997	17°15'
60		179	-1195	21°15'
20	10,11,12	[illegible]	-1436	5°00'
40		52	-1238	11°30'
60		142	-968	20°45'
20	13,14,15	23	-1129	7°52'
40		86	-1160	15°07'
60		117	-1237	20°15'
20	16,17,18	27	-873	13°15'
40		57	-1105	18°30'
60		160	-1350	21°30'

TABLE VIII-9

SHEAR TEST
COMPUTED PRINCIPAL STRESSES
(INCLUDING PRESTRESS)

LOAD KIPS	GAGE POS'N	p MAX PSI	p MIN P.S.I.	Ø DEGREES
20	1,2,3	22	- 1462	7°00'
40		96	- 1310	15°08'
60		249	- 1137	25°07'
20	4,5,6	43	- 1144	10°52'
40		159	- 1251	19°23'
60		315	- 1391	27°23'
20	7,8,9	54	- 890	13°56'
40		165	- 1161	20°57'
60		292	- 1452	24°15'
20	10,11,12	23	- 1351	7°30'
40		125	- 1015	19°20'
60		298	- 950	29°15'
20	13,14,15	33	- 1131	11°00'
40		158	- 1234	19°30'
60		317	- 1371	25°50'
20	16,17,18	50	- 966	13°15'
40		145	- 1203	18°30'
60		259	- 1659	21°35'

TABLE VIII-10

BENDING TEST
MEASURED PRINCIPAL STRESSES
(INCLUDING PRESTRESS)

LOAD KIPS	GAGE POS'N	σ_{MAX} PSI	σ_{MIN} PSI	ϕ DEGREES	τ_{MAX} PSI
20	1,2,3	1805	-808	22°56'	664
40		1405	-910	18°28'	579
60		1350	-686	18°10'	510
20	4,5,6	-219	-1870	1°30'	431
40		-253	-2100	0°	463
60		-344	-2150	6°15'	456
20	7,8,9	312	-998	5°45'	325
40		1435	-440	14°00'	466
60		1956	-1205	16°45'	784
20	10,11,12	-112	-1140	22°30'	313
40		-151	-1100	27°53'	306
60		-281	-1135	33°45'	353
20	13,14,15	-191	-1060	16°30'	217
40		-151	-1025	13°00'	217
60		-75	-1125	20°25'	265
20	16,17,18	-159	-925	16°50'	196
40		70	-1220	21°15'	295
60		25	-1610	24°00'	406

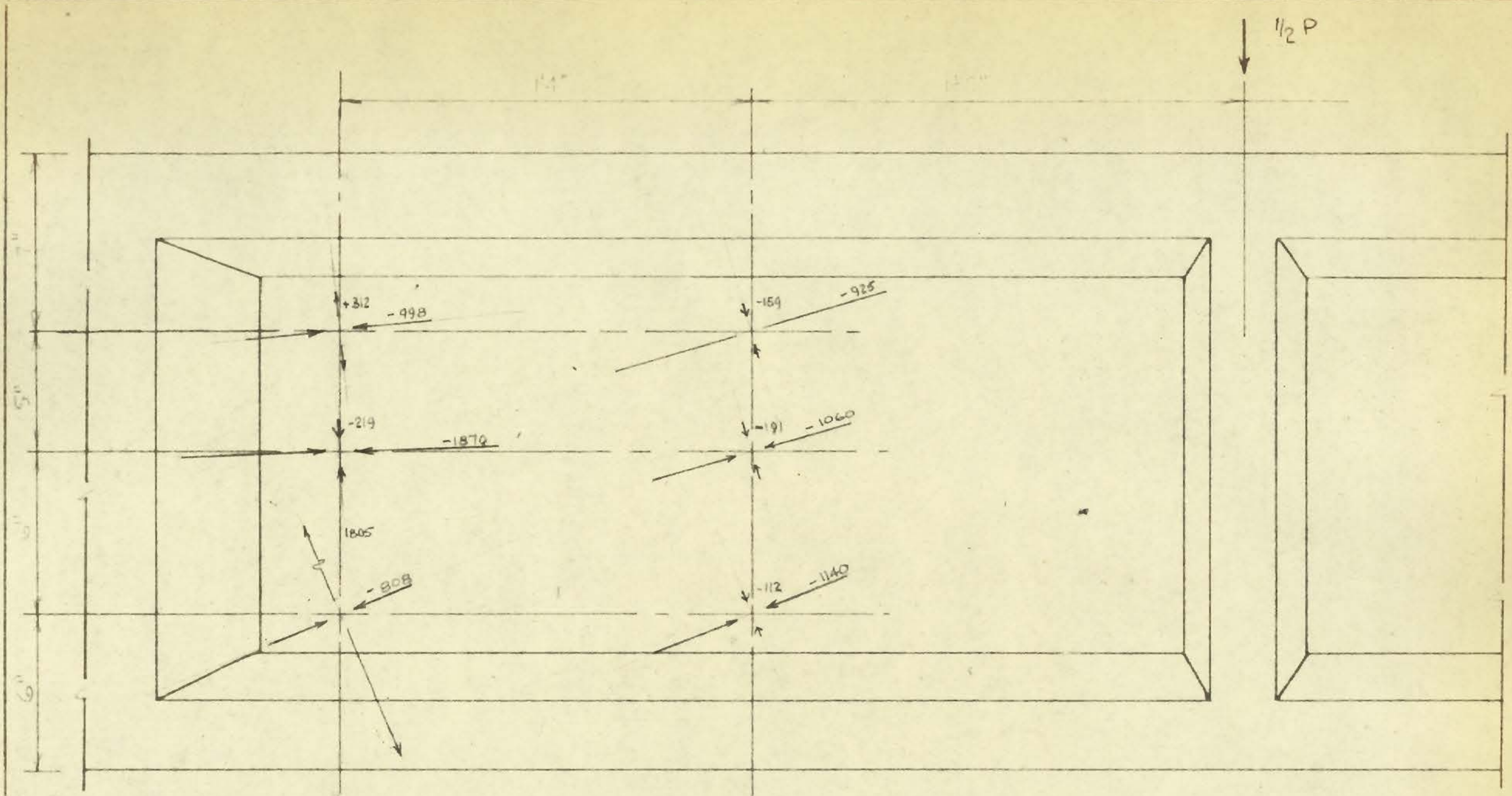

FIG VIII – 1

BENDING TEST
PRINCIPAL STRESSES
MEASURED VALUES
P = 20K
SCALES 1" = 6" 1" = 2000 PSI

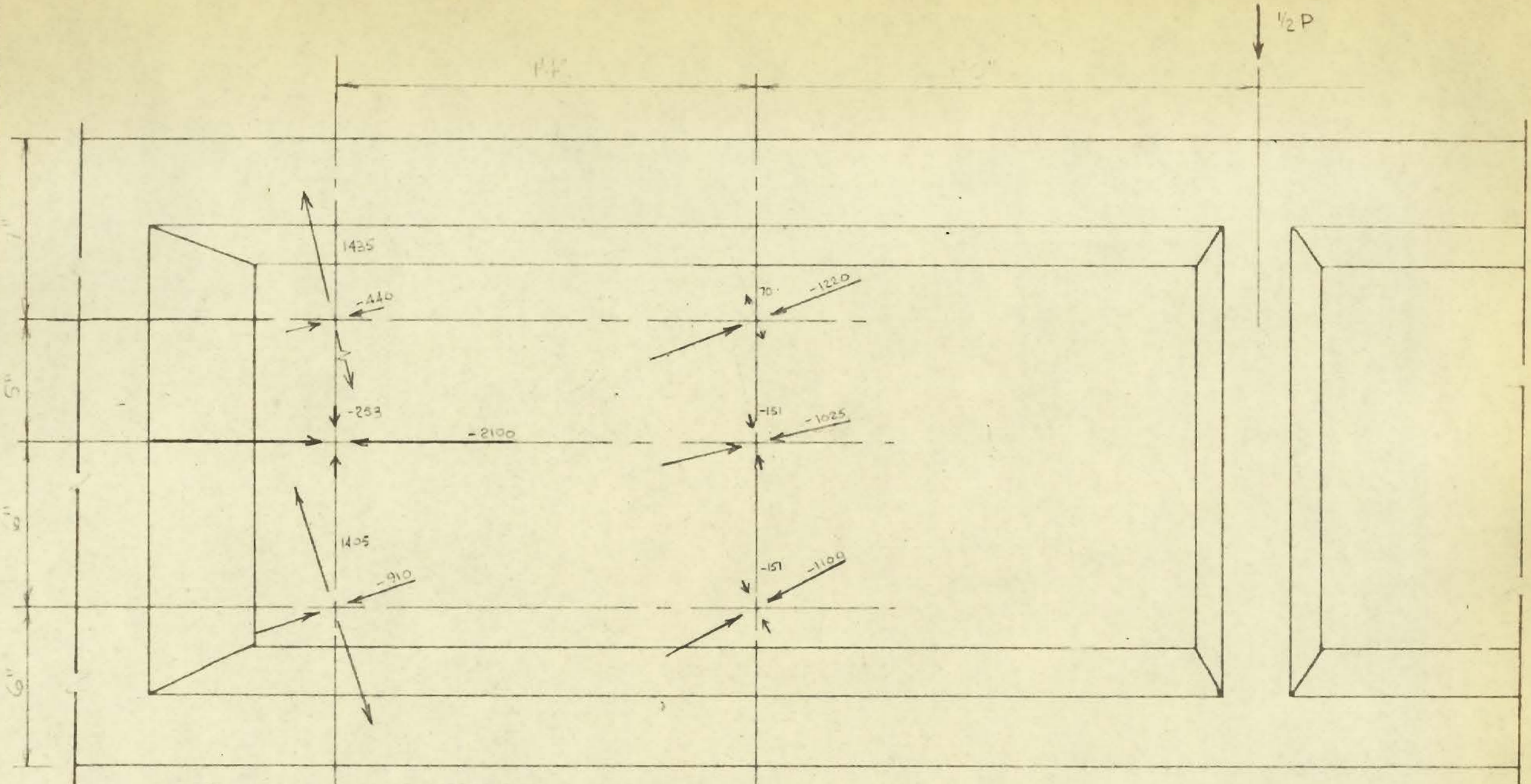

FIG VIII - 2

BENDING TEST
PRINCIPAL STRESSES
MEASURED VALUES
P=40K
SCALES 1" = 6" 1" = 2000 PSI

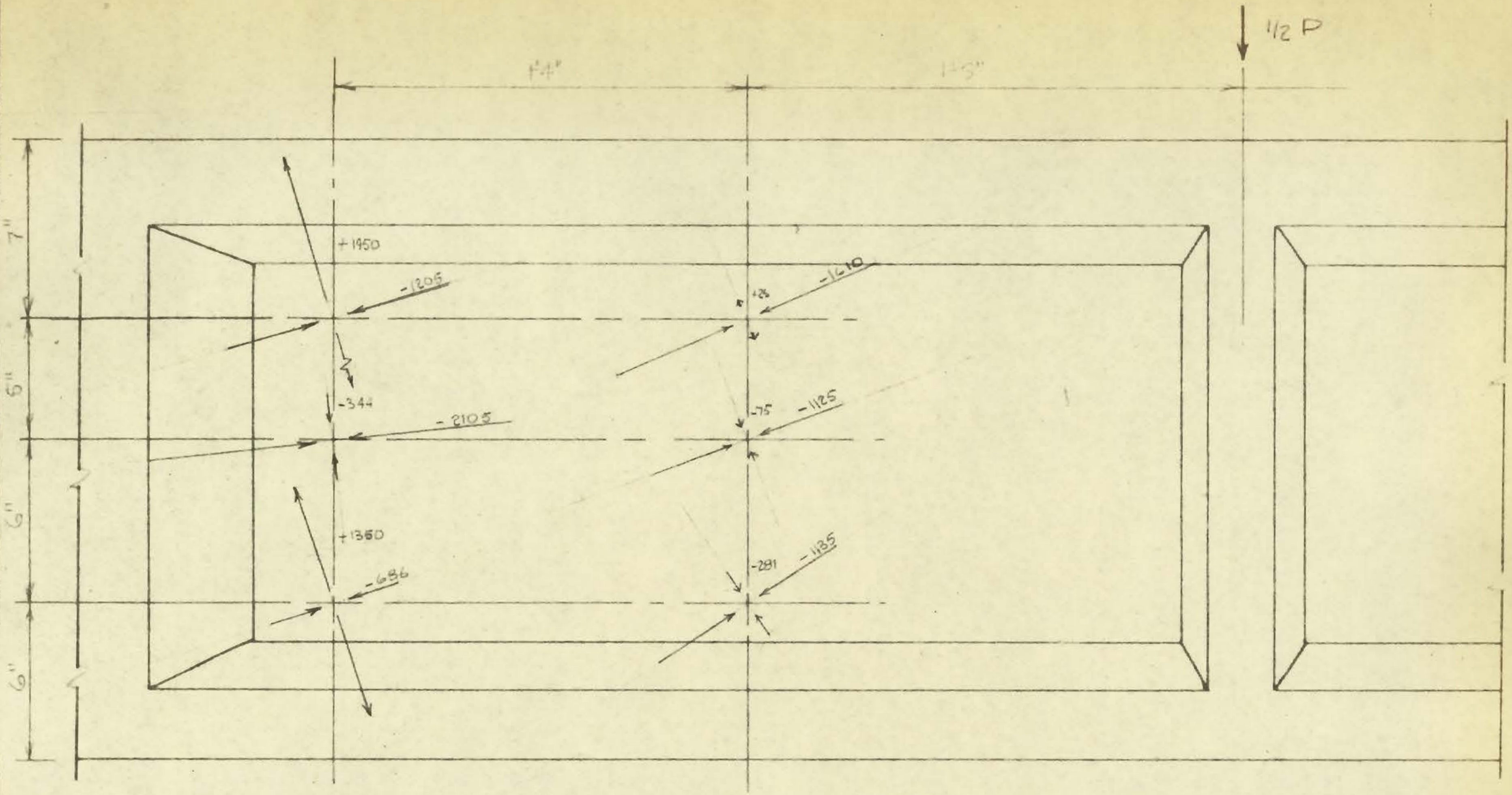

FIG VIII - 3

BENDING TEST
PRINCIPAL STRESSES
MEASURED VALUES
P = 60K
SCALES 1" = 6" 1" = 2000 PSI

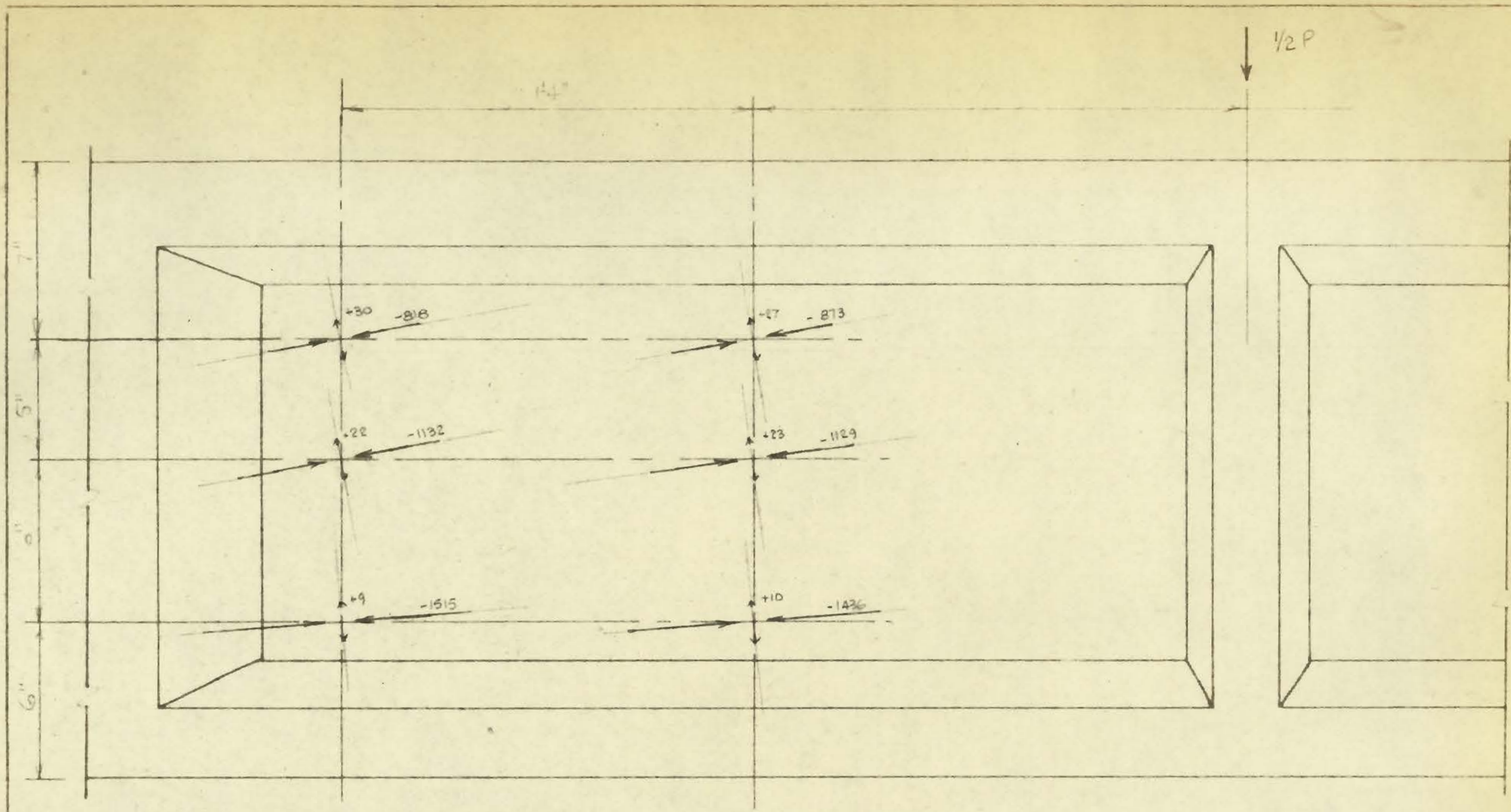

FIG. VIII - 4

BENDING TEST
PRINCIPAL STRESSES
COMPUTED VALUES
P = 20K
SCALES 1" = 6" 1" = 2000 PSI

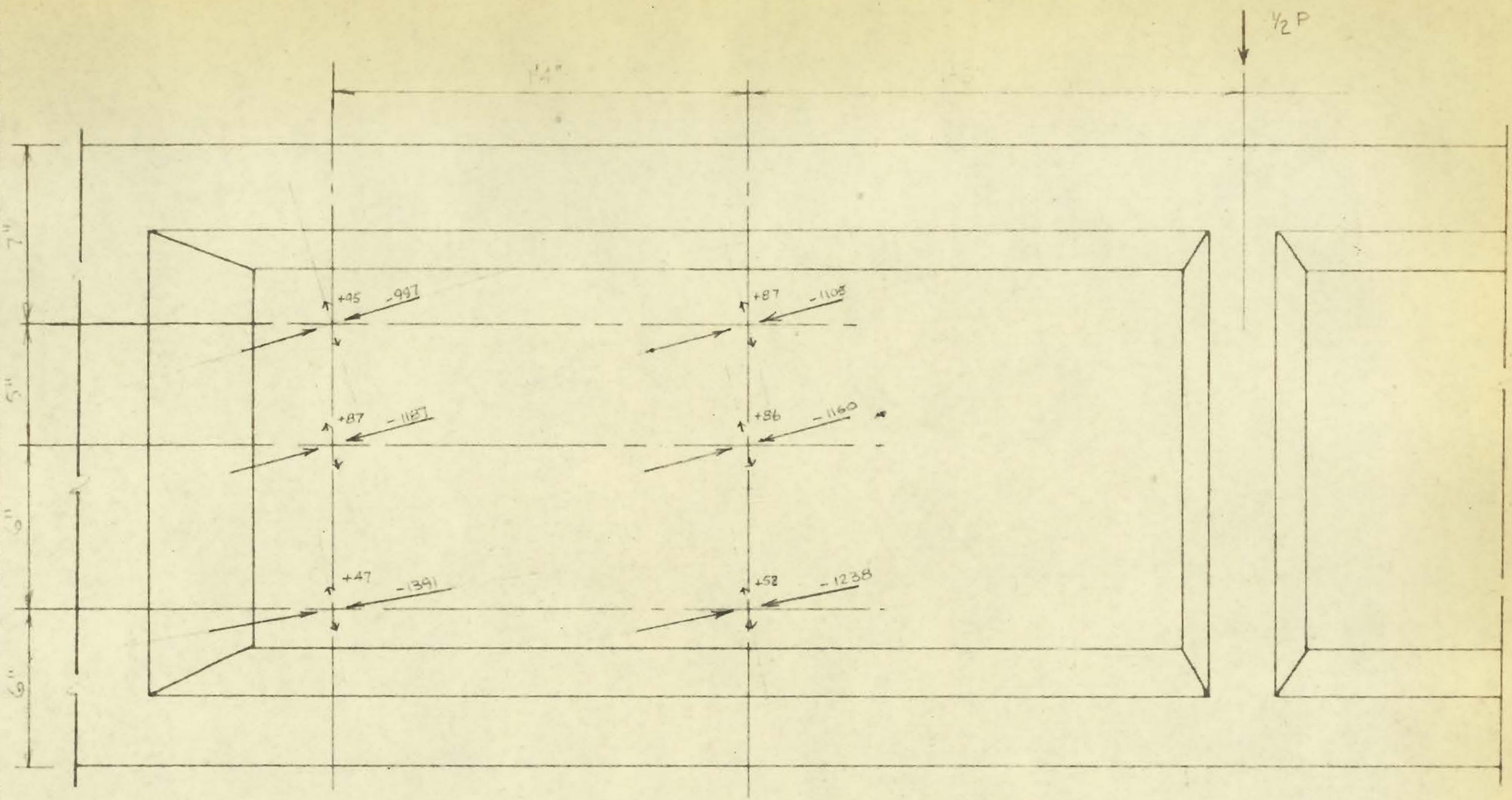

FIG VIII - 5

BENDING TEST

PRINCIPAL STRESSES

COMPUTED VALUES

$P = 40^K$

SCALES 1" = 6" 1" = 2000 PSI

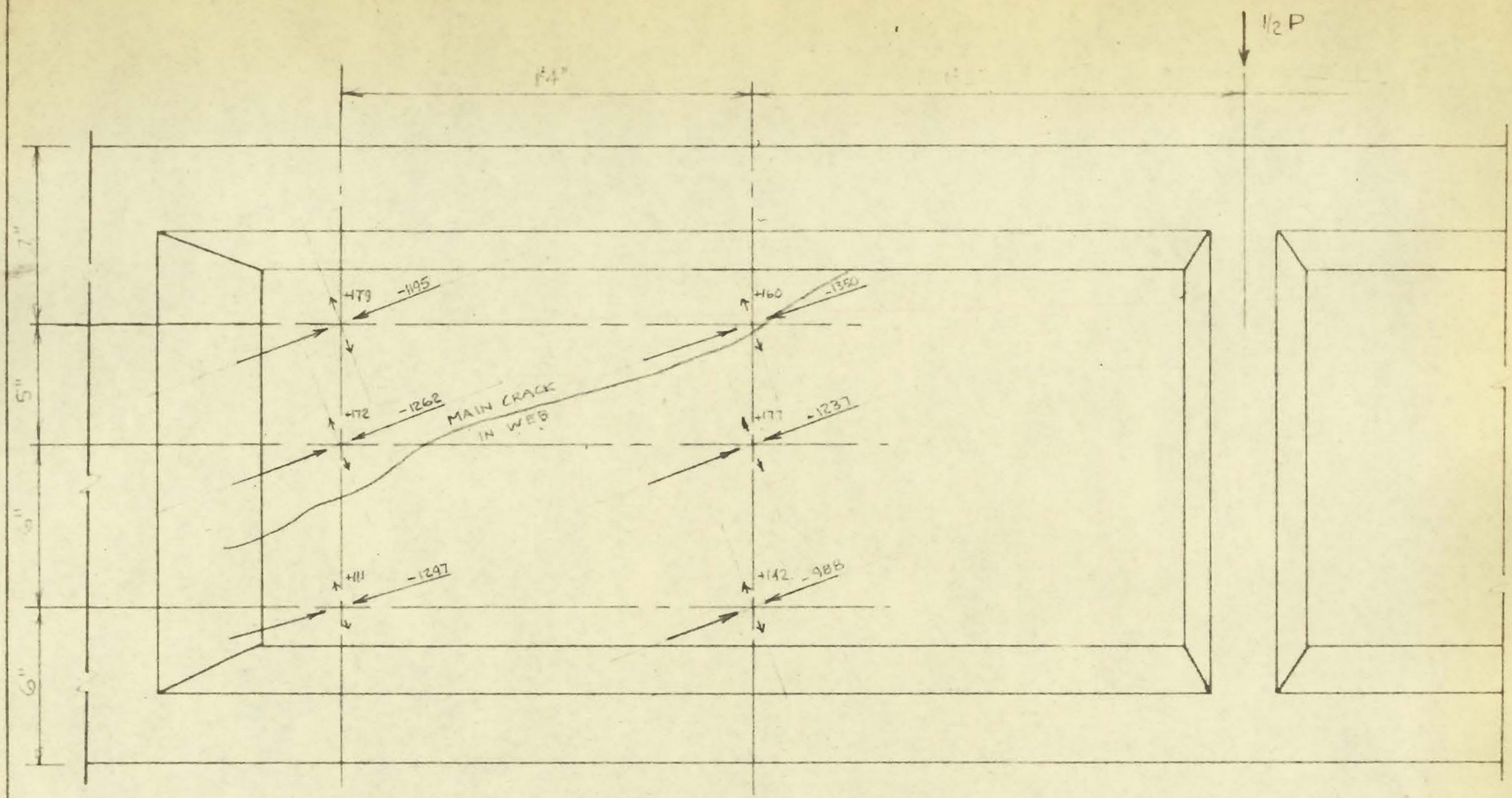

FIG VIII-6

BENDING TEST
PRINCIPAL STRESSES
COMPUTED VALUES
P = 60K
SCALES 1" = 6" 1" = 2000 PSI

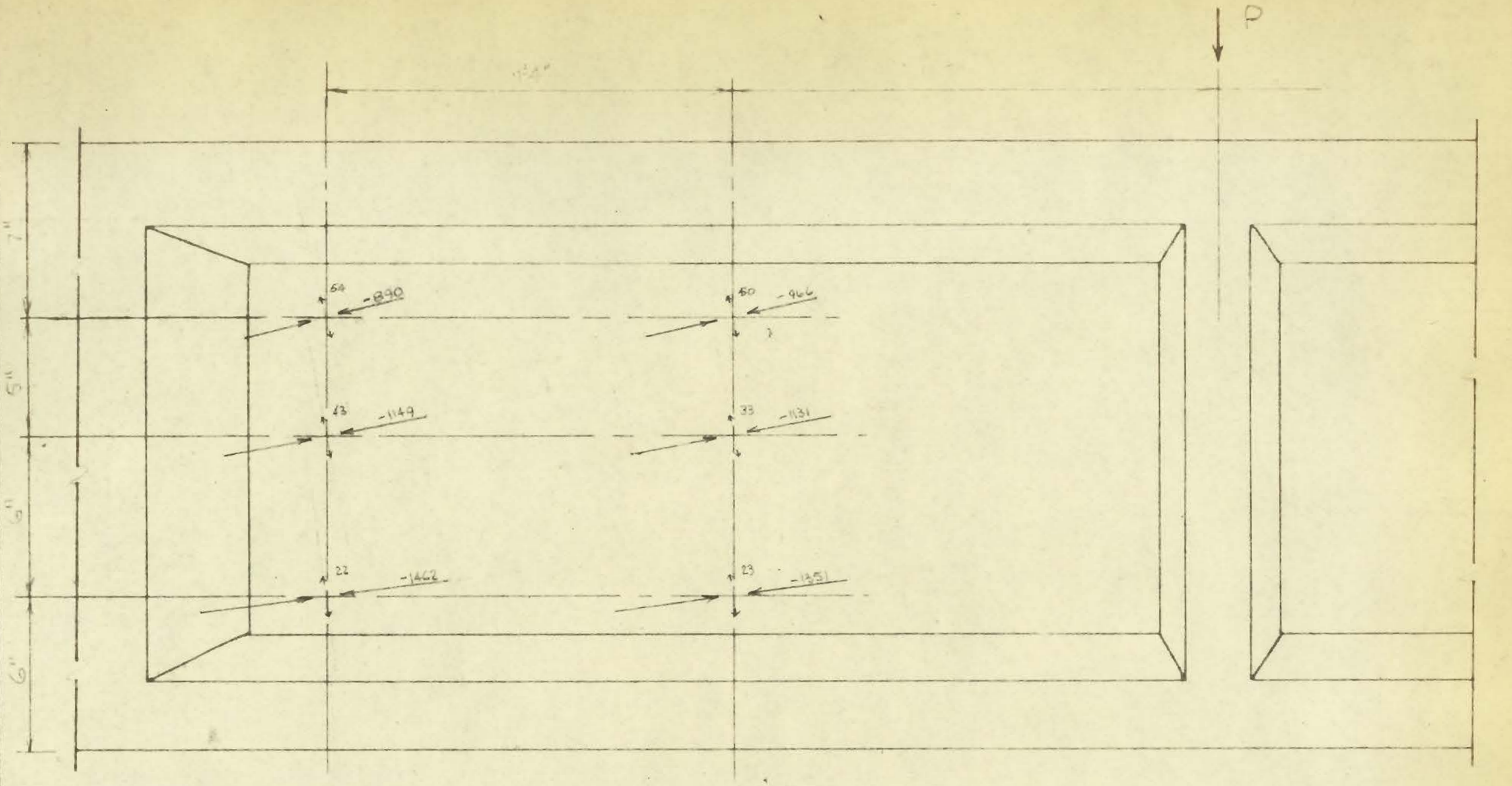

FIG VIII -7

SHEAR TEST
PRINCIPAL STRESSES
COMPUTED VALUES
P = 20k
SCALES 1" = 6" ; 1" = 2000 PSI

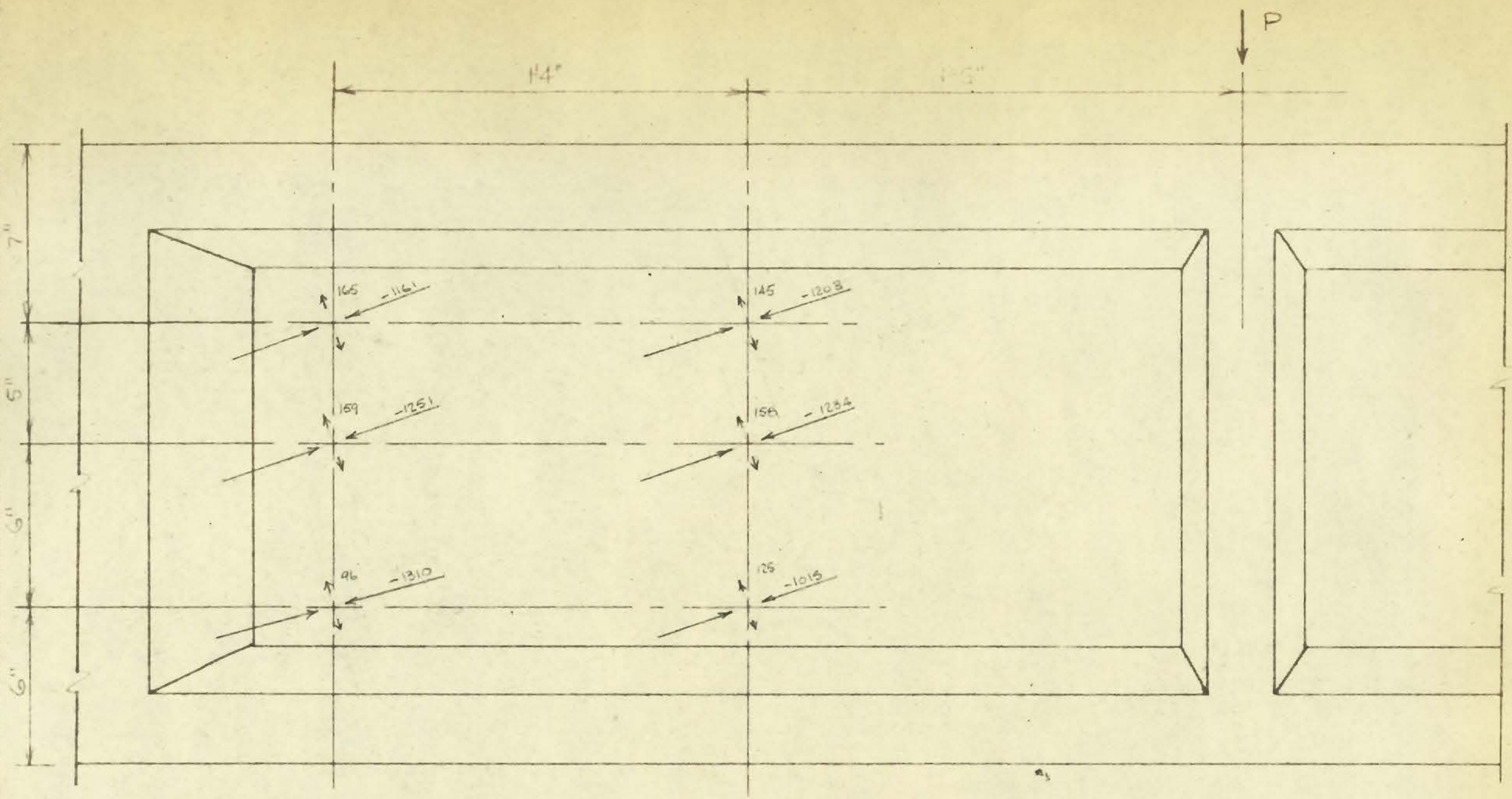

FIG VIII - 8

SHEAR TEST
PRINCIPAL STRESSES
COMPUTED VALUES
P = 40K
SCALES 1" = 6" 1" = 2000 PSI

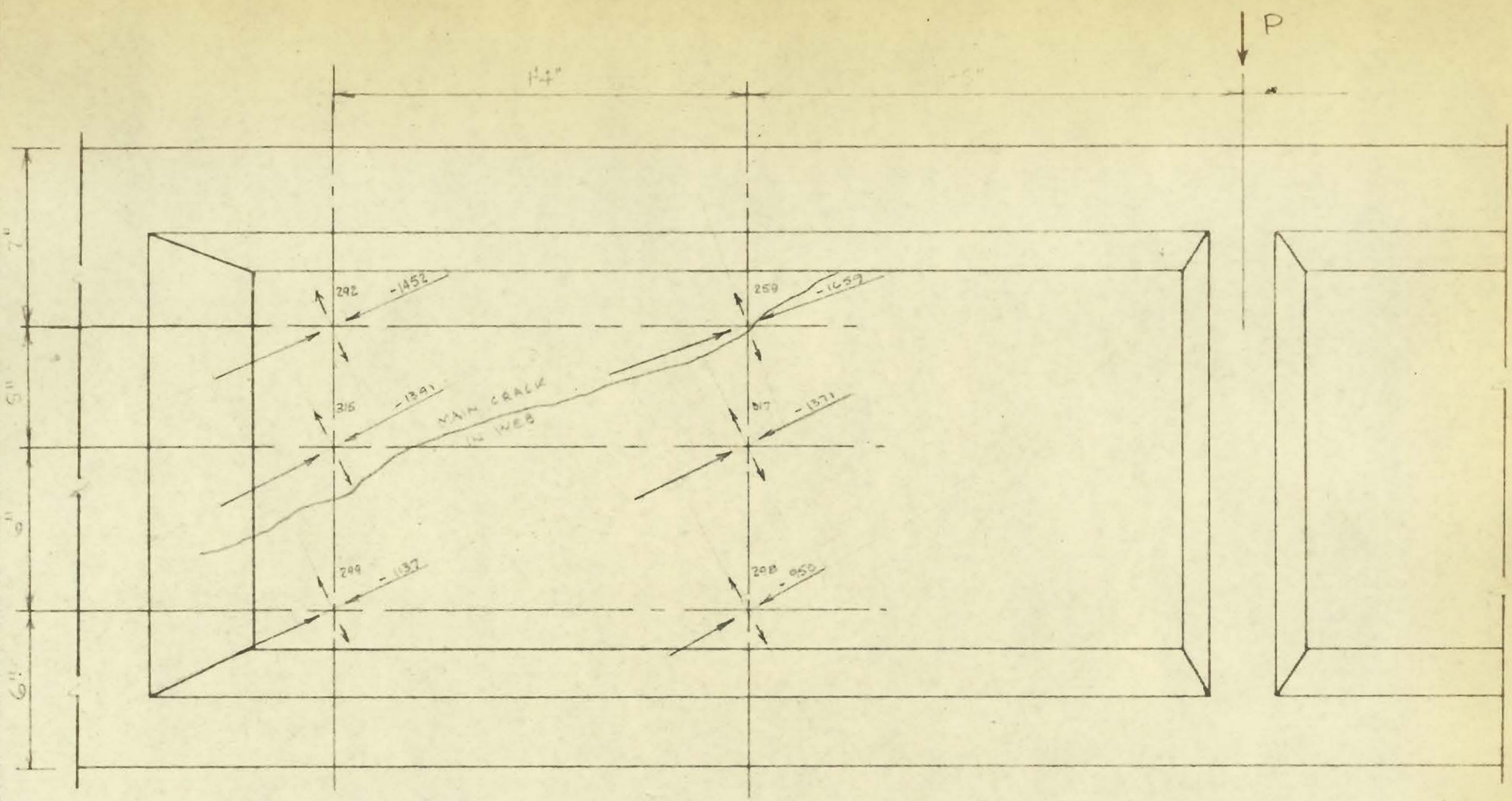

FIG VIII - 9

SHEAR TEST
PRINCIPAL STRESSES
COMPUTED VALUES
P = 60K
SCALES 1" = 6" 1" = 2000 PSI

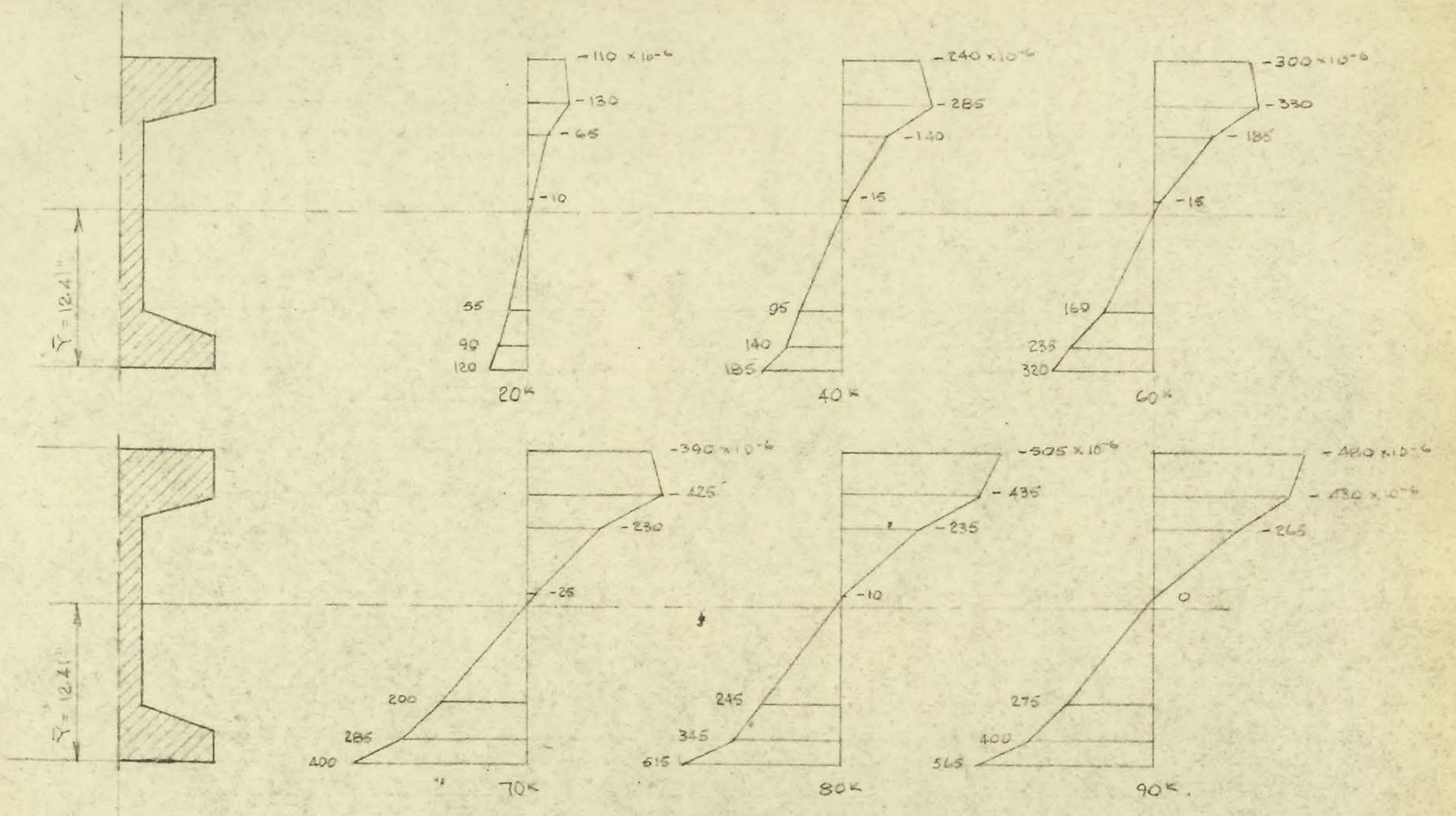

FIG VIII - 10

MEASURED CHANGE OF STRAINS AT CENTER OF BEAM

BENDING TEST

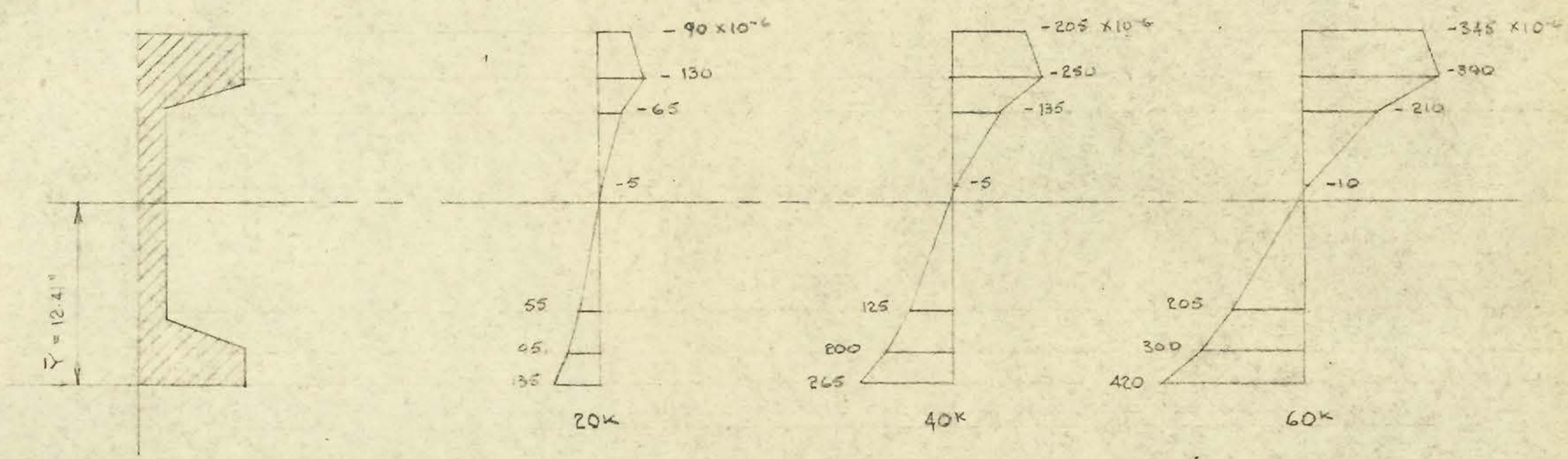

FIG $\overline{\text{VIII}}$ - 11

MEASURED CHANGE OF STRAINS AT CENTER OF BEAM

SHEAR TEST

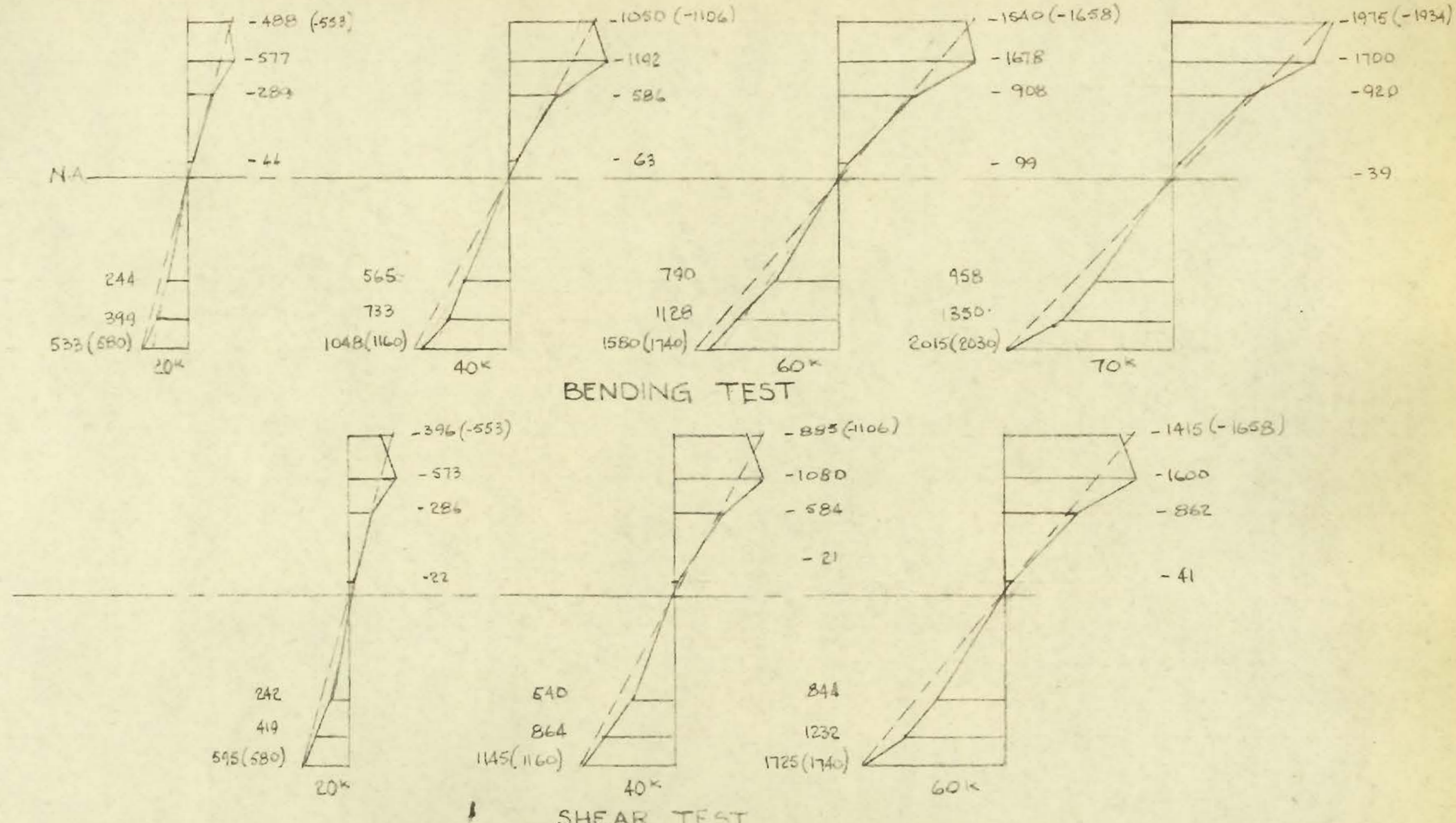

STRESSES IN PSI

NUMBERS IN BRACKETS REFER TO COMPUTED STRESSES

——— MEAS'D STRESS

– – – COMPUTED STRESS

FIG. VIII -12
COMPARISON OF MEASURED AND COMPUTED STRESS AT CENTER OF TEST BEAM

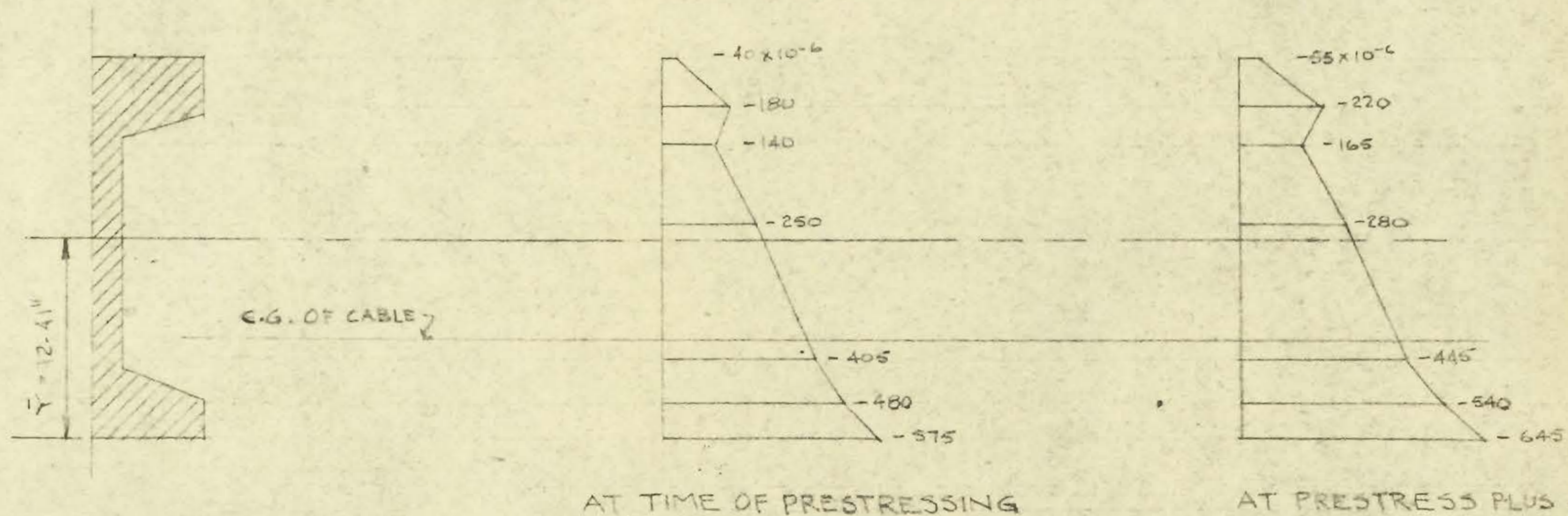

FIG. VIII - 13

MEASURED CHANGE OF STRAIN AT CENTER OF BEAM

DUE TO PRESTRESS ONLY.

SCALES 1" = 12"
1" = 50 MICRO IN/IN

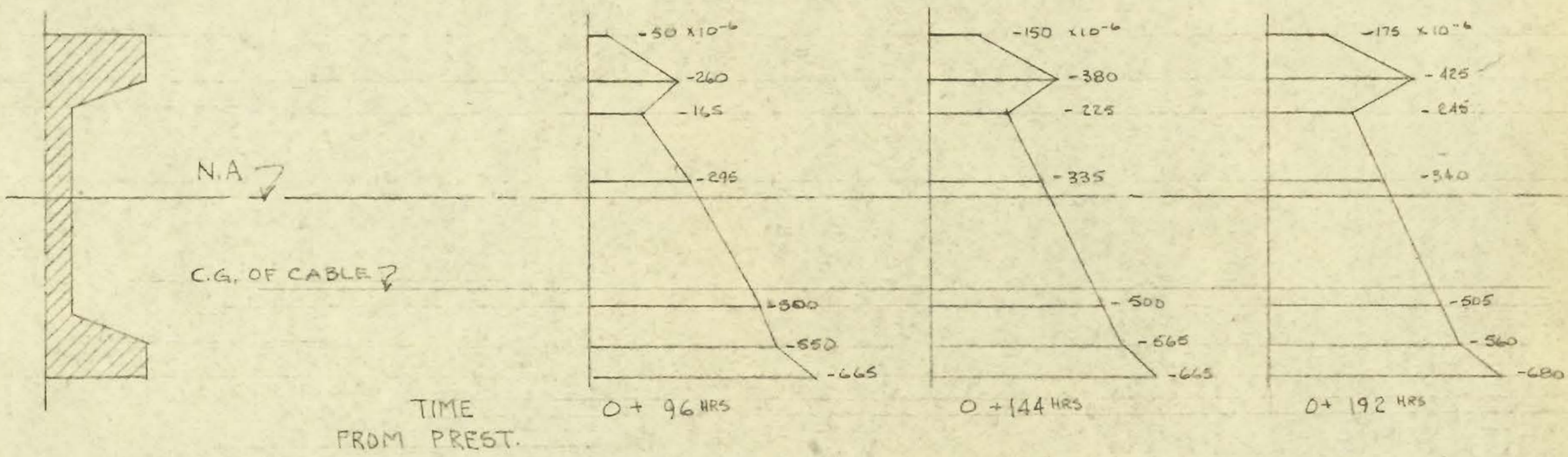

FIG VIII-14

MEASURED CHANGE OF STRAIN AT CENTER OF BEAM

DUE TO PRESTRESS ONLY

SCALES 1" = 12"
1" = 50 MICRO IN/IN

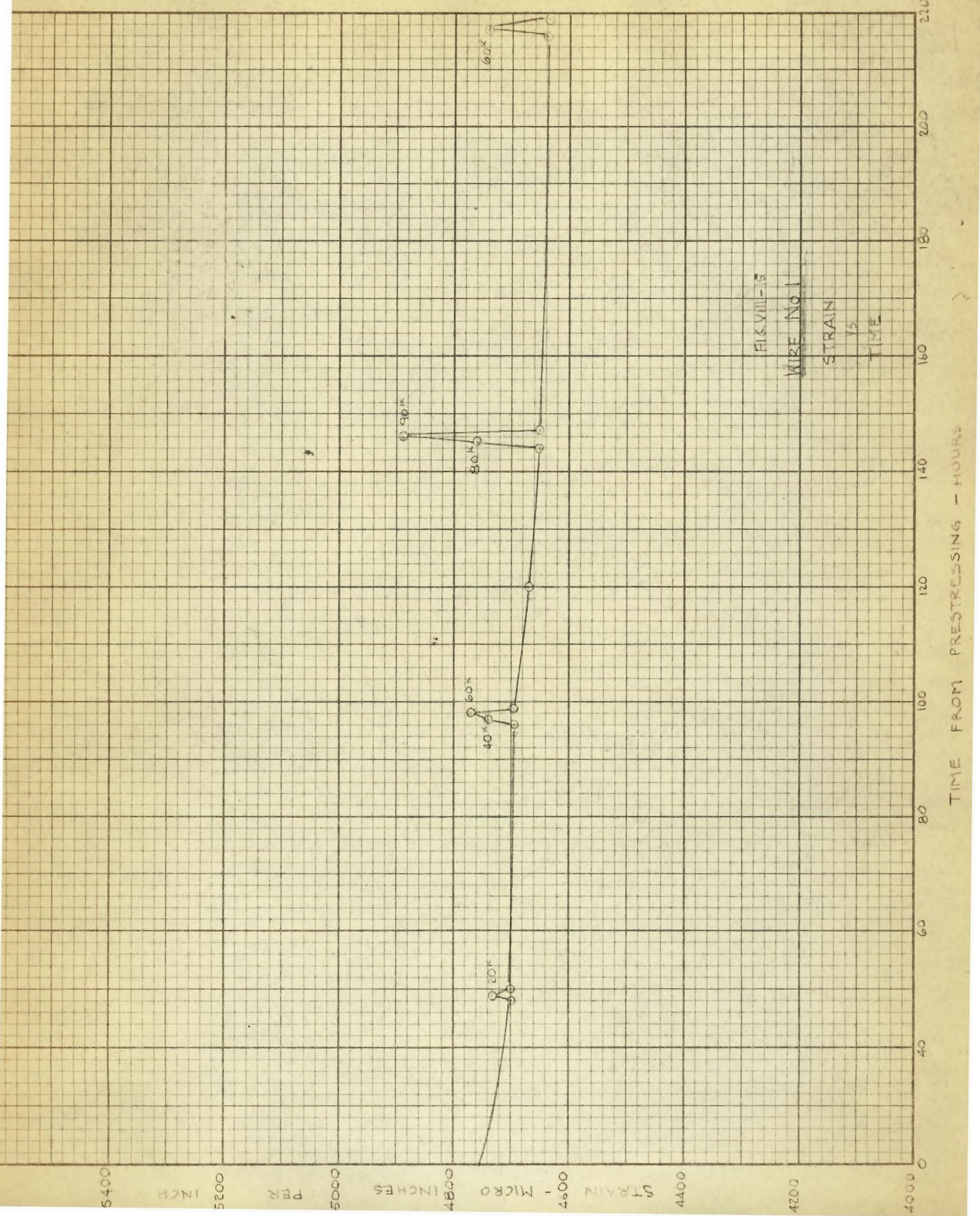
FIG VIII-5
WIRE No 1
STRAIN
VS
TIME
STRAIN - MICRO INCHES PER INCH
TIME FROM PRESTRESSING - HOURS
0
20
40
60
80
100
120
140
160
180
200
220
4000
4200
4400
4600
4800
5000
5200
5400
20k
40k
60k
80k
90k
60k

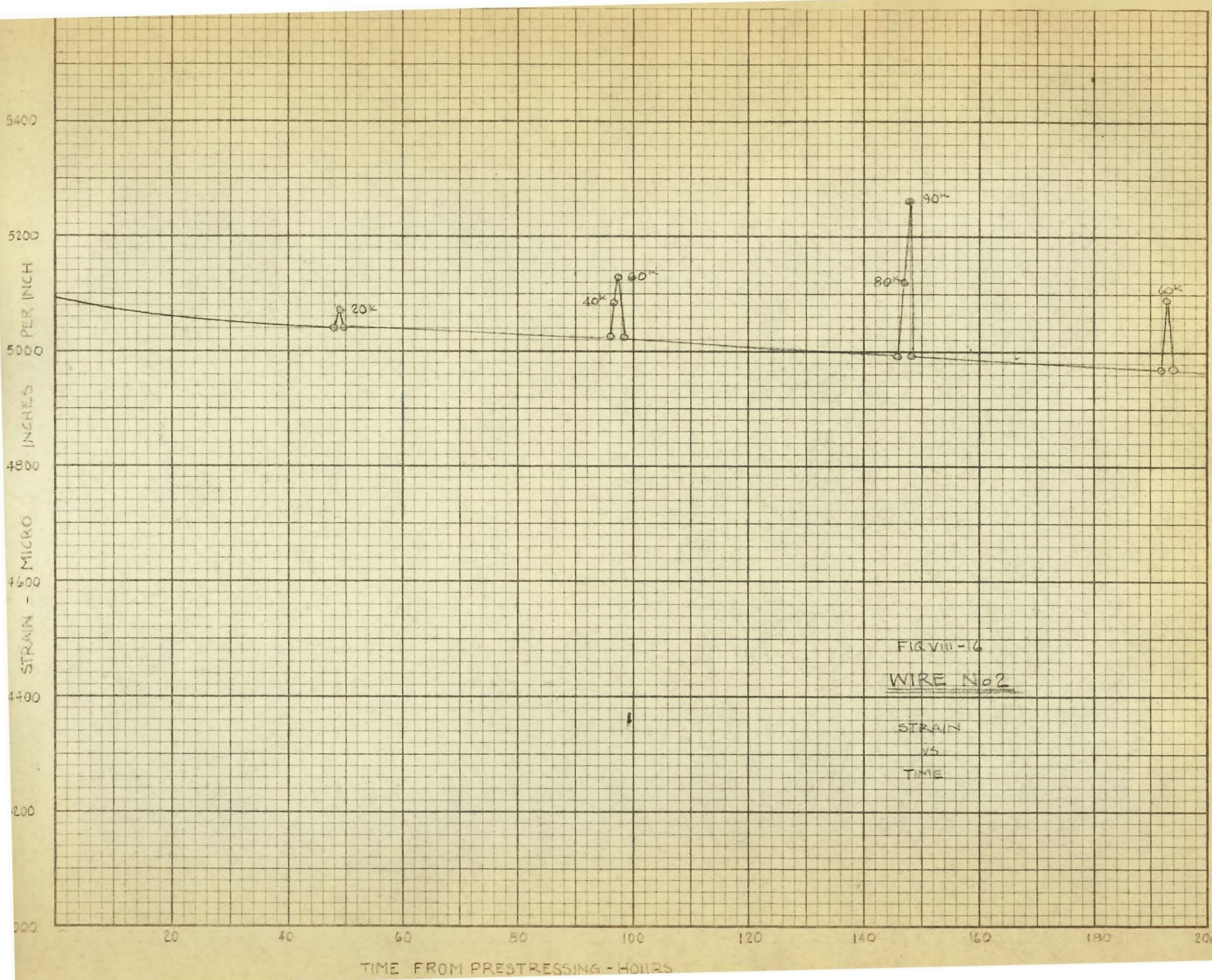

FIG VIII-16

WIRE No 2

STRAIN VS TIME

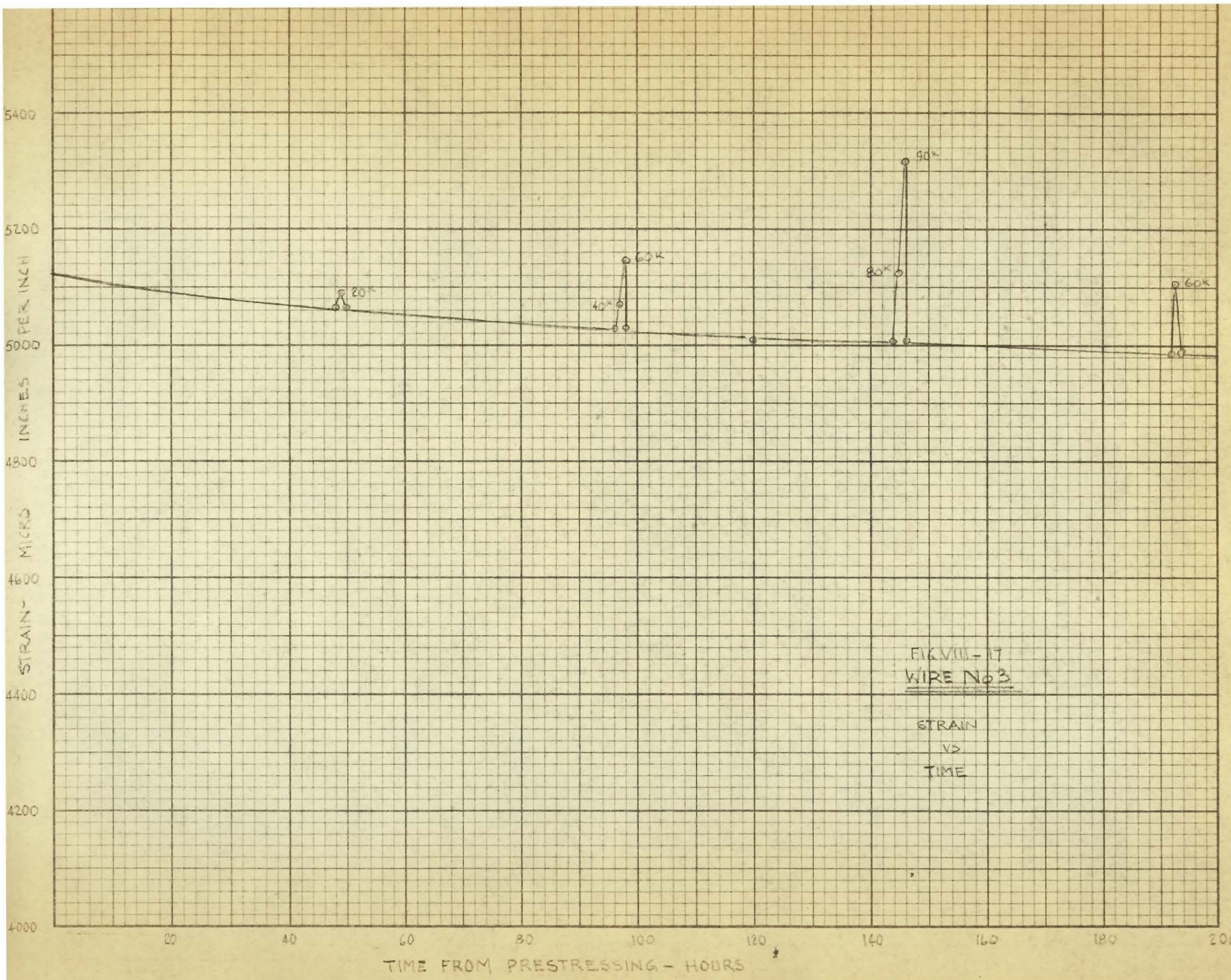

FIG VIII - 17
WIRE No 3

STRAIN
VS
TIME

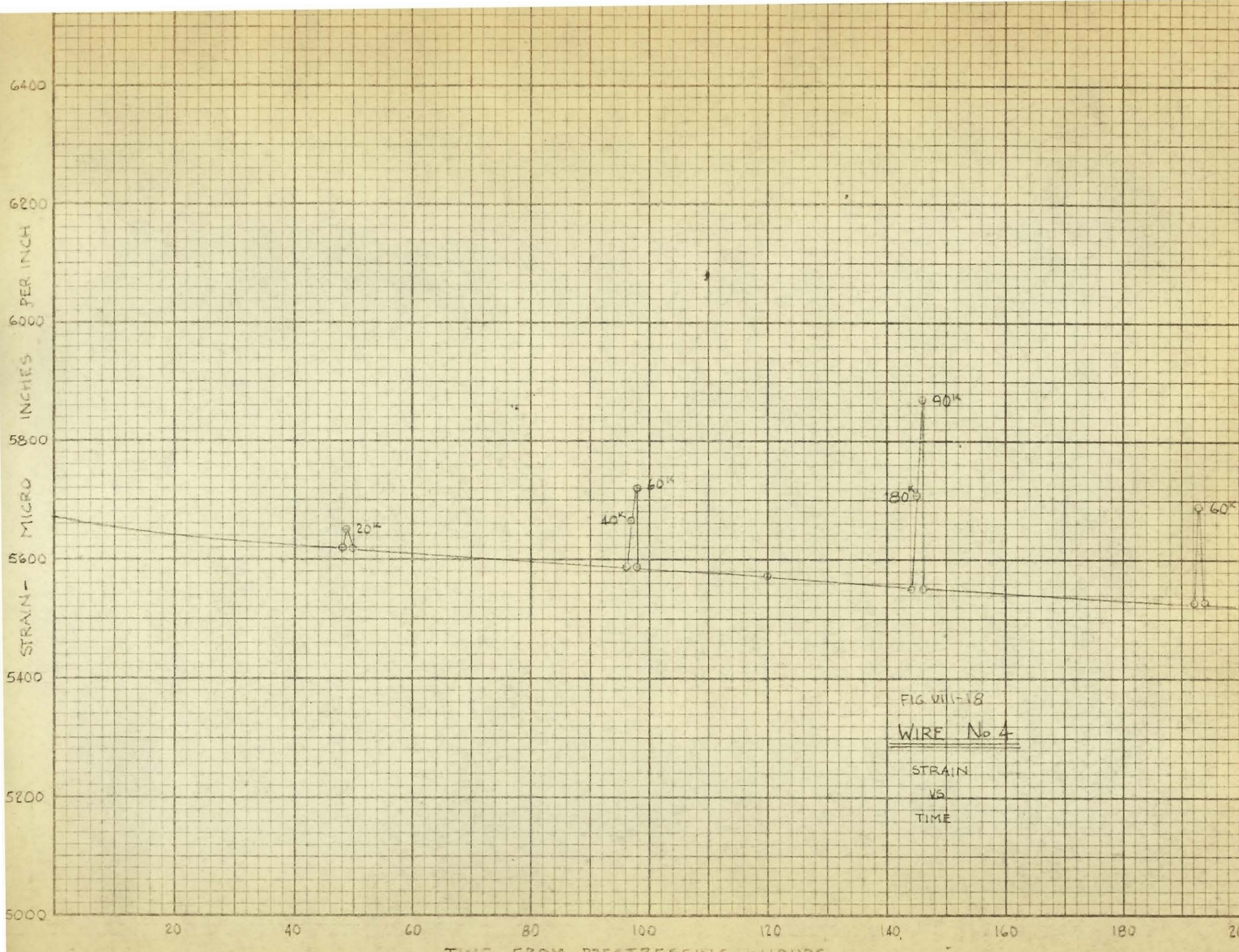
6400
6200
6000
5800
5600
5400
5200
5000
STRAIN - MICRO INCHES PER INCH
20
40
60
80
100
120
140
160
180
200
TIME FROM PRESTRESSING - HOURS
20K
40K
60K
180K
90K
60K
FIG VIII-18
WIRE No 4
STRAIN
VS
TIME

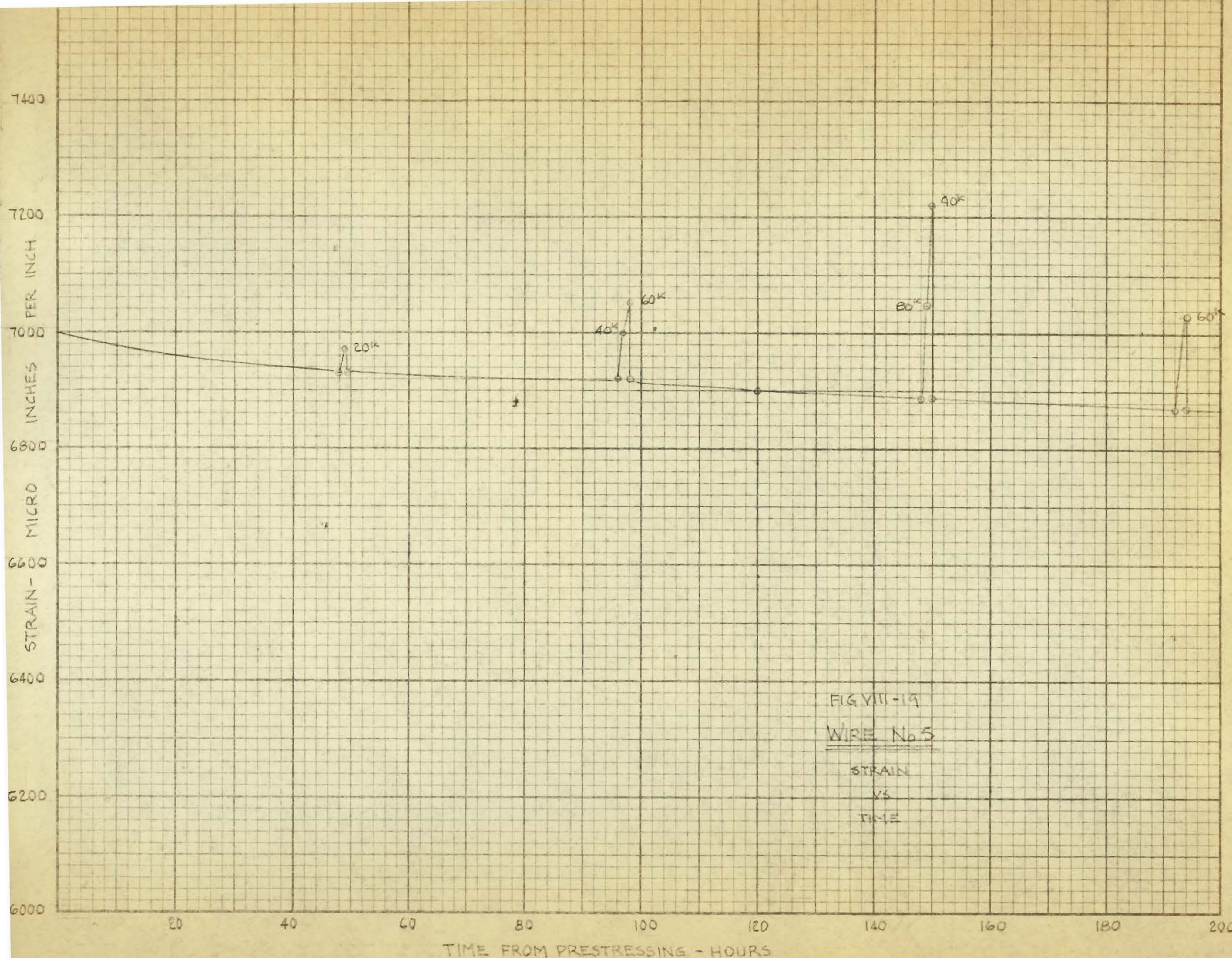
FIG VIII-19
WIRE No.5
STRAIN
VS
TIME
STRAIN - MICRO INCHES PER INCH
TIME FROM PRESTRESSING - HOURS
7400
7200
7000
6800
6600
6400
6200
6000
20
40
60
80
100
120
140
160
180
200
20K
40K
60K
80K
90K
60K

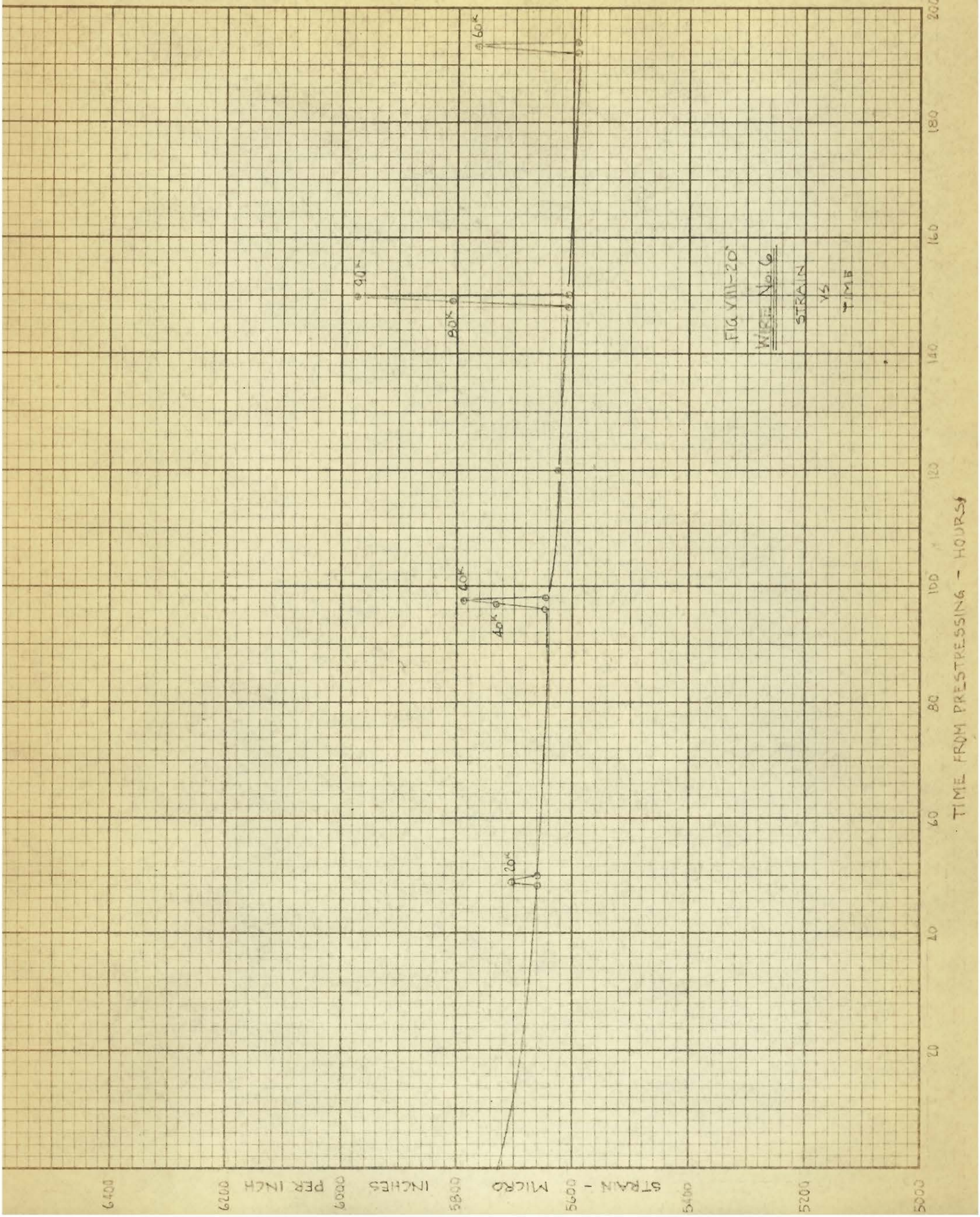
FIG VIII-20
WIRE No. 6
STRAIN
VS
TIME
TIME FROM PRESTRESSING - HOURS
STRAIN - MICRO INCHES PER INCH
20^K
40^K
60^K
80^K
90^K
80^K
60^K
0
20
40
60
80
100
120
140
160
180
200
5000
5200
5400
5600
5800
6000
6200
6400

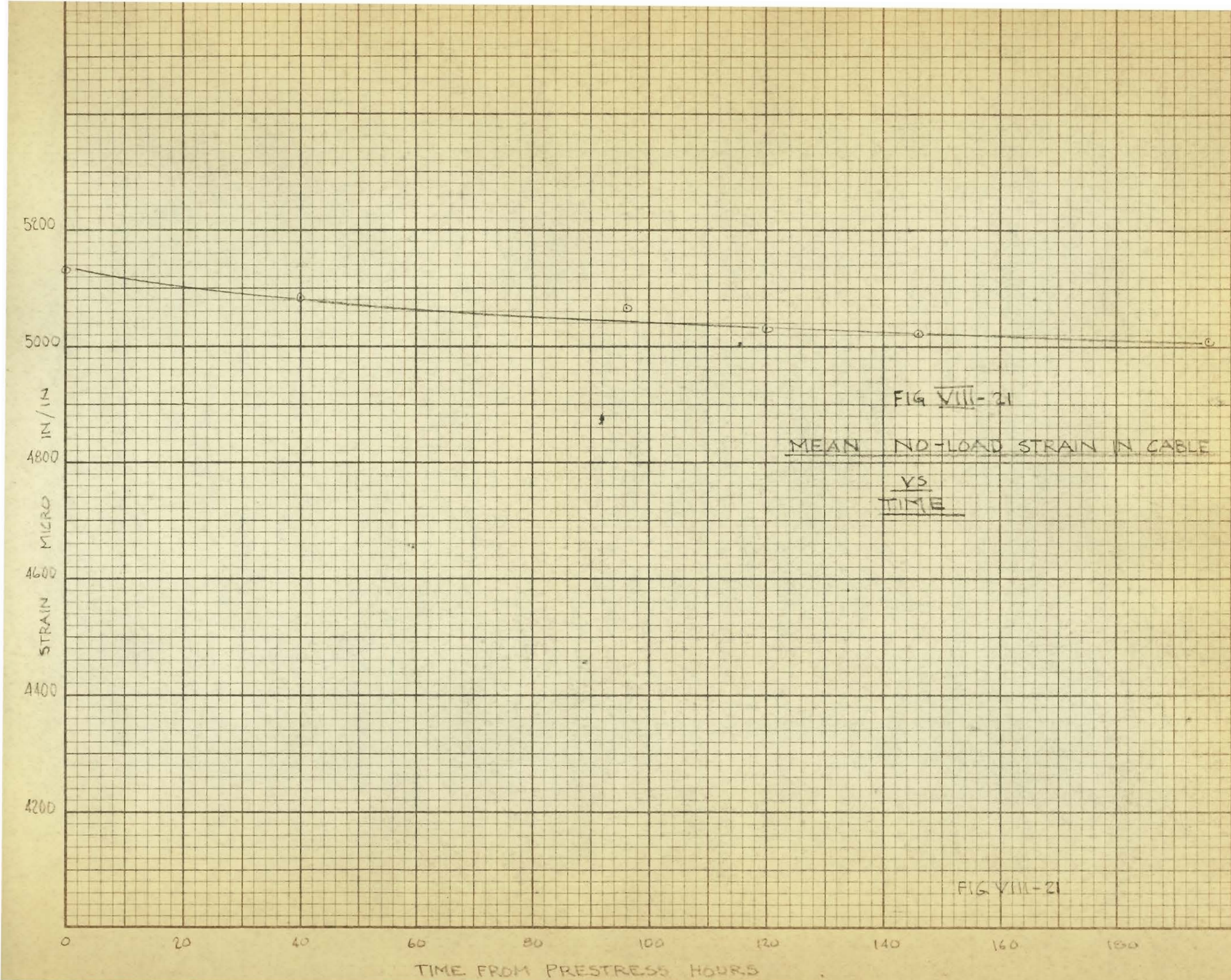
FIG VIII-21
MEAN NO-LOAD STRAIN IN CABLE
VS
TIME
5200
5000
4800
4600
4400
4200
STRAIN MICRO IN/IN
0
20
40
60
80
100
120
140
160
180
TIME FROM PRESTRESS HOURS

FIG VIII-21

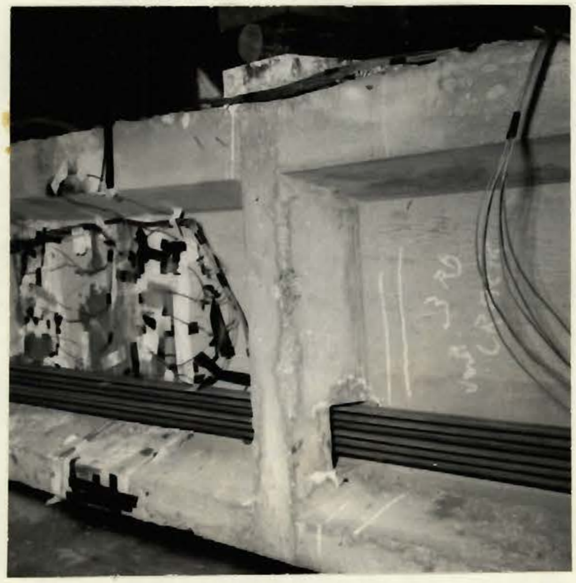

FIG. VIII - 22 a

TEST BEAM APPROACHING FAILURE

Note development of vertical crack near stiffener and diagonal crack in end panel

FIG. VIII - 22 b

FAILURE OF BEAM AT LOAD OF 92 KIPS APPLIED AT STIFFENER

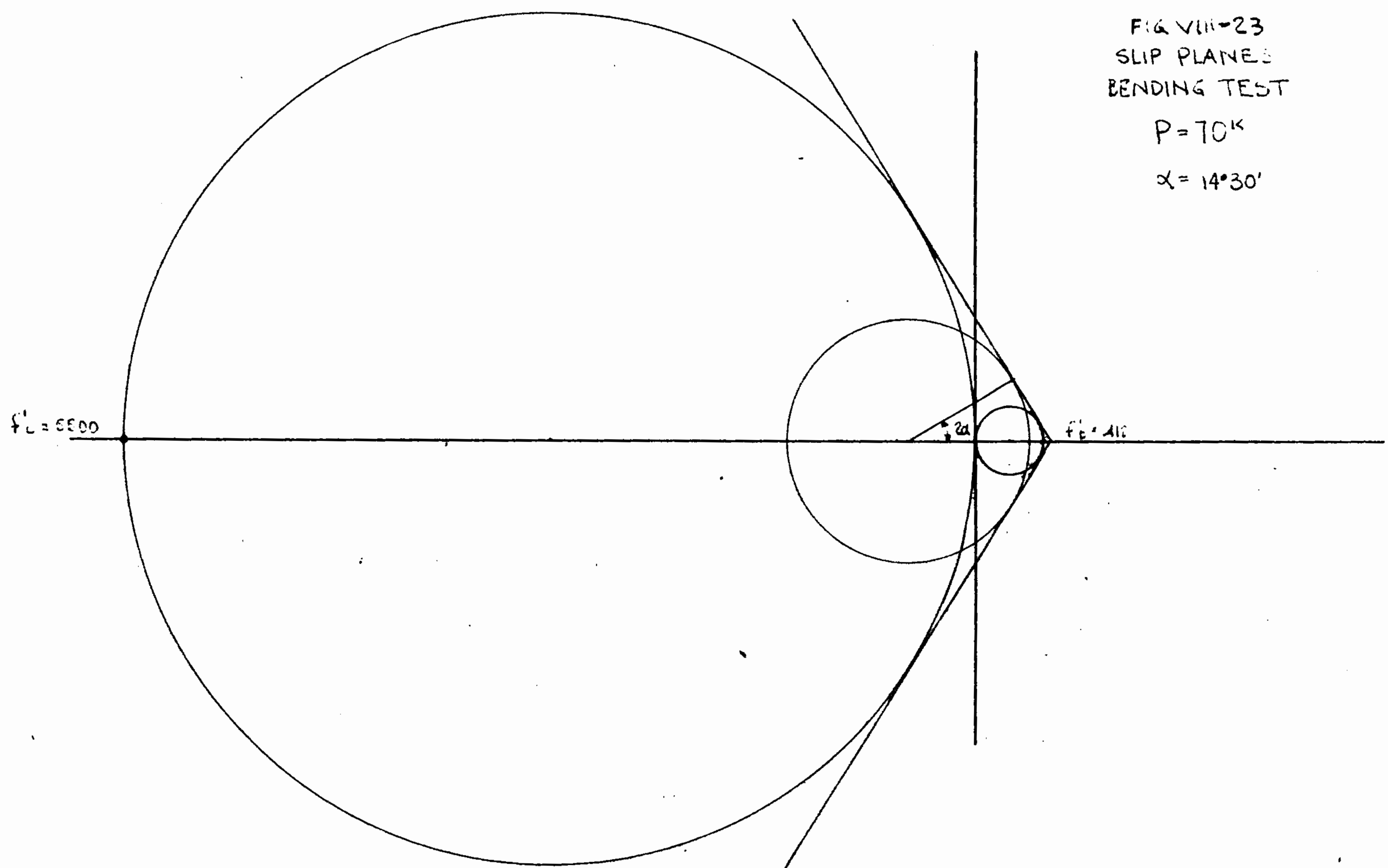

FIG VIII-23
SLIP PLANES
BENDING TEST
P = 70K
α = 14°30'
f'c = 5500
2α
f't = 416

FIG VIII-23

A P P E N D I X I

DETAILS OF THE TEST BEAM

In Fig. I-1 and I-2 are shown the concrete and mild steel details for the test beam used in this experiment.

In Fig. I-3 is shown a photo of the jack and hand pump used to apply the pretension to the wires. As stated previously, the Magnel-Blaton system was used in this experiment. In this system, the wires are tensioned two at a time. The stressing procedure took two days, and much of this time was spent in cutting the ends of the tensioned wires and attaching the pulling device to the wires.

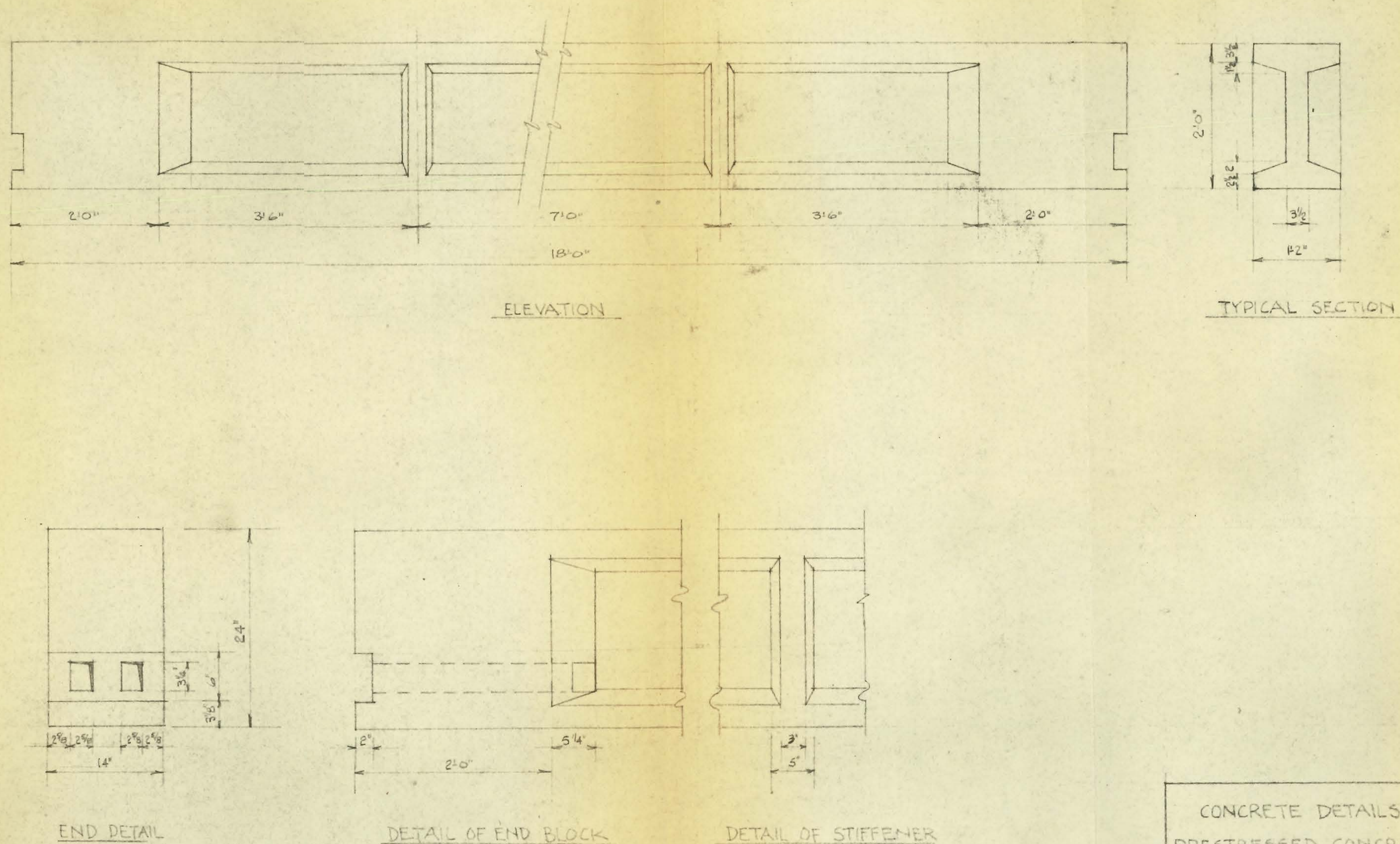

CONCRETE DETAILS

PRESTRESSED CONCRETE BEAM

FIG 1-1

SCALES 3/4" = 1'0" , 1" = 1'0"

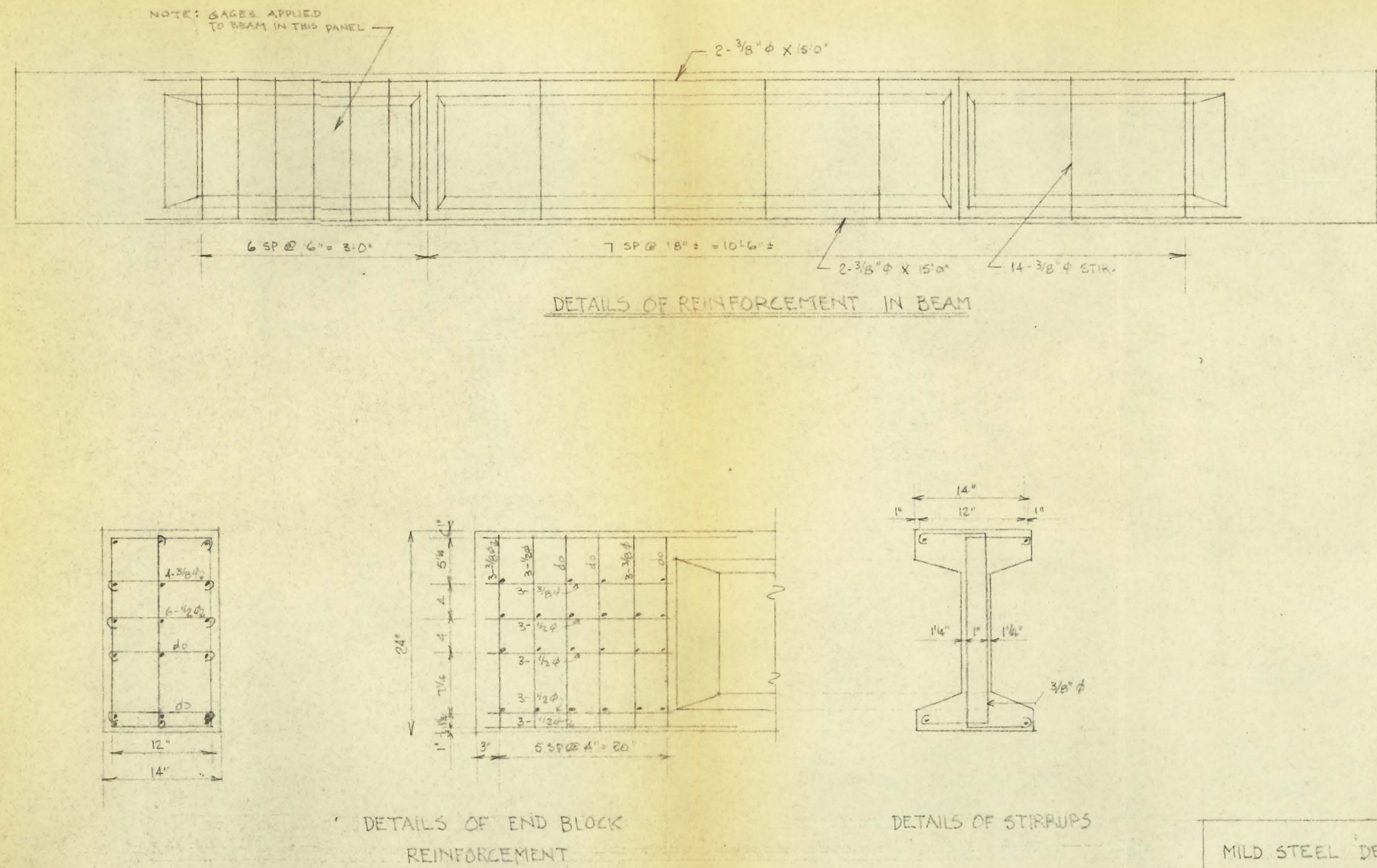

MILD STEEL DETAILS
PRESTRESSED CONCRETE
BEAM
FIG 1-2
SCALES 3/4" = 1'0" 1" = 1'0"

FIG. I - 3

STRESSING SETUP

(Note jack and hand pump)

THE MODULUS OF ELASTICITY DETERMINED BY BALANCING FORCES ACROSS A SECTION THROUGH THE BEAM

Consider a section through the beam along a line of strain gages. Note that if there are rosettes along the line of gages, consider only the one gage of each rosette that is lined up with the lingitudinal axis of the beam. See Fig. 2-1.

Considering the measured strains as the true linear strains, the stress at any gage point will be $E\epsilon$.

Whence the stress at gage number 1 will be $E\epsilon_1$, at gage number 2 it will be $E\epsilon_2$ and so on. Assuming a straight line distribution of stress between gages 1 and 2, the value and point of application of the resultant force acting on the element of area of the cross section between these two gages can be determined. By taking each element of area between strain gages and calculating the moment of the forces acting on it about the neutral axis, the total internal resisting moment can be calculated in terms of E and the measured strains. Since this internal resisting moment must be equal to the external moment at the section, the value of E can be calculated.

Applying this method to the test beam, and ignoring the strain at gage 4 (measured strains are too small to be accurate) we have after collecting terms and simplifying

$$E \times \epsilon_1 \times 271 = m_1$$
$$E \times \epsilon_2 \times 319 = m_2$$
$$E \times \epsilon_3 \times 66 = m_3$$
$$E \times \epsilon_5 \times 112 = m_5$$
$$E \times \epsilon_6 \times 326 = m_6$$
$$E \times \epsilon_7 \times 208 = m_7$$
$$\sum m_i = M_t$$

let $\sum m'E = \sum m_i$

whence $E = \dfrac{M_t}{\sum m'}$

This method gives an average value for E across the section for particular load at a particular rate of loading.

The effect of the increase in steel stress can be taken into account by reducing M by the amount of the external moment carried by the increase in steel stress. However, this reduction is less than 3% and is ignored here.

FIG 2-1

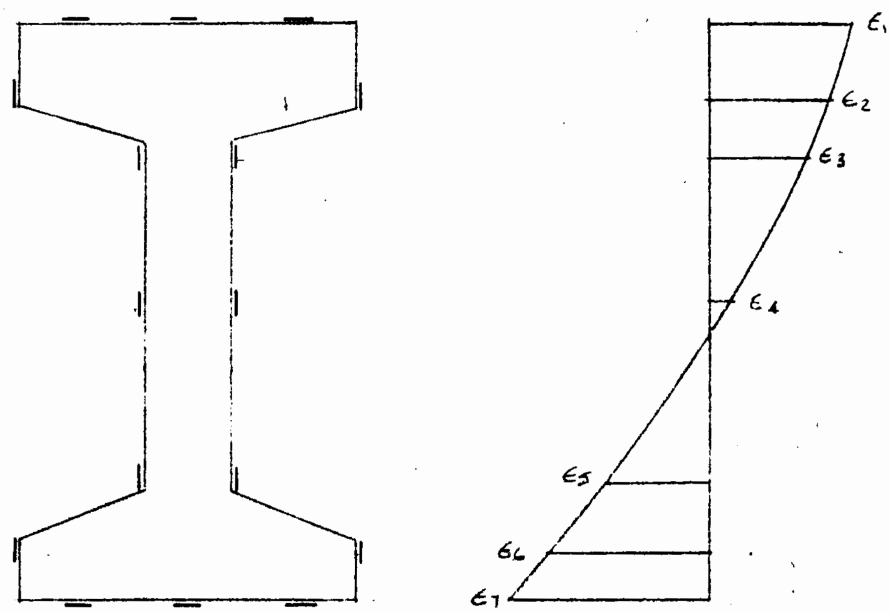

CROSS SECTION AT LINE OF GAGES

STRAIN DISTRIBUTION UNDER A LOADING.

APPENDIX 3

DEFLECTION DUE TO BENDING AND SHEAR

In the case of deep beams and narrow web beams such as I-beams, the deflection due to shearing forces may not be negligible compared to the deflection due to bending.

For this case, the additional deflection due to shear will be numerically equal to the bending moment produced by an imaginary loading P' acting at the same point as the real loading P. The value of this imaginary loading P' is $\frac{mP}{AG}$ or alternately may be calculated from the more familiar form $\frac{PQ}{ItG}$

where m = the ratio of the maximum stress at the neutral axis to the average stress across the section.

P - the real concentrated loads.

A - the cross sectional area.

G - the modulus of rigidity.

Q - the static moment of the area of the section above (or below) the neutral axis, taken about the neutral axis.

t = thickness of the section at the neutral axis.

I = the moment of inertia of the section

It follows that the value of m is = $\frac{QA}{It}$ and for the test beam m = $\frac{170.09 \times 675}{12850 \times 3.56}$ = 2.52. A close approximation can be made by considering the section to be a rectangle, the width being equal to the width of the web and the depth being the overall depth of the beam; m would then be equal to 1.5. The error involved in using this approximation for this test beam would be about 20% overestimation of the shear deflections.

The modulus of rigidity is given by $G = \frac{E}{2(1+\mu)} = \frac{E}{2(1+.164)}$

$$= \frac{E}{2.328}$$

In the case of the plain concrete test beam, the loading was at the third points over a 6'0" span, and the cross section being 6" wide by 8" deep. The center line deflection due to bending alone is given by $\delta_{max} = \frac{Pa}{48EI}(3L^2 - 4a^2)$

$$= \frac{P \times 24}{48 \times E \times 256}(3 \times 72 \times 72 - 4 \times 24 \times 24)$$

$$= 25.9 \frac{P}{E} \text{ inches}$$

The center line deflection due to shear is equal to the center line moment due to the imaginary loading of $\frac{mP}{2AG}$, here m = 1.5.

Whence $M' = \delta_{shear} = \frac{1.5 \times P \times 2.328 \times (36 - 12)}{2 \times 48 \times E} = .872 \frac{P}{E}$ inches

the ratio of shear deflection to bending deflection is therefore

$$\frac{.872}{25.9} = .0337 \quad \text{or} \quad 3.37\%$$

In the case of the prestressed concrete beam, we have two loading conditions to consider:

case (a) two point loading.

case (b) one point loading.

CASE (a) TWO POINT LOADING

Here the loads were applied 5'0" from the end supports over a 17'0" span. The center line deflection due to bending alone is given by $\delta_{bending} = \frac{Pa}{48EI}(3L^2 - 4a^2)$

$$= \frac{P \times 60 \times 144}{48 \times E \times 12,850}(3 \times 17 \times 17 - 4 \times 5 \times 5)$$

$$= 10.75\ \frac{P}{E} \text{ inches}$$

and the center line deflection due to shear is given by

$$M' = \delta_{shear} = \frac{2.52 \times P \times 2.328}{2 \times 170.09 \times E}(102 - 42) = 1.035\ \frac{P}{E} \text{ inches}$$

the ratio of shear deflection to bending deflection is therefore

$$\frac{1.035}{10.75} \quad .0962 \quad \text{or} \quad 9.62\%$$

CASE (b) ONE POINT LOADING

Here the load was applied 5'0" from one end support over a 17'0" span.

On carrying out a similar calculation, as was done for case (a), it was found that the shear deflection was again 9.62% of the bending deflection.

B I B L I O G R A P H Y

1. Abeles, P.W., "The principals and Practice of Prestressed Concrete," Frederick Ungar Publishing Co., New York, 1952.

2. Billig, K., "Prestressed Concrete", McMillan and Co., 1952.

3. Guyon, Y., "Prestressed Concrete", Contractors Record and Municipal Engineering, London, 1953.

4. Hetenyi, M., "Handbook of Experimental Stress Analysis," John Wiley & Sons, Inc., 1950.

5. Komendant, A.E., "Prestressed Concrete Structures," McGraw-Hill Book Company, Inc., 1952.

6. Lin, T.Y., "Prestressed Concrete Structures," John Wiley & Sons, Inc., 1955.

7. Magnel, G., "Prestressed Concrete", Third Edition, Concrete Publications Limited, London, 1954.

8. Parcel, J.I. and G. A. Maney, "Statically Indeterminate Stresses," John Wiley & Sons, Inc., 1936.

9. Popov, E.P., "Mechanics of Materials," Prentice-Hall Inc., 1952.

10. Seely, F.B., and J.O. Smith, "Advanced Mechanics of Materials," Second Edition, John Wiley & Sons, Inc., 1952.

11. Sutherland, H., and R.C. Reese, "Reinforced Concrete Design," Second Edition, John Wiley & Sons, Inc., 1952.

12. Timoshenko, S., and J.M. Lessels, "Applied Elasticity," First Edition, Westinghouse Technical Night School Press, East Pittsburgh, Pa., 1925.

13. Urquhart, L.C., and G.E. O'Rourke, "Design of Concrete Structures," Fifth Edition, McGraw-Hill Book Company, Inc., 1954.

14. American Concrete Institute Proceedings,

(a) October 1952, p.143.

(b) December, 1952.

(c) September 1953.

(d) October, 1953, p.121.

15. Civil Engineering,

(a) September 1951, p.356.

16. Banks and Kennedy, "The Technology of Cement and Concrete", John Wiley and Sons, Inc., 1955.

17. Timoshenko, S., "Applied Elasticity", 2nd Edition, John Wiley and Sons, Inc., 1955.

18. Proceedings of the A.S.C.E. (Paper No.1189)
E. Hognestad "Confirmation of Inelastic Stresses in Concrete".

19. Banks, R.H., "Flexural Stresses And Deflections of a Prestressed Concrete I Beam," McGill M.Eng. Thesis, 1956.

20. Jakobson, G.A., "Web Stresses in a Prestressed Concrete I Beam," McGill M.Eng. Thesis, 1955.

21. Proceedings of the First United States Conference on Prestressed Concrete," Massachusetts Institute of Technology, 1951.